



REBSA: Enhanced backtracking search for multi-threshold segmentation of breast cancer images

Shiqi Xu ^a*, Wei Jiang ^a, Yi Chen ^a, Ali Asghar Heidari ^b, Lei Liu ^c, Huiling Chen ^a*, Guoxi Liang ^d*

^a Institute of Big data and Information Technology, Wenzhou University, Wenzhou 325000, China

^b School of Surveying and Geospatial Engineering, College of Engineering, University of Tehran, Tehran, Iran

^c College of Computer Science, Sichuan University, Chengdu, Sichuan 610065, China

^d Department of Artificial Intelligence, Wenzhou Polytechnic, Wenzhou 325035, China

ARTICLE INFO

Keywords:

Metaheuristic algorithms

BSA

Random reselection strategy

Enhanced quality mechanisms

Image segmentation

Breast cancer

ABSTRACT

Breast cancer has become one of the most common cancers among women globally. Early diagnosis and intervention play a crucial role in breast cancer management. Automatic segmentation of histological images of breast cancer utilizing Multi-Threshold Image Segmentation (MTIS) technology can assist doctors in making more accurate diagnostic decisions for patients. However, traditional methods face challenges in terms of segmentation efficiency and accuracy. This paper proposes a Renyi entropy-based MTIS to address this issue using an improved backtracking search algorithm (REBSA). The proposed method enhances the original BSA by introducing a random reselection strategy to enhance diversity of the population and enhance the algorithm's exploration capability. Additionally, an enhanced quality mechanism is incorporated, which improves the quality of candidate solutions while maintaining a degree of randomness. The integration of these two approaches significantly enhances the performance of the BSA. In order to confirm the performance of the proposed REBSA, several tests were carried out using the CEC 2017 benchmark functions, including diversity balance analysis, parameter sensitivity analysis, and stability analysis. Additionally, REBSA was compared with various basic and advanced algorithms. The results demonstrate that REBSA achieved the top rank on most functions across different dimensions, proving its exceptional optimization performance and robustness. Finally, the proposed REBSA was applied to MTIS tasks on breast cancer histopathological images. The results verified that REBSA achieved higher segmentation accuracy and efficiency. Compared to other approaches, it can retain more pathological tissue details and rank higher than other methods in several image evaluation metrics, demonstrating its ability to handle the difficult problem of breast cancer tissue image segmentation. Moreover, this study utilized a real clinical dataset of breast cancer histopathological images, further demonstrating the suggested method's efficacy in practical diagnostic scenarios. It provides reliable technical support for medical image analysis, assisting doctors in improving diagnostic accuracy and early screening efficiency.

1. Introduction

Breast cancer has become one of the most common cancers among women worldwide, with its incidence and mortality rates leading among various cancers [1]. According to the World Health Organization (WHO), breast cancer causes hundreds of thousands of deaths each year, and the number of cases continues to rise [2]. Early diagnosis and treatment have an important part in the management of breast

cancer [3]. Early detection and treatment of breast cancer can significantly increase the survival rate of patients and even achieve complete recovery. However, the detection and diagnostic processes for breast cancer faces considerable challenges [4]. The morphology of its lesions is extremely complex and diverse, making image interpretation difficult and rendering it hard for medical personnel to make accurate diagnoses based on experience alone. Individual differences in breast density and lesion characteristics among patients complicate the diagnosis.

* Corresponding authors.

E-mail addresses: sergixu977@gmail.com (S. Xu), swxxjw@aliyun.com (W. Jiang), kenyoncy2016@gmail.com (Y. Chen), as_heidari@ut.ac.ir (A.A. Heidari), liulei.cx@gmail.com (L. Liu), chenhuiling.jlu@gmail.com (H. Chen), guoxiliang2017@gmail.com (G. Liang).

Therefore, developing advanced technologies capable of accurately identifying and segmenting breast cancer lesion areas is crucial for enhancing the precision and effectiveness of early detection of breast cancer [5].

Over the past few years, computational intelligence has become an essential instrument in disease diagnosis, significantly improving the precision and effectiveness of medical decision-making [6]. The diagnosis of breast cancer has advanced significantly in recent years, with various advanced technologies offering promising methods for early detection and accurate identification of the disease [7]. In this regard, with the continuous advancement of artificial intelligence and image processing technology, Medical Image Segmentation (MIS) has become a key tool in the early detection and treatment of breast cancer. Recent developments in image segmentation techniques offer promising insights for improving segmentation performance across various medical imaging tasks [8]. MIS technology includes graph theory-based segmentation [9], active contour model-based segmentation [10], edge-based segmentation [11], region-based segmentation [12], deep learning-based segmentation [13], and threshold-based segmentation [14], etc. Among these, threshold-based image segmentation is one of the simplest and most widely applied techniques. This method relies on the grayscale characteristics of the image, setting one or more thresholds to segment the image into different regions, thereby separating tumors from normal tissue. Despite its simplicity, selecting the proper thresholds has an enormous effect on the segmentation outcomes and is crucial for accuracy. Researchers have developed various algorithms and techniques to automatically or semiautomatically select the optimal thresholds to address this issue.

Among the many techniques, Metaheuristic Algorithms (MAs) have gradually become important tools in MIS due to their efficiency and robustness in solving complex optimization problems [15]. Instead of methodically looking for solutions one step at a time, these algorithms are largely motivated by biological behaviors or natural events, learning from search experiences to choose efficient solutions. Consequently, MAs are more adaptable and effective at solving a range of practical optimization issues. By simulating behaviors or evolutionary processes in nature, MAs can automatically find optimal thresholds, thereby enhancing the accuracy and stability of image segmentation. Compared to traditional methods, MAs escape local optimal (LO) to find global optimal solutions and are insensitive to initial conditions and parameter settings. This adaptability enables them to handle complex, high-dimensional image data effectively. The application of MAs in Multi-Threshold Image Segmentation (MTIS) not only enhances segmentation accuracy but also reduces human intervention and increases the degree of automation. This provides more reliable technical support for clinical diagnosis.

In general, MAs can be divided into four primary types. The first is for algorithms that are based on evolution. The principle of biological evolution serves as the foundation for optimization algorithms known as evolutionary algorithms. By imitating processes like crossover, mutation, and natural selection, they explore the solution space. The primary forces behind evolutionary algorithms are individual competition and reproduction. Individuals with higher fitness are more likely to be chosen as a result of continuing iteration and optimization, which leads the population as a whole to superior solutions. Genetic Algorithm (GA) [16], Differential Evolution (DE) [17], and Evolutionary Strategy (ES) [18] are examples of classical evolutionary algorithms.

The second category is bio-inspired algorithms. These algorithms, which have been used to solve a variety of optimization, search, and decision-making problems, are motivated by the collective behaviors seen in nature and offer an innovative viewpoint and method for handling challenging issues. Individual collaboration and information exchange are essential to swarm intelligence algorithms. The group as a whole can more successfully search the feasibility domain and progressively get closer to the ideal solution through interactions and information sharing among members. In the last few years, swarm

intelligence algorithms have gained widespread attention, leading to the emergence of many innovative algorithms, such as Ant Colony Optimization (ACO) [19], Artificial Fish Search (AFS) [20], Particle Swarm Optimization (PSO) [21], Firefly Algorithm (FA) [22], Bacterial Foraging Optimization (BFO) [23], Bat Algorithm (BA) [24], Whale Optimization Algorithm (WOA) [25], Salp Swarm Algorithm (SSA) [26], Moth-Flame Optimization (MFO) [27], Cuckoo Search (CS) [28], Artificial Bee Colony algorithm (ABC) [29], Harris Hawks Optimization (HHO) [30], Grey Wolf Optimizer (GWO) [31], Slime Mould Algorithm (SMA) [32], and Hunger Games Search (HGS) [33], among others.

The third type is math-based algorithms, which are optimization methods that guide the search process through mathematical models and rules. These algorithms typically rely on mathematical principles, equations, or statistical methods to effectively explore the solution space and find optimal or near-optimal solutions. These algorithms include the RUNge Kutta optimizer (RUN) [34] and the Sine Cosine Algorithm (SCA) [35], etc.

The fourth category is those inspired by nature. These algorithms are primarily gathered from the simulation of physical and chemical laws observed in nature. By mimicking the movement of objects or particles, these algorithms change the search agents' locations and use the stability of the environment as an indicator of the optimization state, effectively exploring and optimizing complex solution spaces. Common nature-inspired algorithms include the RIME optimization algorithm (RIME) [36], Biogeography-Based Optimization (BBO) [37], Simulated Annealing (SA) [38], and the Gravitational Search Algorithm (GSA) [39], etc.

Even so, the MAs still have some common drawbacks. For instance, in complicated or high-dimensional domains, they could converge too soon to poor solutions. They often struggle to effectively explore the search space, leading to a lack of diversity among solutions and missing the global optimum. Additionally, these algorithms tend to have slow convergence speeds, requiring many iterations to reach satisfactory solutions. These shortcomings can cause improved MAs to suffer from slow convergence or get trapped in LO when attempting to search the ideal thresholds.

An enhanced BSA method is suggested in this study to address these issues, called REBSA. BSA [40] is a classic population-based optimization method first introduced in 2013, known for its simple, efficient, and fast structure. The proposed REBSA incorporates enhanced quality method and random reselection strategy into the BSA. The CS algorithm inspires the random reselection strategy [28]. In the CS, the idea of cuckoos randomly reselecting parasitic nests with a certain probability of being discovered provides a mechanism for escaping LO, thereby improving the exploratory capabilities of the algorithm. The quality of candidate solutions can be improved, and the likelihood of an individual approaching the best solution can be increased, by implementing the enhanced quality method at the end of the optimization process. It is worth pointing out that enhanced quality method keeps some unpredictability while boosting the quality of candidate solutions. To validate the performance of REBSA, we carried out a variety of comparative experiments on CEC 2017, including balance and diversity analysis, stability analysis, and parameter sensitivity analysis. Additionally, we compared REBSA with several original and advanced methods on CEC 2017. The results demonstrate that REBSA exhibits good global optimization capability and robustness, making it an excellent algorithm.

Finally, this study proposes an MTIS method based on REBSA for segmenting breast cancer images. This approach uses a Non-local Means (NM) 2D histogram to represent image information and Renyi entropy as the objective function to choose the best thresholds. In order to validate the excellent performance of REBSA in the MTIS method, we compared it with several competitive algorithms at different thresholds (15, 20, 25, 30). The segmentation experimental results show that the REBSA-based MTIS method generates segmented images of superior quality and demonstrates greater robustness and stability across different thresholds than other methods.

The following are this paper's primary contributions:

- An enhanced BSA (REBSA) is suggested to address the shortcomings of the BSA algorithm in balancing exploration and exploitation. Extensive experiments show that REBSA has better performance than other advanced methods.
- To increase the algorithm's capacity to avoid local optimal, a random reselection strategy is introduced, which effectively improves population diversity
- A quality enhancement strategy is introduced to enhance the candidate solutions' quality while retaining a certain degree of randomness.
- A Renyi entropy MTIS model based on REBSA is proposed for the segmentation task of breast cancer histopathology images. This model not only achieves better segmentation quality than other comparison methods on the public Databiox dataset, but also verifies the efficiency of this approach on actual clinical data in the breast cancer medical image dataset from the First Affiliated Hospital of Wenzhou Medical University, China, and can effectively solve practical problems in MIS.

The following is how this paper is organized. Image segmentation related work is reviewed in Section 2. Section 3 provides background on MTIS. Section 4 details the proposed REBSA method. Section 5 shows comparative experiments and analyzes the results to demonstrate the superior performance of REBSA. Section 6 applies REBSA to breast cancer image segmentation, showcasing its practical effectiveness. Section 7 discusses and analyzes all experimental findings. Finally, in Section 8, the work and results of this paper are summarized and the direction of future research is pointed out.

2. Related work

In the diagnosis of breast cancer, Image Segmentation (IS) [41] technology plays an indispensable role. It can precisely separate tumor regions from medical images, providing crucial information for subsequent diagnosis. Particularly in the early stages, high-precision IS can significantly improve the accuracy of breast cancer detection, thereby guiding clinical treatment decisions and positively impacting patient outcomes.

Simply put, IS is the process of subdividing a digital image into multiple subsets, aiming to simplify or alter how an image is represented to make it easier to analyze. This technology focuses in particular on extracting clinically significant structures, such as tumors, organs, or other pathological areas, in MIS. In recent years, new IS techniques have continuously emerged, providing more efficient and accurate solutions for MIS of breast cancer [42]. Zhou et al. [43] introduced a multi-task learning framework that includes a multi-scale network for classification and an encoder-decoder network for segmentation. An iterative training strategy is used to refine the feature map. It is applied to tumor segmentation and classification in 3D automated breast ultrasound images, and the performance of these two tasks is improved through joint training. Saber et al. [44] introduced a deep learning model based on transfer learning to automatically detect and classify breast cancer by extracting features from the MIAS dataset using a pre-trained CNN architecture. Shen et al. [45] introduced a novel deep learning model GMIC, which uses weakly supervised localization technology. It first extracts global context information and generates a rough localization map through a global module, then determines which regions of the image are the most informative, and finally extracts fine-grained visual data from these regions using a local module. At last, it aggregates global and local information for prediction through a fusion module, aiming to solve the classification problem of high-resolution breast cancer screening images.

IS, as an important branch of computer vision [46], also plays a key role in other medical image processing. For example, Liu et al. [47] developed a novel optimization model called CLMorph, which integrates a contrastive registration architecture built with Convolutional Neural Networks (CNNs) to achieve unsupervised MIS. The study results

indicate that CLMorph effectively conquers the drawbacks of current unsupervised approaches and significantly surpasses the most advanced unsupervised segmentation methods currently in use on two key medical image datasets. Li et al. [48] proposed a quality control method for identifying failed cardiac IS and measuring their quality. Using a self-reflective reference generator, they created informative references and evaluated image-level and pixel-level quality with a difference investigator. He et al. [49] introduced a prototype segmentation method for computing binary segmentation maps based on deep features. The segmentation capability is measured by calculating the Dice coefficient between the feature segmentation map and the ground truth, referred to as the Segmentation Ability (SA) score. This method quantifies the segmentation capability of deep features across different layers and units, aiding in understanding the segmentation performance of deep neural networks. Gallochet et al. [50] proposed an active learning approach that improves the selection strategy of uncertainty-based MIS algorithms through stochastic batches. This method, which calculates uncertainty at the batch level rather than the sample level, is simple and effective, and can be used with any uncertainty-based metric. Experiments demonstrate that this strategy consistently improves the performance of traditional uncertainty-based sampling methods on two MIS datasets.

However, deep learning models typically require large datasets for effective training [51,52]. Acquiring sufficiently large and diverse datasets will be challenging, especially in specialized medical areas where annotated data is scarce or expensive to be utilized [53]. In the field of MIS, obtaining sufficiently large and accurately annotated datasets is particularly challenging. Medical images often involve patient privacy, leading to strict data access restrictions, and the manual annotation process is both time-consuming and costly. Therefore, deep learning methods may not reach their full potential in such scenarios, whereas MTIS methods demonstrate significant advantages.

The “No Free Lunch” (NFL) [54] theory argues that no one algorithm can be the best at all challenges since every method has benefits and drawbacks depending on the problem area and situations. In response, a few academics have enhanced and optimized algorithms for MTIS. For instance, Zhu et al. [55] proposed an inner-based multi-strategy PSO for MTIS of COVID-19 medical images. The algorithm combines dynamic oscillation weights and an internal selection learning mechanism to enhance global optimization capabilities and avoid LO. A shuffling frog-leaping method based on horizontal and vertical crossover search (HVSFLA) was presented by Chen et al. [56] as an integrated multi-strategy driven algorithm for MTIS. The method balances exploitation and exploration through horizontal and vertical crossover searches, improving segmentation performance. Experimental results demonstrate that HVSFLA performs excellently on the CEC 2017 [57] benchmark and the Berkeley Segmentation Dataset 500 and shows potential in MIS of breast invasive ductal carcinoma. The weighted hierarchical recursive guided RIME method (WHRIME), developed by Xing et al. [58], improves the effectiveness and precision of breast cancer histopathology MIS through a hierarchical guided strategy and elite individual-guided updates of non-elite individuals. Chen et al. [59] introduced an AGDE algorithm to increase precision and effectiveness of MIS. The AGDE algorithm combines chaotic game optimization and correlation strategies to enhance population diversity and global search capabilities. Experiments on thyroid papillary carcinoma IS demonstrate that AGDE outperforms existing technologies across multiple evaluation metrics, showing significant clinical application potential. Shi et al. [60] proposed a SMA method integrating multiple strategies (RWGSMA). The study evaluates RWGSMA on 30 test sets from CEC 2017 and demonstrates its segmentation performance on various typical images, proving its effectiveness in segmenting lupus nephritis images. Yang et al. [61] proposed an MTIS method based on the EACOR algorithm to improve the segmentation quality of malignant melanoma pathological images. By introducing soft encirclement

and pursuit strategies, the EACOR algorithm optimizes search performance in continuous domains, enhances global search capability, and avoids LO. According to experimental findings, EACOR excels in MTIS tasks and the CEC 2014 benchmark functions, effectively providing high-quality melanoma pathological image samples for subsequent analysis.

3. Background

3.1. MTIS

MTIS is a method that splits an image into multiple non-overlapping regions, each corresponding to a specific grayscale range. Traditional single-threshold methods can only distinguish between the foreground and background, whereas multi-threshold methods can better separate the detailed structures within an image, which is particularly significant in medical image processing and tumor recognition. However, selecting the appropriate combination of thresholds is a challenging optimization problem that directly affects the quality of the segmentation. To overcome this issue, various optimization algorithms have been introduced. Among them, MAs have shown excellent performance, effectively finding the global optimal combination of thresholds.

Histogram-based segmentation techniques are commonly used in various MTIS methods. However, one-dimensional histograms fail to capture the spatial relationships between pixels, making them susceptible to noise and leading to lower segmentation accuracy. The segmentation errors can be severe if the goal region only takes up a small portion of the image. In 1989, Abutaleb [62] proposed an IS method based on a 2D histogram, which blends the local mean pixel values with the original grayscale histogram. This approach better reflects the image's spatial features and improves segmentation accuracy. However, this method has high computational complexity and demands significant computational resources. Additionally, Abutaleb's method for generating the 2D histogram ignores features at specific borders and points of the image. To deal with these problems, a 2D histogram based on NM is suggested, and the 2D Renyi entropy is used as the fitness function for the enhanced method.

The flowchart of the Renyi entropy-based MTIS method using REBSA is displayed in Fig. 1. First, a grayscale image is created from the image that is provided. Based on the grayscale image, a NM filtering operation is performed and a 2D histogram is created by combining the grayscale and NM-filtered images. Then, REBSA is utilized as the search algorithm with Renyi entropy as the objective function to search for the optimal threshold combination. Finally, this threshold combination is used to obtain the segmented and color-mapped image.

3.2. NM 2D histogram

The NM filtering method suggested by Buades [63] is an effective technique for noise removal. This denoising technique maximizes the preservation of image detail and fully utilizes the redundant information within the image. The core concept is to estimate the current pixel by calculating a weighted average of neighboring pixels with similar structures. The calculation of NM is as follows, assuming that pixels e and f in the image I have grayscale values $g(e)$ and $g(f)$, we have:

$$NM(e) = \sum_{f \in I} w(e, f)g(f) \quad (1)$$

where $NM(e)$ is the grayscale value of pixel e after denoising with NM, and $w(e, f)$ is the weight corresponding to pixels e and f , calculated as shown in Eq. (2).

$$w(e, f) = \frac{1}{U} \exp \frac{-\|v(e) - v(f)\|^2}{h^2} \quad (2)$$

$$U = \sum_{f \in I} \exp \frac{-\|v(e) - v(f)\|^2}{h^2} \quad (3)$$

$$v(e) = \frac{1}{n \times n} \sum_{p \in B(e)} g(p) \quad (4)$$

$$v(f) = \frac{1}{n \times n} \sum_{q \in B(f)} g(q) \quad (5)$$

here, U represents the normalization factor, h is the control parameter, $v(e)$ and $v(f)$ are the local means, $B(e)$ refers to the $n \times n$ pixel block surrounding pixel e , and $B(f)$ is defined similarly.

The NM image and the grayscale image are used to create the NM 2D histogram. If the grayscale image I_g of image I has a size of $m \times n$, then the NM image G obtained through NM filtering also has a size of $m \times n$. In the 2D histogram, the point (t, s) is derived from the grayscale values of pixel (e, f) in the grayscale image I_g and the grayscale values of pixel (e, f) in the NM image G . Here, $T(t, s)$ represents the occurrence count of point (t, s) , and its joint probability density is given by Eq. (6). The final 2D histogram is obtained after normalization using the formula.

$$p(t, s) = \frac{T(t, s)}{m \times n} \quad (6)$$

3.3. Renyi entropy for 2D histogram

Renyi entropy [64] is a generalized version of Shannon entropy, incorporating a positive parameter α which allows it to better adapt to various types of images in IS compared to Shannon entropy [65]. Here, let the grayscale levels of the grayscale image I_g and the NM image G be $L - 1$. The grayscale level s of the pixels and the NM grayscale level t form a binary tuple of $L - 1$ pairs $(s_1, t_1), (s_2, t_2), \dots, (s_{L-1}, t_{L-1})$. The expression for Renyi entropy $\delta^\alpha(t, s)$ is given in Eq. (7)–(8). By maximizing the total Renyi entropy using Eq. (9), the optimal thresholds can be found. Finally, by setting the binary tuples $(s_1, t_1), (s_2, t_2), \dots, (s_{L-1}, t_{L-1})$ to maximize the total Renyi entropy, the ideal segmentation thresholds s_1, s_2, \dots, s_{L-1} can be determined.

$$\delta^\alpha(t, s) = H_1^\alpha + H_2^\alpha + \dots + H_k^\alpha \quad (7)$$

$$\left\{ \begin{array}{l} H_1^\alpha = \frac{1}{1-\alpha} \ln \sum_{i=0}^{s_1} \sum_{j=0}^{t_1} \left(\frac{p(i, j)}{P_1(s_1, t_1)} \right)^\alpha, \quad P_1(s_1, t_1) = \sum_{i=0}^{s_1} \sum_{j=0}^{t_1} p(i, j) \\ H_2^\alpha = \frac{1}{1-\alpha} \ln \sum_{i=s_1+1}^{s_2} \sum_{j=t_1+1}^{t_2} \left(\frac{p(i, j)}{P_2(s_2, t_2)} \right)^\alpha, \quad P_2(s_2, t_2) = \sum_{i=s_1+1}^{s_2} \sum_{j=t_1+1}^{t_2} p(i, j) \\ \vdots \\ H_{L-1}^\alpha = \frac{1}{1-\alpha} \ln \sum_{i=s_{L-2}+1}^{s_{L-1}} \sum_{j=t_{L-2}+1}^{t_{L-1}} \left(\frac{p(i, j)}{P_{L-1}(s_{L-1}, t_{L-1})} \right)^\alpha, \\ P_{L-1}(s_{L-1}, t_{L-1}) = \sum_{i=s_{L-2}+1, j=t_{L-2}+1}^{s_{L-1}} \sum_{i=t_{L-2}+1}^{t_{L-1}} p(i, j) \end{array} \right. \quad (8)$$

$$fit_{Renyi} = Max(\delta^\alpha(t, s)) \quad (9)$$

4. Proposed REBSA algorithm

4.1. Overview of BSA

BSA is a novel population-based heuristic algorithm that, like most MAs, aims to find the optimal solution through population mutation, crossover, and selection. One distinguishing feature of BSA is its memory population, which gives it a strong capability to exploit historical information. The reproduction operators of BSA, namely mutation and crossover operators, are characteristic features of the algorithm, setting it apart from other evolutionary algorithms. The BSA algorithm consists of five steps: population initialization, selection I, mutation, crossover, and selection II.

Initialization: Initially, each population X in the search area is generated randomly according to Eq. (10).

$$X_{i,j} = LB_j + rand \times (UB_j - LB_j) \quad (10)$$

where $i = 1, 2, 3, \dots, N$, N represents the population size, and $j = 1, 2, 3, \dots, D$ denotes the variable dimension. LB_j and UB_j stand for

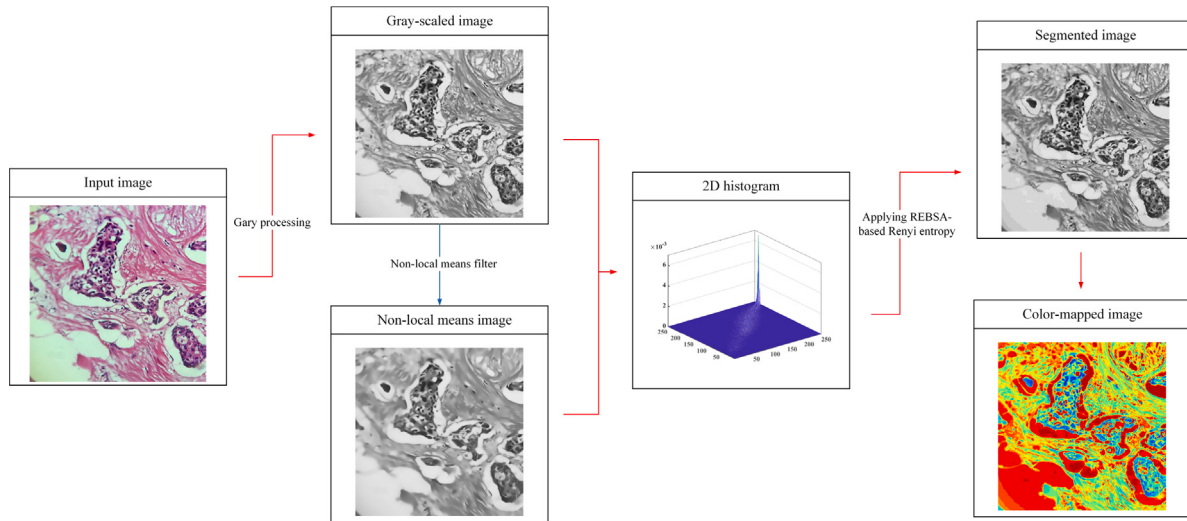


Fig. 1. The flow chart of MTIS method based REBSA.

the lower and upper boundaries, respectively. The term $rand$ is used to generate a random number in the range $[0,1]$.

Selection I: In this phase, the initial historical population $oldX$ used for calculating the search direction is first determined using Eq. (11). At the beginning of each iteration, $oldX$ is redefined through Eq. (12).

$$oldX_{i,j} = LB_j + rand \times (UB_j - LB_j) \quad (11)$$

$$oldX = \begin{cases} X, & a(b|a,b-U(0,1) \\ oldX, & \text{otherwise} \end{cases} \quad (12)$$

It can be seen that BSA has a memory feature, enabling it to designate the previous generation's population, chosen randomly, as the historical population and remember it until it is changed. After determining $oldX$, the order of individuals in $oldX$ is randomly altered using Eq. (13).

$$oldX := \text{permuting}(oldX) \quad (13)$$

where, $:=$ denotes the update operation, and permuting represents the random shuffling function.

Mutation: During the mutation procedure, the initial form of the mutant for the trial individual is generated as shown in Eq. (14).

$$\text{Mutation} := X + F \times (oldX - X) \quad (14)$$

here, the search direction matrix $(oldX - X)$ is controlled by F , where $F = 3 \times rndn$, and $rndn \sim N(0, 1)$, with N representing the standard normal distribution.

Crossover: The final form of the population T is generated through the crossover. BSA's crossover process consists of two steps. First, a binary integer-valued matrix of size $N \times D$ is computed. The final form of the population is determined by Eq. (15). The map is defined by Eqs. (16)–(17). Here, $randi$ is a random integer between $[1, D]$.

$$T_{i,j} = \begin{cases} \text{Mutation}_{i,j}, & \text{if } map_{i,j} = 1 \\ X_{i,j}, & \text{if } map_{i,j} = 0 \end{cases} \quad (15)$$

$$map_{i,u(1:\lceil M \times rand \times D \rceil)} = 0 | u = \text{permutating}(\langle 1, 2, 3, \dots, D \rangle) \quad (16)$$

$$map_{i,randi(D)} = 1 \quad (17)$$

Selection II: The selection step aims to choose the population with better fitness, as shown in Eq. (18). If the fitness value of a new individual is better than the currently obtained global minimum, it is

updated to X_{best} , and the corresponding optimal fitness value is also updated.

$$X_{i,j} = \begin{cases} T_{i,j}, & \text{if } f(T_{i,j}) < f(X_{i,j}) \\ X_{i,j}, & \text{otherwise} \end{cases} \quad (18)$$

The BSA algorithm demonstrates unique advantages in solving global optimization problems. The algorithm effectively accelerates convergence speed and improves solution quality by integrating principles of randomness and determinism in key stages such as population initialization, selection I, mutation, crossover, and selection II. However, when dealing with high-dimensional or specific optimization problems, the BSA algorithm's exploration and exploitation capabilities still have room for improvement. Sometimes, it may struggle to balance diversity and solution quality effectively. Therefore, this study suggests an enhanced BSA algorithm to address these issues.

4.2. Random reselection strategy

Since the original BSA has the defect of easily falling into LO in the process of searching for solutions, to improve the algorithm's performance in global searches, a more efficient mechanism must be implemented.

Random Reselection (RR) simulates the behavior of a cuckoo in searching for the best nesting site. This method uses the Levy Flight mechanism to provide new solutions to explore the search space more efficiently, while reselecting nests with a certain probability to expand the search range. Here, the nest represents a candidate solution, and the cuckoo egg corresponds to a randomly generated new solution. The Levy flying mechanism is used to find new solutions, as shown in Eq. (19).

$$X_{i,j}(\text{new}) = X_{current} + \alpha \times (X_{current} - X_{best}) \times \frac{u}{|v|^{\frac{1}{\beta}}} \quad (19)$$

the position of the individual in the j -dimension of the i th candidate solution is denoted by $X_{i,j}$. The flight's step size is α . Additionally, X_{best} represents the optimal solution. From Eq. (20) to Eq. (23), u and v are computed.

$$u \sim N(0, \sigma_u^2) \quad (20)$$

$$v \sim N(0, \sigma_v^2) \quad (21)$$

$$\sigma_u = \left[\frac{\sin\left(\frac{\beta\pi}{2}\right) \times \Gamma(1+\beta)}{2^{\frac{\beta-1}{2}} \times \beta \times \Gamma\left(\frac{1+\beta}{2}\right)} \right]^{\frac{1}{\beta}} \quad (22)$$

$$\sigma_v = 1 \quad (23)$$

where β represents the Levy exponent; $\Gamma(\cdot)$ stands for the *Gamma* function.

$$X_{i,j}(\text{new}) = \begin{cases} \left\{ \begin{array}{ll} X_{\text{current}} + \text{rand} \times (X_{m_1} - X_{m_2}) & \text{if } K > P_a \\ X_{\text{current}} & \text{else} \end{array} \right. & (24) \end{cases}$$

The regeneration process, as shown in Eq. (1), uses a random method to find a new solution with probability P_a . In this case, individuals m_1 and m_2 are chosen at random. K is uniformly distributed random number in the range 0 to 1.

When specific requirements are achieved (such as the maximum number of iterations, number of evaluations, or time limit), the algorithm randomly provides a new candidate solution to substitute the current solution and continues the search. This random reselection behavior can significantly expand the search space coverage, effectively avoid LO traps, and enhance the algorithm's capacity for global exploration. In addition, the RR can also enhance the flexibility of the algorithm while maintaining solution diversity, making the algorithm more robust in complex optimization problems.

4.3. Enhancing the quality of solutions

In order to further improve the method's exploitation capabilities and balance the performance of the method in all aspects, we introduced the Enhanced Quality (EQ) mechanism. The EQ aims to raise the quality of individuals and strengthen the algorithm's capacity for both local and global search by dynamically adjusting the generation method of candidate solutions to meet the optimization needs of different stages. When $\text{rand} < 0.5$, the EQ strategy is executed. Specifically, the operation process of EQ is described below:

$$\begin{cases} X_{\text{new2}} = X_{\text{new1}} + r_1 \times \omega \times |(X_{\text{new1}} - X_{\text{avg}}) + \text{randn}| & \omega < 1 \\ X_{\text{new2}} = (X_{\text{new1}} - X_{\text{avg}}) + r_1 \times \omega \times |(\mu \times X_{\text{new1}} - X_{\text{avg}}) + \text{randn}| & \omega \geq 1 \end{cases} \quad (25)$$

$$X_{\text{new1}} = r_2 \times X_{\text{avg}} + (1 - \beta) \times X_{\text{best}} \quad (26)$$

$$X_{\text{avg}} = \frac{X_1 + X_2 + X_3}{3} \quad (27)$$

$$w = \text{rand}(0, 2) \times \exp\left(-c \left(\frac{F_{\text{Es}}}{\text{Max}F_{\text{Es}}}\right)\right) \quad (28)$$

where r_1 is an integer between $[-1, 1]$. The calculation of X_{new1} is shown in Eq. (26). X_{avg} is the average value of three random individuals (X_1, X_2, X_3). r_2 is randomly obtained on $[0, 1]$. The calculation of w is shown in Eq. (28), where as the number of evaluations rises, its value reduces. That is, when $\omega \geq 1$ in the beginning phases, the strategy performs a global search; when $\omega < 1$ in the later stages, the method tends to focus more on local search. c is randomly selected from the range $[0, 5]$. F_{Es} and $\text{Max}F_{\text{Es}}$ represent the current and maximum number of evaluations, respectively. μ is used to increase population diversity.

When $F(X_{\text{new2}}) > F(X)$, i.e., the fitness obtained by X_{new2} is not better than the current solution, and $\text{rand} < w$ is also satisfied, a new solution X_{new3} will be created. The calculation of X_{new3} is shown in Eq. (29).

$$X_{\text{new3}} = (X_{\text{new2}} - \text{rand} \times X_{\text{new2}}) + SF \times (\text{rand} \times X_{\text{RK}} + (v \times X_{\text{best}} - X_{\text{new2}})) \quad (29)$$

$$SF = 2 \times (0.5 - \text{rand}) \times f \quad (30)$$

$$f = a \times \exp\left(-b \times \text{rand} \times \left(\frac{F_{\text{Es}}}{\text{Max}F_{\text{Es}}}\right)\right) \quad (31)$$

$$X_{\text{RK}} = k_1 + 2 \times k_2 + 2 \times k_3 + k_4 \quad (32)$$

among them, v takes a random value between 0 and 2, utilized to emphasize how important the ideal solution is. SF acts as an adaptive factor. In the early phases, a larger value of SF is assigned to promote diversity and boost exploratory search, after which its value is gradually reduced as the iterations increase to improve the exploitation search capability. a and b are set to 20 and 12 respectively in this paper. X_{RK} is created using Runge Kutta, where k_1, k_2, k_3, k_4 are represented by Eqs. (33)–(36).

$$k_1 = \frac{1}{2\Delta x} (\text{rand} \times X_w - u \times X_b) \quad (33)$$

$$k_2 = \frac{1}{2\Delta x} (\text{rand} \times (X_w + \text{rand}_1 \times k_1 \times \Delta x) - (u \times X_b + \text{rand}_2 \times k_1 \times \Delta x)) \quad (34)$$

$$\begin{aligned} k_3 = \frac{1}{2\Delta x} & \left(\text{rand} \times \left(X_w + \text{rand}_1 \times \left(\frac{k_2}{2} \right) \times \Delta x \right) \right. \\ & \left. - \left(u \times X_b + \text{rand}_2 \times \left(\frac{k_2}{2} \right) \times \Delta x \right) \right) \end{aligned} \quad (35)$$

$$k_4 = \frac{1}{2\Delta x} (\text{rand} \times (X_w + \text{rand}_1 \times k_3 \times \Delta x) - (u \times X_b + \text{rand}_2 \times k_3 \times \Delta x)) \quad (36)$$

where, $\text{rand}_1, \text{rand}_2, \text{rand}_3$ are all random numbers between 0 and 1. X_b and X_w represent the best solution and the worst solution, respectively. u refers to the significance of X_b , as shown in Eq. (37). Δx denotes the position increment, calculated by Eq. (38).

$$u = 2 \times (1 - \text{rand}) \quad (37)$$

$$\Delta x = 2 \times \text{rand} \times |\text{rand} \times ((X^* - \text{rand} \times X_{\text{avg}}) + \gamma)| \quad (38)$$

$$\gamma = \text{rand} \times \left(X_i - \text{rand} \times \left(u - (UB - LB) \times \exp\left(-4 \times \frac{F_{\text{Es}}}{\text{Max}F_{\text{Es}}}\right)\right) \right) \quad (39)$$

where, γ is the scaling factor, which shows an exponentially decreasing trend. The calculation of γ is given by Eq. (39).

As shown in Fig. 2, the optimization process of EQ involves three possible paths. First, X_{n+1} is generated using the RK search. In the first and second optimization paths, a new position X_{new2} is first generated. If $F(X_{n+1}) < F(X_{\text{new2}})$, a new position X_{new3} is generated. If $F(X_{\text{new3}}) > F(X_{n+1})$, X_{n+1} is retained (the first optimization path), otherwise, X_{new3} is replaced as a better solution (the second optimization path). If $F(X_{\text{new2}}) < F(X_{n+1})$, X_{new2} is retained as the better solution (the third optimization path).

4.4. Modified BSA (REBSA)

Because no single method is optimal for every situation, [54], even though BSA improves search efficiency by introducing a memory mechanism that learns from previous search experiences, issues such as early convergence, slow convergence, and the inability to find the global optimum remain. Seeking strategies that can improve solution variety and exploitation capacity is therefore essential.

In summary, this paper proposes an improved BSA algorithm that incorporates two effective strategies to improve the basic BSA's efficiency. These two methods are the RR and the EQ. On the one hand, the RR strategy can improve population diversity and make it easier for the algorithm to find the best individual. On the other hand, the introduction of the EQ strategy can effectively improve the quality of solutions, improve the development capability of the method, prevent it from getting stuck in LO, and increase convergence precision. Furthermore, the proposed REBSA employs an active greedy selection mechanism. Unlike the selection mechanism of traditional MAs, the algorithm does not fully adopt newly generated solutions but uses a greedy selection mechanism to compare the newly generated solutions with the original ones. If the new individual's function value is better, it is chosen as a replacement. Since newly generated populations will inevitably produce worse individuals than the previous generation, which is not

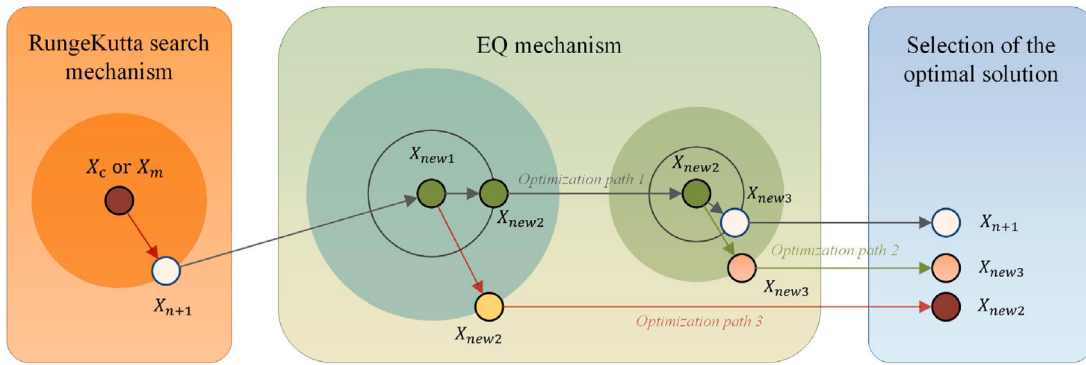


Fig. 2. EQ Strategy Schematic.

conducive to converging to better solutions, this active population replacement method ensures that the population continuously retains superior individuals. This effectively enhances the search efficiency and quality of the global optimum, resolving the defects of the classic BSA.

REBSA mainly includes the following steps:

Step 1: Randomly generate an initial population position X within the search space.

Step 2: Compute the fitness values of the population and retain the best fitness and the best agent, and create the initial historical population $oldX$.

Step 3: Use the original BSA update method to perform selection, mutation, and crossover operations on the population, as shown in Eqs. (12)–(18).

Step 4: If $rand < 0.5$, introduce the EQ method to enhance the quality of candidate solutions. First, create another solution based on Eq. (25). If the fitness value of the newly generated solution is greater than the old fitness value, generate another new solution and then make a judgment, as shown in Eq. (29).

Step 5: Use the RR method to randomly reselect new solutions, giving the individual a chance to get away from LO, as shown in Eq. (24).

Step 6: Use a greedy selection mechanism to compare the recently produced solution with the old candidate solution. If it is better than the original solution, substitute it and simultaneously update the optimal candidate solution and the smallest fitness value.

Step 7: Check whether the stopping criterion for iterative search is met. If satisfied, output the solution; if not satisfied, jump to **Step 3**.

According to the description above, Fig. 3 displays the detailed REBSA flowchart, and Algorithm 1 displays the pseudocode execution procedure.

4.5. Analysis of computational complexity

The computational complexity of the REBSA algorithm is mainly influenced by factors such as the maximum evaluation count, population size, and dimension size. First, let the population size be N and the dimension of each individual be dim . During algorithm execution, let T be the number of iterations obtained through the maximum evaluation count $MaxFEs$, assuming the algorithm evaluates M times per iteration. Thus, T can be expressed as $MaxFEs/M$. Then, we have: $O(BSA) = O(N \times dim + T \times N \times dim)$, $O(RR) = O(T \times N \times dim)$, $O(EQ) = O(T \times N \times dim)$. Consequently, the overall complexity of the REBSA is: $O(REBSA) = O(T \times N \times dim)$.

5. Results and analysis of benchmark test functions experiment

A series of experiments were conducted in this chapter to assess the optimization effectiveness of the proposed REBSA. First, a balance and diversity analysis of REBSA was performed to measure its

Algorithm 1 The Pseudo-code for REBSA

Input: UB , LB , FEs , $MaxFEs$, N , D

Output: The best solution X_{best}

```

1: Initialize the population  $X$ ;
2: Initialize the historical population information  $oldX$ ;
3: Calculate the fitness values for every individuals and select the best
   agent  $X_{best}$ ;
4: while  $FEs < MaxFEs$  do
5:   for  $i = 1$  to  $N$  do
6:     Perform Selection-I according to Eqs.(12)-(13);
7:     Perform Mutation and Crossover operations to generate new
       test individuals. As shown in Eqs. (14)-(15);
8:     Perform boundary control on the newly generated individuals
       and execute Selection-II. Select the better agent between the
       target and test individuals according to Eq. (18) and update the
       agents in the population set;
9:   end for
10:  Update the parameters  $f$  and  $SF$  according to Eqs. (30)-(31)
    and compute  $X_{avg}$ ;
11:  Generate  $K$  randomly;
12:  for  $i = 1$  to  $N$  do
13:    Update the parameters  $\gamma$ ,  $\omega$  with Eqs.(39),(28) respectively,
    and compute the incremental  $\Delta x$  of the position based on the Eq.
    (38);
14:    if  $rand < 0.5$  then
15:      Calculate  $X_{new2}$  as shown in equation Eq. (25);
16:      if  $fitness(x_{new2}) < fitness(X)$  then
17:        if  $rand < \omega$  then
18:          Calculate  $X_{new3}$  from Eq. (29);
19:        end if
20:      end if
21:    end if
22:    Randomly select the solutions using Eq. (24);
23:    if  $F(X_i(new)) < F(X_i)$  then
24:      Update  $X_{best}$ .
25:    end if
26:  end for
27: end while
28: return  $X_{best}$ 

```

capacity to achieve a balance between the method's exploration and exploitation stages, providing a deeper understanding of its complexity. Additionally, REBSA was compared and analyzed against 10 MAs and the original BSA across dimensions of 10, 30, 50, and 100. These 10 algorithms include classical original algorithms, BSA variants, and improved algorithms with superior performance. Ultimately, this validated the stability of the suggested REBSA in resolving problems of

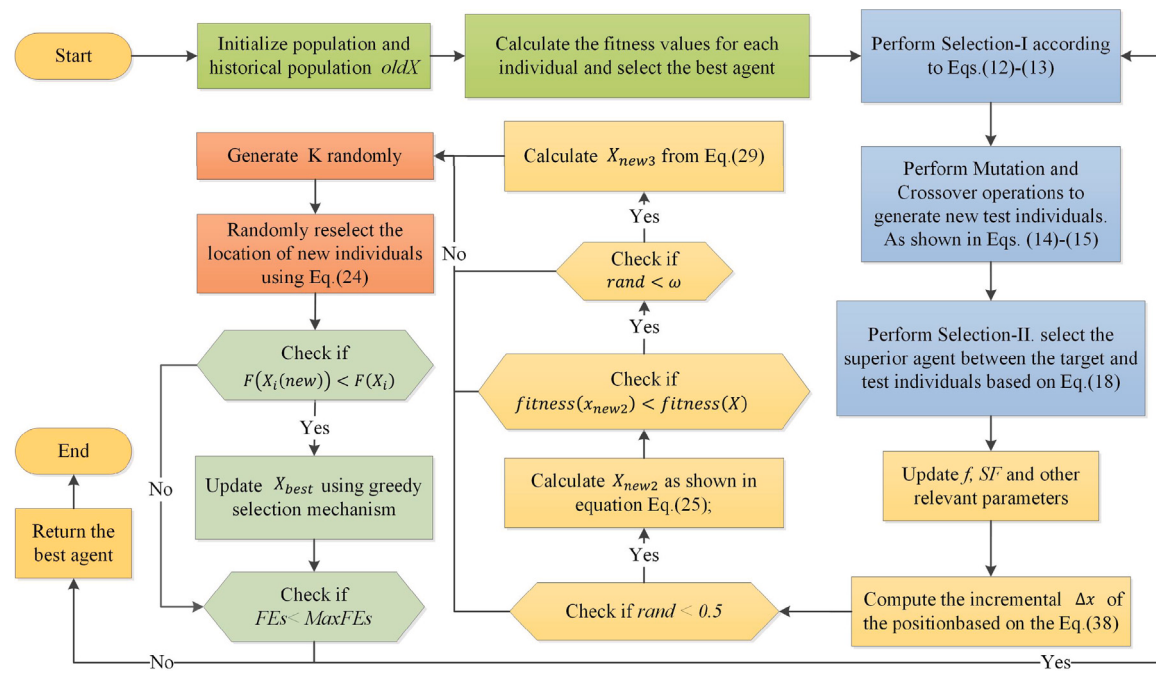


Fig. 3. The flowchart of the proposed REBSA.

varying dimensions. Subsequently, we conducted parameter sensitivity analysis, focusing on key parameters within the algorithm. By adjusting various parameter values, we aimed to identify the optimal settings that further enhance the algorithm's performance. Finally, the enhanced REBSA was compared with various original and advanced methods at CEC 2017 [57], demonstrating its global optimization performance in exploration. To validate the superiority and stability of evaluating method effectiveness, average (Avg) and standard deviation (Std) analyses of the results were conducted, with the best results highlighted in bold. Smaller Avg values indicate the algorithm's proximity to the best solutions, while smaller Std values reflect the algorithm's stability and reliability. Subsequently, the Friedman Test (FT) [66] ranking was utilized to demonstrate the average performance comparison results of the methods visually. Furthermore, the Wilcoxon Signed-Rank Test (WSRT) [67] was utilized further to confirm the effectiveness and robustness of the methods, estimating whether the improved algorithm has statistical significance. The statistical significance level for this test was set at 0.05; if the resulting *p*-value from the comparison is less than 0.05, it indicates a significant improvement in the performance of REBSA compared to the optimizer. Conversely, if the *p*-value is greater than 0.05, it suggests REBSA performs similarly in terms of performance. The symbol '+' implies cases where the algorithm outperforms alternative functions across all test cases; '-' shows cases where its performance is inferior; '=' indicates cases where the performance is comparable. Finally, convergence comparison graphs were provided and analyzed to facilitate a more intuitive comprehension and comparison of the algorithms' convergence behavior, confirming the performance superiority of REBSA compared to its peers.

5.1. Description of the experiment settings

The REBSA optimizer's performance is thoroughly compared to that of a number of different optimization method in this study using the same hardware setup. We aim to guarantee the authenticity and dependability of our results through extensive comparative analysis tests. These experiments were implemented in the Windows 10 with MATLAB 2020a software platform, on the same Intel i7-12700 (2.10 GHz) and 32 GB of RAM. This study selected 29 functions from the IEEE CEC 2017 [57] standard test suite for testing. This suite consists of 30

Table 1
Parameter setting for the algorithm involved.

Algorithm	Other parameters
REBSA	<i>mixrate</i> = 1; <i>pa</i> = 0.1; <i>a</i> = 20; <i>b</i> = 12
DE	<i>ScalingFactor</i> = [0.2, 0.8]; <i>CrossoverProbability</i> = 0.2
HHO	<i>k</i> = 0
PSO	<i>c1</i> = 2; <i>c2</i> = 2; <i>vMax</i> = 6
GWO	<i>a</i> = [2, 0]
WOA	<i>a1</i> = [2, 0]; <i>a2</i> = [-2, -1]; <i>b</i> = 1
SMA	<i>z</i> = 0.03
SCA	<i>a</i> = 2
MFO	<i>b</i> = 1; <i>t</i> = [-1, 1]; <i>a</i> ∈ [-1, -2]
BA	<i>a</i> = 0.5; <i>r</i> = 0.5
FA	<i>a</i> = 0.5; <i>β</i> = 0.2; <i>γ</i> = 1
JADE	<i>Afactor</i> = 1; <i>p</i> = 0.05; <i>c</i> = 0.1; <i>CRm</i> = 0.5; <i>Fm</i> = 0.5
EBOwithCMAR	<i>ce</i> = 0; <i>PS₁</i> = 30; <i>PS₂</i> = 14; <i>PS</i> = 44
LSHADE_cnEpSi	<i>freq_{ini}</i> = 0.5; <i>arc</i> = 1.4; <i>p</i> = 0.11; <i>pb</i> = 0.4; <i>ps</i> = 0.5; <i>memory_{size}</i> = 5
WHRIME	<i>W</i> = 5; <i>K₀</i> = 7; <i>K_{min}</i> = 5
CLPSO	<i>ω</i> ∈ [0.9, 0.2]; <i>c</i> = 1.496; <i>m</i> = 5
CGPSO	<i>c1</i> = <i>c2</i> = 2; <i>W_max</i> = 0.9; <i>W_min</i> = 0; <i>V_max</i> = 6
MLBSA	<i>NP</i> = 50
OBSCA	<i>a</i> = 2
LGWO	<i>a</i> = [2, 0]
ISNMWOA	<i>a₁</i> = [0, 2]; <i>a₂</i> = [-2, -1]; <i>alpha</i> = 0.5

different types of continuous functions: F1–F3 are unimodal functions, F4–F10 are multimodal functions, F11–F20 are hybrid functions, and F21–F30 are composition functions. Further details about CEC 2017 can be found in Table A.1 in the appendix. In the experiments, to guarantee the experiments' validity and fairness, we used the number of evaluations rather than iterations. We set the population size at 30, the maximum number of evaluations to 300,000, and all methods were tested independently 30 times on each benchmark function to minimize the impact of random factors. Additionally, Table 1 provides the parameter configurations used for the competing methods in the experiments. After a series of experiments, the advantages and characteristics of the REBSA algorithm were identified.

5.2. Balance and diversity analysis of REBSA and BSA

It is essential for optimization field to balance the capabilities of exploration and exploitation. If an algorithm only focuses on strong

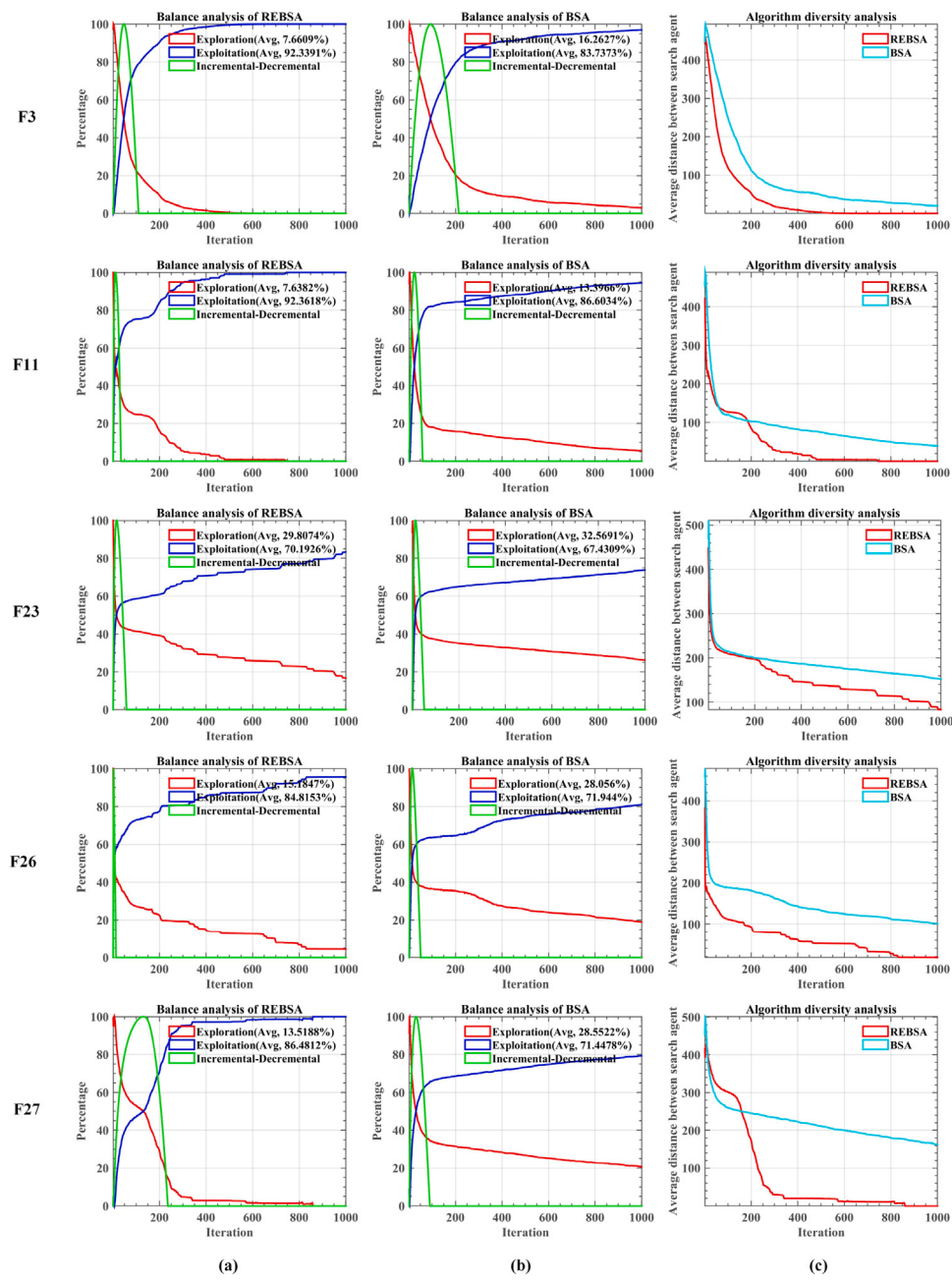


Fig. 4. (a) balance analysis of the REBSA, (b) balance analysis of the BSA, (c) algorithm diversity analysis.

exploitation, it may converge quickly but risks getting trapped in LO, missing out on the global optimal. On the other hand, prioritizing exploration increases the chances of finding the optimal solution but can lead to slower convergence, potentially missing the expected optimum. Therefore, to assess the performance of the suggested REBSA, we first carried out a balanced diversity analysis to gain an in-depth understanding of its ability to balance exploration and exploitation phases.

Fig. 4(a) and (b) show the balance analysis results of REBSA and BSA, respectively. In addition to the red and blue curves representing the exploration and exploitation phases of the algorithms, a green curve has been introduced to evaluate the degree of exploration. If the method's capacity to search globally exceeds its local exploitation capacity, this curve will show an upward trend. Additionally, when the value is negative, it is set to 0. It is evident that in the early phases of iteration, the method is in the exploration phase, where it tends to show

a broad global exploration within the feasibility domain. In the later stages, the algorithm converges quickly and allocates most of its time to exploit solutions. Compared to the BSA, the phases of exploration and exploitation can be more evenly distributed by REBSA, avoid getting trapped in LO, and thus find the global optimum. Additionally, Fig. 4(c) shows the diversity analysis curve of the algorithm. As the population iterates, its diversity gradually decreases and then stabilizes. It is evident that the curve of REBSA converges quicker and stabilizes earlier than that of BSA, indicating the potential of the REBSA algorithm.

5.3. Parameter sensitivity analysis

5.3.1. Analysis of the control parameters of SF

In the EQ strategy, SF is an adaptation factor, given by Eq. (30)–(31). Its main control parameters include a and b . This subsection compares different combinations of parameters tested at CEC 2017,

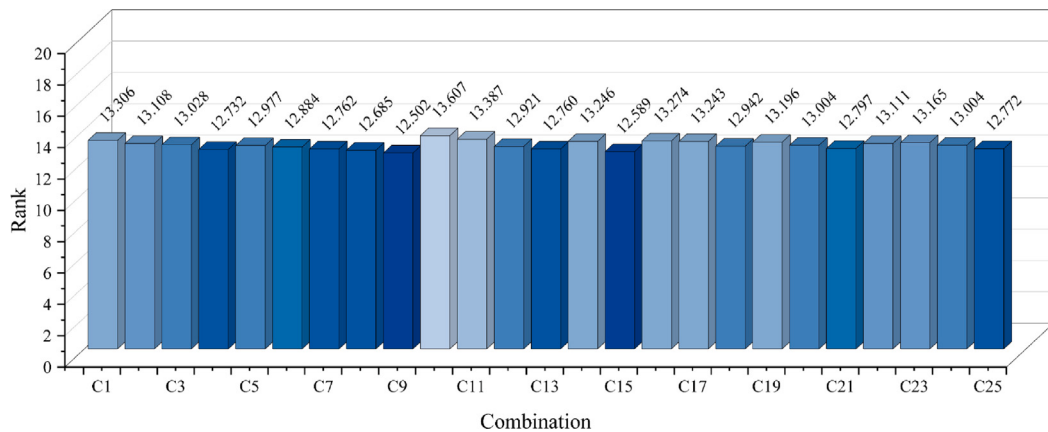


Fig. 5. Average ranks of all combinations.

where $a = [5, 10, 20, 30, 40]$ and $b = [4, 8, 12, 16, 20]$ are the definitions of the values of each parameter. Because each parameter has 5 values, there are a total of 25 parameter combinations in this experiment. Fig. 5 shows the average FT rankings of each combination. Among them, C9 ($a = 10, b = 16$) attained the highest rating, averaging 12.501. It is obvious that the rankings of all the combinations are very close to each other, demonstrating how insensitive the suggested method is to changes in the parameters. Considering all factors, the parameter in the original paper, i.e., C13 ($a = 20, b = 12$, this parameter combination ranks third in the results of our experiment), is selected as the parameter setting of this algorithm.

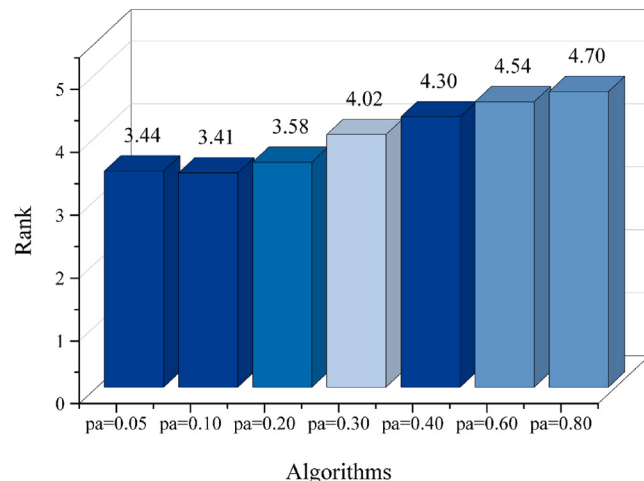
5.3.2. Analysis of the parameter pa

The population is randomly regenerated in the RR approach employed in REBSA, which finds new individuals with a probability of pa . We systematically examined the values of pa in order to maximize the method's efficiency. We tested on CEC 2017 with seven distinct pa values (0.05, 0.10, 0.20, 0.30, 0.40, 0.60, and 0.80) to examine how they affected the algorithm's performance. The method obtains the optimal FT ranking when pa is set to 0.10, as seen in Fig. 6. Additionally, we can observe that beyond a certain range, as the pa value rises, the effectiveness of the method deteriorates. This is due to the excessive randomness causing the algorithm to conduct a substantial amount of random explorations within the feasibility domain, blocking the method's ability to benefit from the information in the current solution. Consequently, this affects the convergence speed and, in some cases, may prevent the algorithm from converging to the best solution, causing the algorithm's performance to gradually deteriorate.

From the above analysis, it can be seen that pa should be controlled within a smaller value range to maintain the stability and effectiveness advantages of the method. The results demonstrate that within a small value range, the ranking difference between each group of parameters is not significant. Therefore, to further optimize the results while ensuring the effectiveness of the method, we finally selected the best-ranked $pa = 0.1$ as the parameter value.

5.4. Comparison in different dimensions

The stability of a method plays a significant part in measuring its effectiveness in optimization. In this paper, we extensively compared the effectiveness of REBSA and several other algorithms across different dimensions using the 29 benchmark functions from CEC 2017. This evaluation aimed to examine the stability and optimization effectiveness of the REBSA algorithm. The experimental design covered four different dimensions: 10, 30, 50, and 100, and included comparisons with the original BSA algorithm, basic variants of BSA, and other advanced algorithms. Through this series of dimensionality tests, we

Fig. 6. The Friedman ranking of different parameters pa .

aimed to gain deeper insights into the adaptability and stability of REBSA when tackling problems of varying scales.

Table A.2 in the appendix presents the Avg and Std of REBSA compared to the BSA across various dimensions. It is evident from the statistics in the table that except for a few multimodal functions, REBSA consistently outperforms BSA in both Avg values and Std across the four different dimensions. This indicates that REBSA not only exhibits strong exploitation capabilities and high accuracy in solving optimization problems but also demonstrates its suitability for tackling complex problems. Moreover, it shows good stability and reliability across problems of varying scales.

Fig. 7 presents the results of using FT between REBSA and 10 different algorithms across four dimensions. In all four dimensions, REBSA is clearly ranked top, demonstrating its superior performance. Additionally, it is evident that other algorithms show varying performance across different dimensions: some perform well in one dimension but poorly in others, resulting in significant fluctuations in their overall performance; others show poor overall performance and are prone to LO. In contrast, the improved REBSA effectively overcomes these shortcomings. It not only shows relatively consistent performance across dimensions (with the best performance observed in 30 dimensions while maintaining competitive results in other dimensions) but also achieves the best solutions, ranking first.

Based on the comprehensive analysis above, we can conclude that in multi-dimensional optimization tasks, REBSA provides high-quality solutions and exhibits superior stability and optimization performance

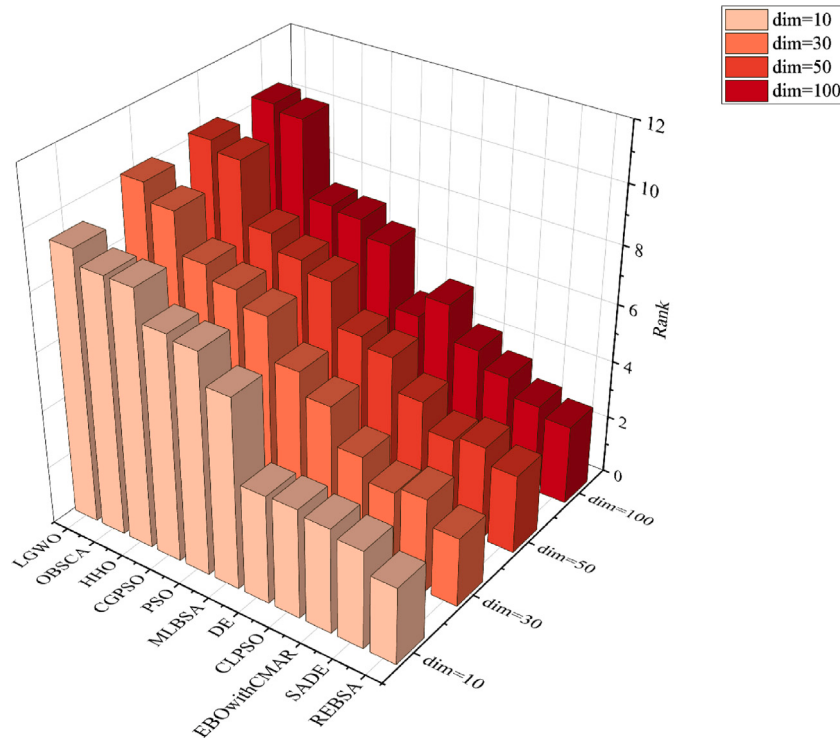


Fig. 7. Friedman-rank of REBSA and other algorithms in different dimensions.

compared to other algorithms. These findings validate REBSA as an effective optimization tool capable of maintaining strong performance in complex and dynamic optimization environments.

5.5. Comparison with original MAs

In this part, ten basic algorithms were compared to REBSA, including DE [17], HHO [30], PSO [21], GWO [31], WOA [25], SMA [32], SCA [35], MFO [27], BA [24], and FA [22].

Table 2 displays the Avg and Std of REBSA and the 10 original algorithms after 30 independent runs. Because F1–F3 are unimodal functions with no LO in the solution space, they could be used to assess algorithms' exploitation capabilities. In Table 2, It is evident that in both unimodal functions F1 and F3, REBSA comes in first and possesses the smallest Std value, which indicates that it performs well in determining the optimal solution of these benchmark functions with good robustness. However, although REBSA can find the optimal solution in several multimodal functions in some cases, it is not as stable as the DE algorithm. In the hybrid functions and composition functions F11–F30, REBSA also demonstrates exceptional performance, achieving the minimum Avg and Std values for the majority of functions. This showcases its strong exploitation capabilities and capacity to get out of LO. The introduction of the RR improves the method's exploration ability, while the EQ strategy ensures that the algorithm has strong exploitation capabilities and opportunities to avoid LO. This indicates that REBSA works better at resolving complicated issues. Fig. 8 gives the FT rankings for all comparison algorithms, allowing a more intuitive observation of how REBSA significantly outperforms the other methods.

To comprehend the convergence of the algorithm more intuitively, Fig. 9 presents the convergence curves of REBSA and other basic methods. We selected the convergence graphs of 9 functions, including the unimodal function F1, multimodal functions F5 and F8, hybrid functions F14, F15, and F19, and composition functions F22, F26, and F30. In the figures, the curve represented by the red line is the convergence curve of the suggested REBSA algorithm. As seen in all convergence

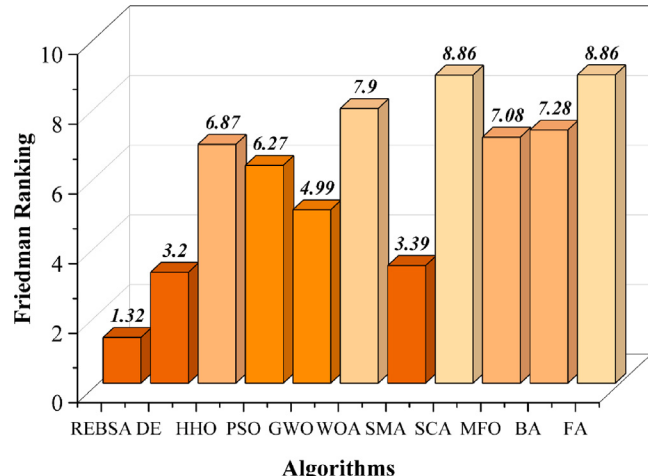


Fig. 8. The Friedman ranking of REBSA and original algorithms.

graphs, the red curve is always at the bottom, proving that REBSA shows a significant advantage in finding the best result to the problem. In the unimodal function F1, although DE, PSO, and BA have slightly higher convergence speeds than REBSA in the early stages, REBSA's final precision of convergence is significantly superior to that of the other methods. The reason for this improvement is the EQ mechanism, which enhances the ability of the algorithm to find the optimal. For the multimodal functions F5 and F8, REBSA achieves higher quality solutions, showcasing its excellent exploration capabilities. This proves the efficiency of combining the RR and EQ strategies, which provide the algorithm with opportunities to escape from LO and obtain better solutions. Finally, in the hybrid and composition functions, REBSA not only achieves the optimal solution among several algorithms but also has the fastest convergence speed. This indicates that REBSA effectively balances exploration and exploitation capabilities, making

Table 2
Comparison of REBSA with original algorithm at CEC 2017.

	F1		F3		F4	
	Avg	Std	Avg	Std	Avg	Std
REBSA	1.0000E+02	1.5958E-13	3.0000E+02	2.6862E-08	4.2049E+02	2.6782E+01
DE	1.6739E+03	2.3434E+03	2.1015E+04	4.8847E+03	4.8957E+02	6.8810E+00
HHO	1.1087E+07	1.9570E+06	9.0306E+03	3.7020E+03	5.2822E+02	2.9397E+01
PSO	1.3019E+08	1.2359E+07	6.5329E+02	4.2265E+01	4.8139E+02	2.9261E+01
GWO	2.4544E+09	1.6526E+09	3.2024E+04	9.1706E+03	6.1065E+02	8.3855E+01
WOA	2.8604E+06	1.9853E+06	1.3987E+05	6.4154E+04	5.5632E+02	5.3854E+01
SMA	4.6491E+03	6.0835E+03	3.0001E+02	8.1608E-03	4.8471E+02	1.4264E+01
SCA	1.2472E+10	1.9556E+09	3.8539E+04	6.8635E+03	1.4622E+03	2.4164E+02
MFO	1.2277E+10	8.9085E+09	1.0459E+05	7.7241E+04	1.4055E+03	1.0731E+03
BA	6.3518E+05	4.4450E+05	3.0010E+02	7.4155E-02	4.7614E+02	2.9404E+01
FA	1.4769E+10	1.2554E+09	6.1963E+04	8.4407E+03	1.3611E+03	1.3144E+02
	F5		F6		F7	
	Avg	Std	Avg	Std	Avg	Std
REBSA	5.7424E+02	1.4155E+01	6.0000E+02	3.0696E-03	7.9391E+02	1.7696E+01
DE	6.0696E+02	9.5979E+00	6.0000E+02	2.1111E-14	8.4273E+02	9.2901E+00
HHO	7.3612E+02	2.8495E+01	6.6060E+02	7.8475E+00	1.2518E+03	6.7941E+01
PSO	7.4687E+02	2.8224E+01	6.5115E+02	1.4089E+01	9.1822E+02	1.3214E+01
GWO	6.0122E+02	2.0641E+01	6.0672E+02	2.6385E+00	8.7548E+02	4.0378E+01
WOA	7.8368E+02	5.4050E+01	6.6975E+02	1.2671E+01	1.2475E+03	1.0118E+02
SMA	5.8635E+02	2.3541E+01	6.0107E+02	8.8855E-01	8.2974E+02	2.9492E+01
SCA	7.7682E+02	1.8044E+01	6.5010E+02	5.3944E+00	1.1292E+03	3.8989E+01
MFO	7.0181E+02	4.4883E+01	6.4102E+02	1.1057E+01	1.1780E+03	2.3285E+02
BA	8.2454E+02	6.3179E+01	6.7310E+02	1.1391E+01	1.6608E+03	1.8252E+02
FA	7.5944E+02	1.1091E+01	6.4508E+02	2.3959E+00	1.3912E+03	3.8020E+01
	F8		F9		F10	
	Avg	Std	Avg	Std	Avg	Std
REBSA	8.7027E+02	9.1829E+00	9.9182E+02	1.2682E+02	3.5024E+03	2.4476E+02
DE	9.1284E+02	8.0726E+00	9.0000E+02	1.0125E-13	5.8698E+03	2.7930E+02
HHO	9.5859E+02	2.0796E+01	6.8779E+03	7.3781E+02	5.5667E+03	7.8407E+02
PSO	9.9460E+02	1.9995E+01	5.4599E+03	2.2429E+03	6.0707E+03	5.9371E+02
GWO	8.8616E+02	1.7437E+01	2.0534E+03	7.4706E+02	3.9085E+03	5.7482E+02
WOA	1.0037E+03	3.6952E+01	7.4400E+03	2.6727E+03	6.0626E+03	9.0149E+02
SMA	8.8838E+02	1.6994E+01	2.1848E+03	1.1445E+03	4.0274E+03	7.3308E+02
SCA	1.0419E+03	1.9272E+01	5.5579E+03	1.1291E+03	8.1554E+03	3.6547E+02
MFO	1.0282E+03	3.8951E+01	7.2917E+03	1.7143E+03	5.3678E+03	7.0094E+02
BA	1.0499E+03	6.0865E+01	1.3794E+04	5.1299E+03	5.7500E+03	7.1106E+02
FA	1.0515E+03	1.2553E+01	5.2284E+03	5.2864E+02	7.9763E+03	2.8706E+02
	F11		F12		F13	
	Avg	Std	Avg	Std	Avg	Std
REBSA	1.1336E+03	2.1069E+01	1.2544E+04	9.3008E+03	1.3778E+03	4.3675E+01
DE	1.1624E+03	2.4835E+01	1.9096E+06	1.0094E+06	4.1678E+04	2.5796E+04
HHO	1.2513E+03	5.0969E+01	9.6608E+06	6.3115E+06	5.1502E+05	9.8171E+05
PSO	1.2814E+03	3.9277E+01	2.7325E+07	1.3181E+07	4.8788E+06	1.1043E+06
GWO	1.8699E+03	8.9748E+02	5.2844E+07	6.2799E+07	9.9883E+05	3.9115E+06
WOA	1.5368E+03	8.1774E+01	3.6828E+07	2.6700E+07	1.5659E+05	1.0040E+05
SMA	1.2176E+03	4.9537E+01	9.5137E+05	8.0066E+05	2.1428E+04	2.2452E+04
SCA	2.1220E+03	3.7423E+02	1.1682E+09	3.2165E+08	3.6519E+08	1.4722E+08
MFO	6.8598E+03	7.4312E+03	3.1207E+08	4.6519E+08	3.8154E+07	1.9332E+08
BA	1.3293E+03	7.4446E+01	2.9902E+06	3.0652E+06	3.0325E+05	1.2952E+05
FA	3.4409E+03	4.7508E+02	1.5385E+09	2.3759E+08	6.4786E+08	1.9493E+08
	F14		F15		F16	
	Avg	Std	Avg	Std	Avg	Std
REBSA	1.4278E+03	1.0390E+01	1.5202E+03	1.0941E+01	2.0892E+03	1.7770E+02
DE	4.0999E+04	2.1276E+04	8.8475E+03	6.0205E+03	2.0653E+03	1.4360E+02
HHO	7.2199E+04	8.5905E+04	7.5723E+04	4.8330E+04	3.1005E+03	4.1737E+02
PSO	8.2262E+03	5.0277E+03	4.5767E+05	2.0427E+05	2.8991E+03	2.6903E+02
GWO	1.6890E+05	2.4018E+05	3.7496E+05	8.1695E+05	2.3814E+03	2.6550E+02
WOA	1.0003E+06	1.1287E+06	8.0304E+04	6.5414E+04	3.5002E+03	4.3596E+02
SMA	3.7707E+04	1.7271E+04	2.5678E+04	1.4455E+04	2.3110E+03	3.0368E+02
SCA	1.2536E+05	6.5648E+04	1.2200E+07	9.8917E+06	3.5964E+03	2.0899E+02
MFO	1.1381E+05	1.6308E+05	3.0179E+07	1.6485E+08	3.2496E+03	4.2127E+02
BA	6.8367E+03	4.4672E+03	1.0717E+05	6.2402E+04	3.4426E+03	3.9768E+02
FA	2.1154E+05	1.0052E+05	6.2223E+07	2.1065E+07	3.4424E+03	1.7988E+02
	F17		F18		F19	
	Avg	Std	Avg	Std	Avg	Std
REBSA	1.7870E+03	5.5441E+01	2.4635E+03	9.2122E+02	1.9129E+03	3.4382E+00
DE	1.8368E+03	5.2783E+01	3.0815E+05	1.4521E+05	7.1301E+03	3.8452E+03

(continued on next page)

Table 2 (continued).

HHO	2.5251E+03	3.0831E+02	1.0629E+06	1.0256E+06	3.0184E+05	2.0105E+05
PSO	2.3436E+03	2.6675E+02	2.1663E+05	1.5591E+05	1.4708E+06	5.7576E+05
GWO	2.0044E+03	1.3406E+02	1.3381E+06	4.8619E+06	2.0874E+06	6.2081E+06
WOA	2.5871E+03	2.9103E+02	2.5933E+06	2.2269E+06	2.4645E+06	2.0817E+06
SMA	2.1585E+03	1.9898E+02	3.7512E+05	3.5944E+05	2.6772E+04	1.8911E+04
SCA	2.3942E+03	1.8252E+02	2.9328E+06	1.8248E+06	2.7336E+07	1.6793E+07
MFO	2.5920E+03	3.2448E+02	2.3967E+06	5.5841E+06	1.2169E+07	2.5228E+07
BA	2.8867E+03	2.9838E+02	1.5143E+05	1.0988E+05	5.3101E+05	2.4154E+05
FA	2.5171E+03	1.1506E+02	3.6805E+06	1.5463E+06	9.0037E+07	3.4142E+07
	F20		F21		F22	
	Avg	Std	Avg	Std	Avg	Std
REBSA	2.1215E+03	5.6557E+01	2.3529E+03	3.0491E+01	2.5897E+03	8.8454E+02
DE	2.1463E+03	6.7547E+01	2.4093E+03	9.0878E+00	3.6190E+03	1.7280E+03
HHO	2.7851E+03	1.9925E+02	2.5545E+03	5.1083E+01	6.7473E+03	1.4991E+03
PSO	2.6207E+03	1.4196E+02	2.5380E+03	2.7932E+01	5.6869E+03	2.6246E+03
GWO	2.3710E+03	1.3626E+02	2.3817E+03	2.4112E+01	3.7010E+03	1.3141E+03
WOA	2.6126E+03	1.5845E+02	2.5799E+03	8.0891E+01	6.3655E+03	2.3544E+03
SMA	2.4262E+03	1.9044E+02	2.3958E+03	2.0148E+01	5.4219E+03	1.1536E+03
SCA	2.6671E+03	1.1773E+02	2.5549E+03	2.0312E+01	7.7734E+03	2.6772E+03
MFO	2.7686E+03	2.5554E+02	2.5029E+03	4.5633E+01	6.3904E+03	1.6176E+03
BA	3.0169E+03	2.4072E+02	2.6305E+03	7.1782E+01	7.2220E+03	1.3277E+03
FA	2.6023E+03	7.5320E+01	2.5397E+03	1.1087E+01	3.9112E+03	1.5079E+02
	F23		F24		F25	
	Avg	Std	Avg	Std	Avg	Std
REBSA	2.7010E+03	1.3955E+01	2.8800E+03	1.5766E+01	2.8848E+03	2.3897E+00
DE	2.7534E+03	1.0347E+01	2.9590E+03	1.0843E+01	2.8874E+03	4.5840E-01
HHO	3.1335E+03	9.4105E+01	3.4360E+03	1.4288E+02	2.9116E+03	1.7617E+01
PSO	3.1494E+03	1.1818E+02	3.2078E+03	8.3111E+01	2.9047E+03	2.2980E+01
GWO	2.7612E+03	3.7186E+01	2.9435E+03	5.4159E+01	2.9832E+03	4.3001E+01
WOA	3.0358E+03	9.6275E+01	3.2076E+03	9.5471E+01	2.9442E+03	2.7059E+01
SMA	2.7384E+03	2.3487E+01	2.9159E+03	2.0592E+01	2.8870E+03	1.2196E+00
SCA	2.9908E+03	2.5733E+01	3.1596E+03	2.6070E+01	3.2055E+03	7.4503E+01
MFO	2.8416E+03	4.5114E+01	3.0004E+03	3.4695E+01	3.2109E+03	3.6432E+02
BA	3.2996E+03	1.2797E+02	3.3615E+03	1.3827E+02	2.9073E+03	2.4070E+01
FA	2.9164E+03	1.2919E+01	3.0663E+03	1.1459E+01	3.5478E+03	9.1959E+01
	F26		F27		F28	
	Avg	Std	Avg	Std	Avg	Std
REBSA	3.2960E+03	6.5994E+02	3.2013E+03	7.1148E+00	3.1123E+03	3.8556E+01
DE	4.6161E+03	1.0360E+02	3.2055E+03	3.9680E+00	3.2001E+03	4.4511E+01
HHO	6.2055E+03	2.1106E+03	3.3543E+03	1.5413E+02	3.2535E+03	2.3034E+01
PSO	5.4702E+03	1.9246E+03	3.1948E+03	9.2717E+01	3.2459E+03	2.5280E+01
GWO	4.6905E+03	4.6642E+02	3.2480E+03	2.1397E+01	3.3927E+03	7.6185E+01
WOA	7.2435E+03	1.1056E+03	3.3858E+03	1.2583E+02	3.3067E+03	2.9015E+01
SMA	4.5799E+03	2.7472E+02	3.2119E+03	1.0004E+01	3.2444E+03	5.5620E+01
SCA	6.9047E+03	2.7496E+02	3.3980E+03	2.9393E+01	3.8107E+03	1.0444E+02
MFO	5.9008E+03	3.7561E+02	3.2639E+03	2.6658E+01	4.5291E+03	1.0300E+03
BA	9.1192E+03	2.4070E+03	3.4663E+03	1.7899E+02	3.1406E+03	5.9937E+01
FA	6.5045E+03	1.5450E+02	3.3292E+03	1.8681E+01	3.8914E+03	8.3140E+01
	F29		F30			
	Avg	Std	Avg	Std		
REBSA	3.3891E+03	4.6561E+01	5.4176E+03	3.7165E+02		
DE	3.5136E+03	7.8807E+01	1.2111E+04	2.7740E+03		
HHO	4.3998E+03	4.3400E+02	1.5176E+06	7.5953E+05		
PSO	4.3672E+03	2.6133E+02	3.6348E+06	1.6072E+06		
GWO	3.7170E+03	1.4601E+02	6.4582E+06	6.6021E+06		
WOA	4.6295E+03	4.2336E+02	1.3004E+07	1.0606E+07		
SMA	3.8085E+03	1.8044E+02	1.6705E+04	4.1268E+03		
SCA	4.6820E+03	2.1338E+02	7.1334E+07	3.2390E+07		
MFO	4.3233E+03	3.3808E+02	4.4001E+05	5.4455E+05		
BA	4.8217E+03	3.6961E+02	1.1900E+06	6.4649E+05		
FA	4.7355E+03	1.3628E+02	9.6931E+07	2.9662E+07		
	Overall Rank					
	Rank	+/-/=	Avg			
REBSA	1	~	1.1379			
DE	2	25/2/2	3.0345			
HHO	6	29/0/0	6.7241			
PSO	5	28/1/0	5.8621			
GWO	4	29/0/0	5.2414			
WOA	9	29/0/0	8.1034			
SMA	3	28/0/1	3.1034			
SCA	11	29/0/0	8.9310			
MFO	8	29/0/0	7.6207			
BA	7	29/0/0	7.4828			
FA	10	29/0/0	8.7586			

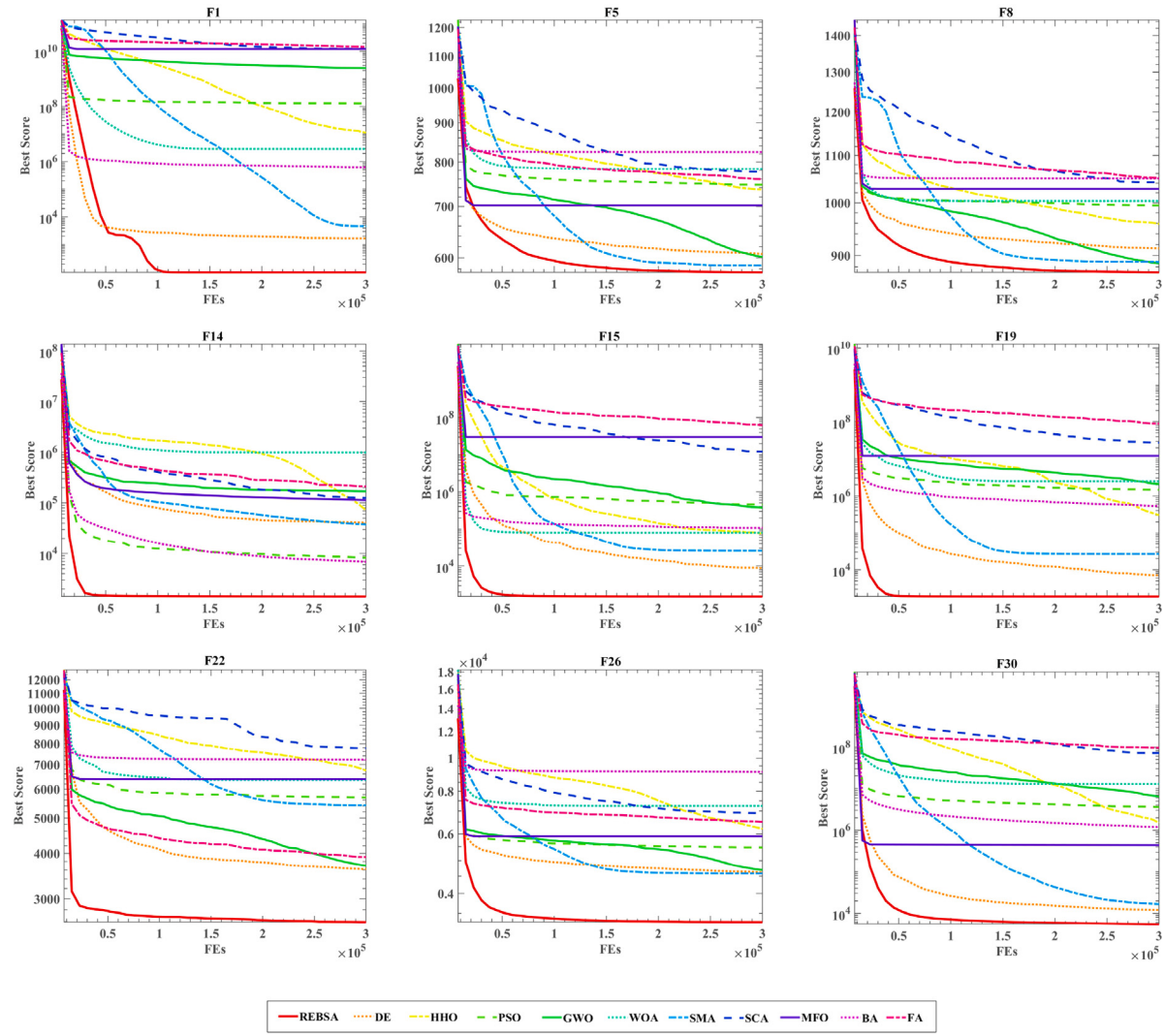


Fig. 9. Convergence curves of the REBSA algorithm and the original algorithm at CEC 2017.

it an successful optimization method with a clear advantage in solving complex problems.

5.6. Comparison with advanced MAs

To better demonstrate the advantages of the REBSA algorithm, this section selects 10 enhanced MAs, including classic champion algorithms, BSA variants, and the latest optimization improvement methods, for comparison with REBSA. The specific algorithms include JADE [68], EBOwithCMAR [69], LSHADE_cnEpSi [70], WHRIME [58], CLPSO [71], CGPSO [72], MLBSA [73], OBSCA [74], LGWO [75], and ISNMWOA [76].

Table 3 presents the comparative results of REBSA and several other methods, showing the Avg and Std for each algorithm. It is evident that REBSA achieves the optimal values for unimodal functions F1 and F3, proving its strong exploitation capability. Furthermore, REBSA achieves the best Avg and Std values on almost all composite functions (F11–F20). This suggests that in addition to balancing the algorithm's capacity for exploitation and LO escape, the REBSA, in conjunction with the RR approach and EQ mechanism, guarantees stability and dependability while seeking more prospective areas. Fig. 10 shows the FT comparison results, providing a more intuitive demonstration of REBSA's superiority.

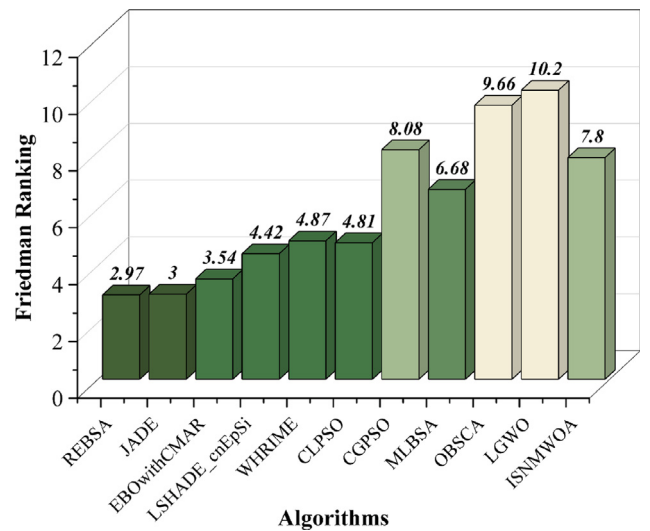


Fig. 10. The Friedman ranking of REBSA and advanced algorithms.

Table 3

Comparison of REBSA with advanced algorithm at CEC 2017.

	F1		F3		F4	
	Avg	Std	Avg	Std	Avg	Std
REBSA	1.0000E+02	9.2053E-13	3.0000E+02	6.3275E-09	4.2004E+02	2.7418E+01
JADE	1.0000E+02	2.7048E-13	1.4182E+03	4.6037E+03	4.2731E+02	2.9403E+01
EBOwithCMAR	1.0000E+02	7.6412E-08	3.7971E+04	3.8836E+04	4.0172E+02	2.0071E+00
LSHADE_cnEpSi	1.0000E+02	7.0486E-10	3.0002E+02	1.2575E-01	4.6471E+02	4.2020E+01
WHRIME	6.7765E+03	9.8849E+03	9.7641E+02	4.2525E+02	4.4590E+02	2.7684E+01
CLPSO	1.3297E+02	7.2145E+01	9.2042E+03	2.2220E+03	4.5791E+02	2.5852E+01
CGPSO	1.3658E+08	1.5891E+07	7.7272E+02	6.0929E+01	4.7986E+02	3.4357E+01
MLBSA	1.0866E+02	1.4550E+01	3.0000E+02	1.0161E-03	4.4883E+02	3.8741E+01
OBSCA	1.7113E+10	2.7732E+09	6.0686E+04	7.7026E+03	2.5155E+03	7.6043E+02
LGWO	1.7950E+10	1.7685E+09	5.7631E+04	6.1229E+03	2.9724E+03	5.1646E+02
ISNMWOA	5.2120E+02	1.8924E+03	3.0000E+02	6.8546E-04	4.1261E+02	2.4375E+01
	F5		F6		F7	
	Avg	Std	Avg	Std	Avg	Std
REBSA	5.7285E+02	1.7379E+01	6.0001E+02	5.0710E-03	7.9244E+02	1.4798E+01
JADE	5.3191E+02	6.7196E+00	6.0000E+02	0.0000E+00	7.6323E+02	6.2516E+00
EBOwithCMAR	5.2277E+02	5.7618E+00	6.0022E+02	3.3232E-01	7.5996E+02	9.2332E+00
LSHADE_cnEpSi	5.3905E+02	1.0920E+01	6.0172E+02	1.4379E+00	7.8185E+02	1.4967E+01
WHRIME	5.3937E+02	1.2663E+01	6.0000E+02	2.1755E-05	7.7317E+02	1.6136E+01
CLPSO	5.4705E+02	7.3840E+00	6.0000E+02	6.6759E-14	7.8301E+02	7.6314E+00
CGPSO	7.7617E+02	3.8046E+01	6.6070E+02	1.1304E+01	9.3265E+02	1.7262E+01
MLBSA	6.9637E+02	4.8148E+01	6.4954E+02	5.0071E+00	1.1671E+03	1.0449E+02
OBSCA	8.1210E+02	2.0695E+01	6.5577E+02	4.9064E+00	1.1596E+03	5.4469E+01
LGWO	7.9840E+02	1.4366E+01	6.5669E+02	4.1120E+00	1.1744E+03	3.0334E+01
ISNMWOA	8.7072E+02	7.4240E+01	6.6381E+02	8.6317E+00	1.0189E+03	1.0714E+02
	F8		F9		F10	
	Avg	Std	Avg	Std	Avg	Std
REBSA	8.7169E+02	1.3358E+01	9.9612E+02	9.7479E+01	3.4741E+03	3.5695E+02
JADE	8.3428E+02	8.5035E+00	9.0270E+02	3.3142E+00	3.0220E+03	2.7428E+02
EBOwithCMAR	8.2471E+02	5.9700E+00	9.3514E+02	4.3988E+01	2.9533E+03	2.9358E+02
LSHADE_cnEpSi	8.4083E+02	1.1833E+01	1.1625E+03	2.1259E+02	2.9862E+03	2.6208E+02
WHRIME	8.3688E+02	9.0170E+00	9.5495E+02	3.8064E+01	3.5087E+03	5.4608E+02
CLPSO	8.5502E+02	8.6621E+00	9.0908E+02	7.4163E+00	3.4084E+03	2.5665E+02
CGPSO	1.0124E+03	2.5384E+01	7.1050E+03	1.9862E+03	6.3479E+03	5.0463E+02
MLBSA	9.5564E+02	2.9022E+01	4.8178E+03	1.0301E+03	5.3401E+03	8.1678E+02
OBSCA	1.0706E+03	1.9054E+01	6.6857E+03	1.1571E+03	7.3965E+03	4.8695E+02
LGWO	1.0670E+03	1.4614E+01	6.5733E+03	7.3132E+02	8.1609E+03	2.5718E+02
ISNMWOA	1.1167E+03	6.2019E+01	9.7772E+03	1.9007E+03	5.4623E+03	7.2997E+02
	F11		F12		F13	
	Avg	Std	Avg	Std	Avg	Std
REBSA	1.1240E+03	7.5516E+00	1.2147E+04	7.3877E+03	1.3618E+03	2.1932E+01
JADE	1.1759E+03	4.9390E+01	2.0031E+04	9.1553E+04	3.5632E+03	5.6396E+03
EBOwithCMAR	1.2037E+03	2.9245E+01	7.4637E+03	5.4600E+03	3.5370E+03	1.1276E+03
LSHADE_cnEpSi	1.2641E+03	4.3722E+01	8.9036E+03	6.1580E+03	4.1384E+03	1.1925E+03
WHRIME	1.1331E+03	9.6502E+00	6.9101E+05	7.6972E+05	2.1619E+04	2.2474E+04
CLPSO	1.1412E+03	1.5782E+01	4.6601E+05	3.1103E+05	1.6788E+03	2.8885E+02
CGPSO	1.2872E+03	3.2435E+01	2.7998E+07	1.2344E+07	5.6439E+06	1.5781E+06
MLBSA	1.2530E+03	4.3396E+01	2.0734E+04	1.4185E+04	1.8920E+04	1.4747E+04
OBSCA	2.8251E+03	7.1182E+02	1.9976E+09	5.8984E+08	7.0012E+08	2.8265E+08
LGWO	3.0124E+03	2.9785E+02	2.7640E+09	4.0038E+08	1.2494E+09	3.6123E+08
ISNMWOA	1.2715E+03	4.8791E+01	1.7063E+04	1.3765E+04	1.4226E+04	1.4494E+04
	F14		F15		F16	
	Avg	Std	Avg	Std	Avg	Std
REBSA	1.4310E+03	9.7149E+00	1.5176E+03	6.9657E+00	2.0262E+03	1.2325E+02
JADE	4.8013E+03	6.6023E+03	1.9563E+03	6.7215E+02	2.0610E+03	1.7385E+02
EBOwithCMAR	1.5844E+03	7.1590E+01	1.7891E+03	1.1341E+02	2.0832E+03	1.7423E+02
LSHADE_cnEpSi	1.6053E+03	6.4648E+01	1.8447E+03	1.4310E+02	2.0693E+03	1.8066E+02
WHRIME	1.8776E+04	1.7983E+04	1.1286E+04	1.0646E+04	2.0373E+03	2.1067E+02
CLPSO	3.0073E+04	3.3139E+04	1.6321E+03	7.5080E+01	2.0955E+03	1.3448E+02
CGPSO	1.5264E+04	1.1171E+04	6.3654E+05	2.1853E+05	3.0407E+03	2.4960E+02
MLBSA	1.6033E+03	7.7116E+01	3.6574E+03	2.5184E+03	2.8443E+03	3.2296E+02
OBSCA	2.9604E+05	2.3216E+05	1.1280E+07	1.0656E+07	3.8353E+03	2.2866E+02
LGWO	2.7508E+05	1.4161E+05	8.4977E+06	5.4818E+06	3.9226E+03	1.8200E+02
ISNMWOA	3.2838E+03	3.2224E+03	1.2703E+04	9.5721E+03	2.9953E+03	3.8390E+02
	F17		F18		F19	
	Avg	Std	Avg	Std	Avg	Std
REBSA	1.7681E+03	4.4691E+01	1.9296E+03	9.9705E+01	1.9124E+03	4.2771E+00
JADE	1.8043E+03	6.7883E+01	7.6729E+03	2.0557E+04	2.8404E+03	4.2156E+03
EBOwithCMAR	1.8339E+03	8.2001E+01	4.1969E+03	2.2175E+03	2.0586E+03	7.2217E+01
LSHADE_cnEpSi	1.8744E+03	9.1790E+01	2.3459E+03	6.7107E+02	2.1216E+03	1.4043E+02
WHRIME	1.8540E+03	1.0990E+02	3.1645E+05	3.8956E+05	1.2931E+04	1.5435E+04

(continued on next page)

Table 3 (continued).

CLPSO	1.8284E+03	7.1783E+01	1.4126E+05	8.2406E+04	2.0039E+03	9.3984E+01
CGPSO	2.3599E+03	2.3229E+02	2.3068E+05	9.8801E+04	1.5723E+06	6.7382E+05
MLBSA	2.4906E+03	3.1359E+02	3.9555E+03	2.0818E+03	3.1476E+03	2.6768E+03
OBSCA	2.5298E+03	2.0634E+02	3.7864E+06	2.1510E+06	4.3376E+07	3.1224E+07
LGWO	2.7384E+03	1.4274E+02	3.9439E+06	2.2029E+06	4.7638E+07	1.8196E+07
ISNMWOA	2.6169E+03	3.6966E+02	4.0479E+04	1.3826E+04	1.3055E+04	1.4551E+04
	F20		F21		F22	
	Avg	Std	Avg	Std	Avg	Std
REBSA	2.1246E+03	5.3855E+01	2.3600E+03	1.3501E+01	2.4796E+03	6.8353E+02
JADE	2.1559E+03	6.0666E+01	2.3345E+03	6.4790E+00	2.6880E+03	8.9200E+02
EBOwithCMAR	2.1862E+03	8.9861E+01	2.3230E+03	6.7221E+00	2.3000E+03	2.1035E-01
LSHADE_cnEpSi	2.1899E+03	8.5888E+01	2.3391E+03	1.0262E+01	2.5188E+03	6.4051E+02
WHRIME	2.1493E+03	1.0367E+02	2.3390E+03	7.7955E+00	4.6053E+03	1.0824E+03
CLPSO	2.1704E+03	7.1983E+01	2.3471E+03	2.7363E+01	2.3640E+03	1.2745E+02
CGPSO	2.5787E+03	1.3736E+02	2.5426E+03	3.3525E+01	3.8210E+03	2.5095E+03
MLBSA	2.5543E+03	2.0554E+02	2.4861E+03	4.1655E+01	5.8205E+03	2.2788E+03
OBSCA	2.6740E+03	1.4274E+02	2.4779E+03	1.1427E+02	4.0666E+03	3.1837E+02
LGWO	2.6964E+03	1.0997E+02	2.5904E+03	1.9183E+01	6.9970E+03	2.4381E+03
ISNMWOA	2.9779E+03	3.1380E+02	2.6455E+03	7.6274E+01	6.9735E+03	1.5788E+03
	F23		F24		F25	
	Avg	Std	Avg	Std	Avg	Std
REBSA	2.6986E+03	1.1371E+01	2.8857E+03	1.7597E+01	2.8845E+03	2.0150E+00
JADE	2.6841E+03	8.0721E+00	2.8545E+03	1.0921E+01	2.8879E+03	7.0610E+00
EBOwithCMAR	2.6892E+03	1.4765E+01	2.8561E+03	1.4321E+01	2.8955E+03	1.5509E+01
LSHADE_cnEpSi	2.7110E+03	2.7459E+01	2.8787E+03	1.6910E+01	2.8915E+03	7.5943E+00
WHRIME	2.7030E+03	1.6979E+01	2.8756E+03	1.3891E+01	2.8784E+03	9.1445E-01
CLPSO	2.7065E+03	8.7586E+00	2.8546E+03	1.1197E+02	2.8864E+03	1.1477E+00
CGPSO	3.0987E+03	1.0816E+02	3.2104E+03	9.0683E+01	2.9174E+03	2.4676E+01
MLBSA	2.9262E+03	7.6373E+01	3.0921E+03	9.4935E+01	2.9112E+03	2.5558E+01
OBSCA	3.0150E+03	3.0402E+01	3.1890E+03	2.4704E+01	3.4443E+03	1.9957E+02
LGWO	3.0559E+03	2.1469E+01	3.2202E+03	2.5620E+01	3.4484E+03	9.3356E+01
ISNMWOA	3.2634E+03	1.9240E+02	3.2121E+03	9.2185E+01	2.8876E+03	2.1772E+00
	F26		F27		F28	
	Avg	Std	Avg	Std	Avg	Std
REBSA	3.4618E+03	7.1575E+02	3.2054E+03	8.5322E+00	3.1104E+03	3.1618E+01
JADE	3.8733E+03	3.7197E+02	3.2133E+03	9.8952E+00	3.1233E+03	4.8374E+01
EBOwithCMAR	3.3032E+03	5.6954E+02	3.2292E+03	1.3502E+01	3.1228E+03	4.7558E+01
LSHADE_cnEpSi	4.1276E+03	4.8264E+02	3.2318E+03	1.7912E+01	3.1528E+03	6.3600E+01
WHRIME	4.1638E+03	2.6122E+02	3.2000E+03	3.5550E-04	3.2977E+03	4.5931E+00
CLPSO	3.5084E+03	5.2349E+02	3.2125E+03	5.6074E+00	3.2137E+03	6.5698E+00
CGPSO	4.5781E+03	1.9878E+03	3.1837E+03	5.2915E+01	3.2575E+03	2.3267E+01
MLBSA	6.4913E+03	1.9888E+03	3.3154E+03	7.1698E+01	3.1573E+03	6.8802E+01
OBSCA	6.9200E+03	6.1211E+02	3.4769E+03	5.6216E+01	4.2387E+03	3.1443E+02
LGWO	7.8087E+03	2.8023E+02	3.5178E+03	3.9852E+01	4.3359E+03	1.5509E+02
ISNMWOA	7.3833E+03	2.5050E+03	3.3351E+03	7.0843E+01	3.1681E+03	6.7267E+01
	F29		F30			
	Avg	Std	Avg	Std		
REBSA	3.3879E+03	2.9610E+01	5.2507E+03	2.7221E+02		
JADE	3.4606E+03	9.8411E+01	5.5219E+03	1.1995E+03		
EBOwithCMAR	3.4483E+03	7.0154E+01	8.4178E+03	3.1170E+03		
LSHADE_cnEpSi	3.5444E+03	1.3408E+02	6.3509E+03	2.2399E+03		
WHRIME	3.3301E+03	8.5763E+01	6.4701E+03	4.4205E+03		
CLPSO	3.4642E+03	7.3665E+01	8.3477E+03	1.1383E+03		
CGPSO	4.3390E+03	2.1771E+02	8.3844E+06	1.8776E+06		
MLBSA	4.2807E+03	3.2317E+02	6.5393E+03	1.5537E+03		
OBSCA	4.9494E+03	2.2784E+02	1.0261E+08	3.6528E+07		
LGWO	4.8855E+03	1.8114E+02	1.2868E+08	4.1086E+07		
ISNMWOA	4.3598E+03	3.0177E+02	9.8662E+03	4.0249E+03		
	Overall Rank					
	Rank	+/-=	Avg			
REBSA	1	~	2.7241			
JADE	3	19/9/0	3.3448			
EBOwithCMAR	2	17/12/0	3.2414			
LSHADE_cnEpSi	5	22/7/0	4.6207			
WHRIME	6	19/10/0	4.8966			
CLPSO	4	20/9/0	4.4828			
CGPSO	9	28/1/0	8.1034			
MLBSA	7	29/0/0	6.5172			
OBSCA	10	29/0/0	9.5517			
LGWO	11	29/0/0	10.4138			
ISNMWOA	8	28/1/0	8.0690			

Fig. 11 shows the convergence curves on selected test functions from the 29 functions of CEC 2017. Several convergence plots show that other compared algorithms easily get trapped in LO during the iteration process. In contrast, REBSA, due to the introduction of the RR strategy

and the EQ mechanism, dramatically enhances its ability to escape LO, better explore the space, and quickly converge to the optimal solution. This demonstrates REBSA's strong exploitation capability and superior performance.

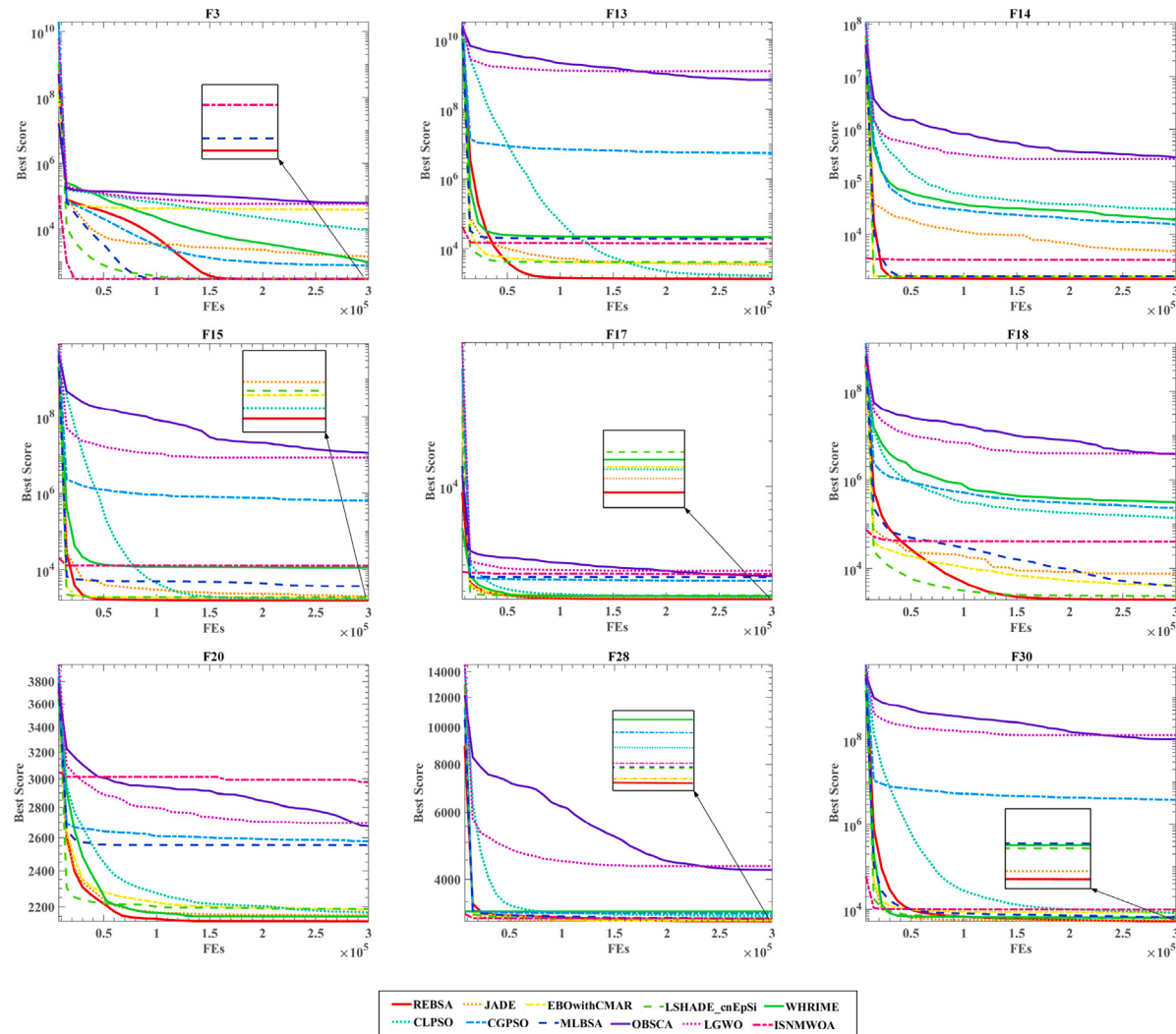


Fig. 11. Convergence curves of the REBSA algorithm and the advanced algorithm at CEC 2017.

6. Experiments on MTIS

6.1. Experiment setup and database

Practice is the sole criterion for testing truth. In this chapter, we utilize the suggested REBSA method to MTIS to demonstrate its efficacy in practical applications. A portion of the image data used in this study was sourced from Databio [77], a widely utilized dataset for breast invasive ductal carcinoma, containing 922 images. Another portion of the images was obtained from the First Affiliated Hospital of Wenzhou Medical University in China. To validate the performance of the REBSA, we selected 9 images from each dataset for experimentation. Here, nine images from the public dataset are labeled as A, B, C, D, E, F, G, H, and I. The selected images and their NM 2D histograms are shown in Fig. 12. Meanwhile, Fig. 13 displays the breast cancer pathology images from the hospital along with their 2D histograms, labeled as Image 1, 2, 3, 4, 5, 6, 7, 8, and 9. Every method that was compared was tested in the identical conditions to guarantee study fairness. The number of evaluations was set to 2000, and the population size to 20. Every algorithm was independently tested 30 times. Additionally, to accurately assess the performance of each method at various threshold levels for IS, threshold levels were set to 15, 20, 25, and 30. The comparison algorithms included BSA [40], DE [17], GLSMA [78], IGWO [79], MDE [80], and MGSMA [81].

6.2. Metrics for performance evaluation

This paper employs three image quality evaluation metrics: Peak Signal to Noise Ratio (PSNR) [82], Structural Similarity Index (SSIM) [83], and Feature Similarity Index (FSIM) [84] to assess the quality of segmented images. The maximum value of these evaluation results represents the optimal solution.

The distinction between the segmented image and the original image is evaluated using PSNR, expressed by Eq. (40). A higher PSNR value indicates less distortion.

$$PSNR = 20 \times \log_{10} \left(\frac{255}{RMSE} \right) \quad (40)$$

$$RMSE = \sqrt{\frac{\sum_{i=0}^{M-1} \sum_{j=0}^{N-1} (I_{ij} - Seg_{ij})^2}{M \times N}} \quad (41)$$

where $RMSE$ refers to the root mean square error, defined as Eq. (41). I_{ij} stands for the pixel grayscale value of the input image, Seg_{ij} is the pixel grayscale value of the segmented image. $M \times N$ denotes the image size.

SSIM is another widely utilized objective evaluation metric that is mostly used to measure the structural integrity of images. Let I denote the original image and S denote the segmented image. The calculation

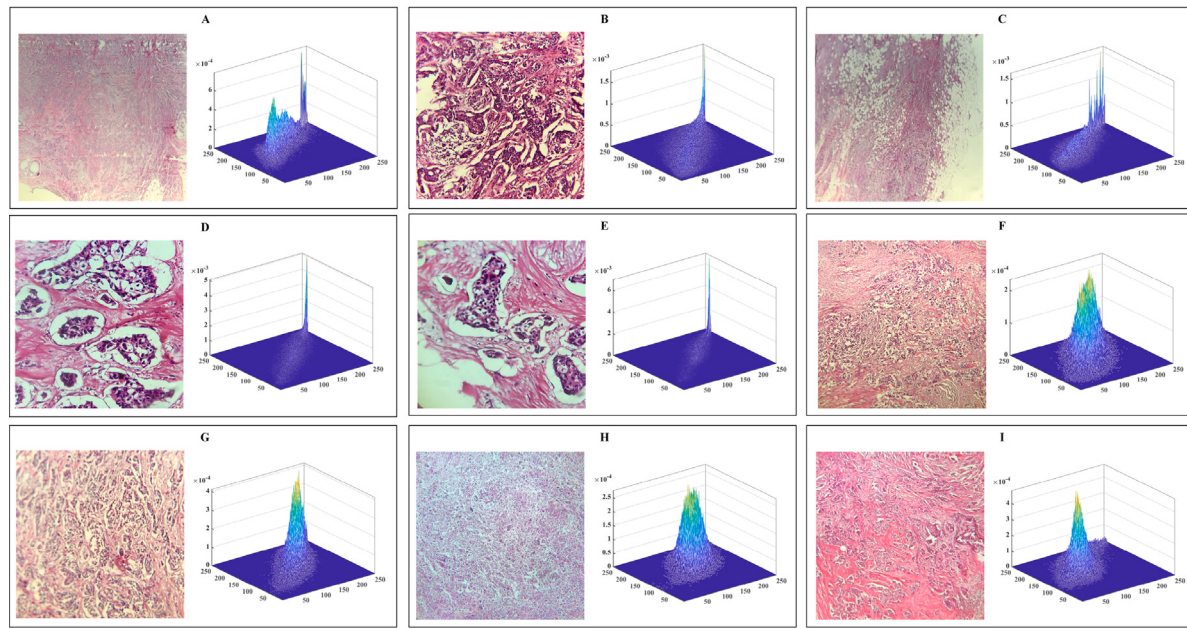


Fig. 12. The test images and corresponding histograms.

of their structural similarity is as follows:

$$SSIM = \frac{(2\mu_I\mu_S + c_1)(2\sigma_{I,S} + c_2)}{(\mu_I^2 + \mu_S^2 + c_1)(\sigma_I^2 + \sigma_S^2 + c_2)} \quad (42)$$

where the average gray level of images I and S is represented by μ_I and μ_S , respectively. The variance of images I and S is denoted by σ_I^2 and σ_S^2 , respectively. $\sigma_{I,S}$ refers to the covariance of images I and S . Two constants, c_1 and c_2 , are employed to keep the system stable.

FSIM is utilized to reflect the feature similarity, which is a variant of SSIM. It utilizes phase congruence to explain the structure in the image and gradient magnitude to capture the contrast distortion. FSIM ranges from 0 to 1, where a higher value shows that the segmented image is closer to the reference image. The definition of FSIM is given by Eqs. (43)–(46).

$$FSIM = \frac{\sum_{I \in \Omega} S_L(X)PC_m(X)}{\sum_{I \in \Omega} PC_m(X)} \quad (43)$$

$$S_L(X) = S_{PC}(X)S_G(X) \quad (44)$$

$$S_{PC}(X) = \frac{2PC_1(X)PC_2(X) + T_1}{PC_1^2(X)PC_2^2(X) + T_1} \quad (45)$$

$$S_G(X) = \frac{2G_1(X)G_2(X) + T_2}{G_1^2(X)G_2^2(X) + T_2} \quad (46)$$

$$G = \sqrt{G_x^2 + G_y^2} \quad (47)$$

$$PC(X) = \frac{E(X)}{(\varepsilon + \sum_m A_n(X))} \quad (48)$$

the test image's pixel domain is denoted by Ω . S_L represents similarity. $PC_m(X)$ denotes the phase consistency measure. To prevent the denominator from becoming 0, ε is an extremely tiny value. $E(X)$ is the response vector magnitude at location X . $A_n(X)$ is the amplitude value at location X on scale n . T_1 and T_2 are constants.

6.3. Experimental analysis of a public breast cancer dataset

To evaluate the IS performance of REBSA at various threshold levels, we selected 9 images from the public dataset for segmentation, with each image set to a size of 512×512 . Using REBSA and other comparative algorithms, segmentations were conducted at threshold levels

of 15, 20, 25, and 30. The segmentation outcomes were assessed using PSNR, SSIM, and FSIM. Further analysis of the results was conducted using Avg, Std, and WSRT ranking.

Tables 4–6 present the results of the PSNR, SSIM, and FSIM analyses, respectively. Where “Thresholds” indicates the threshold levels, “Mean” represents the average value of the overall ranking, and “Rank” represents the ranking level. The symbols “+” indicate that REBSA outperformed the comparative algorithm, “=” indicates performance equality, and “−” indicates that REBSA underperformed compared to the comparative algorithm. It is clear from the WSRT data that at all threshold levels, the segmented images obtained using the REBSA threshold sets consistently demonstrated superior performance across multiple metrics. The average value of the overall ranking is the lowest, consistently achieving first place, proving REBSA’s superiority in threshold-based IS.

Tables A.3 to A.6 in the appendix provide detailed outcomes for the average PSNR, SSIM, and FSIM metrics, along with their Std and ranking results for all methods at different threshold levels. From the data in these tables, it is evident that the images segmented using thresholds identified by REBSA achieve the best results on most images. Most FSIM values are around 0.98 or 0.99, indicating that, in terms of general characteristics, edges and textures, and structural information, the images that REBSA segmented are very close to the original images. The images segmented using REBSA also achieved high SSIM values, ranking first in most cases, demonstrating that the segmented images are very close to the original images in terms of local contrast, brightness, and structural patterns, and retain good details. Additionally, PSNR values are around 30, indicating that the segmentation results have a small error compared to the reference images, with low noise and distortion, and retain most of the original image information, meaning the image quality is high and the segmentation results are close to the reference images. In summary, the results show that the proposed REBSA method has excellent threshold searching capability and demonstrates strong stability across different threshold levels, as evidenced by the consistently low standard deviation values. Additionally, Table A.7 in the appendix shows the Renyi entropy fitness values acquired by all methods on the breast cancer pathology images. It is evident that REBSA achieved the maximum fitness values across all threshold levels and images.

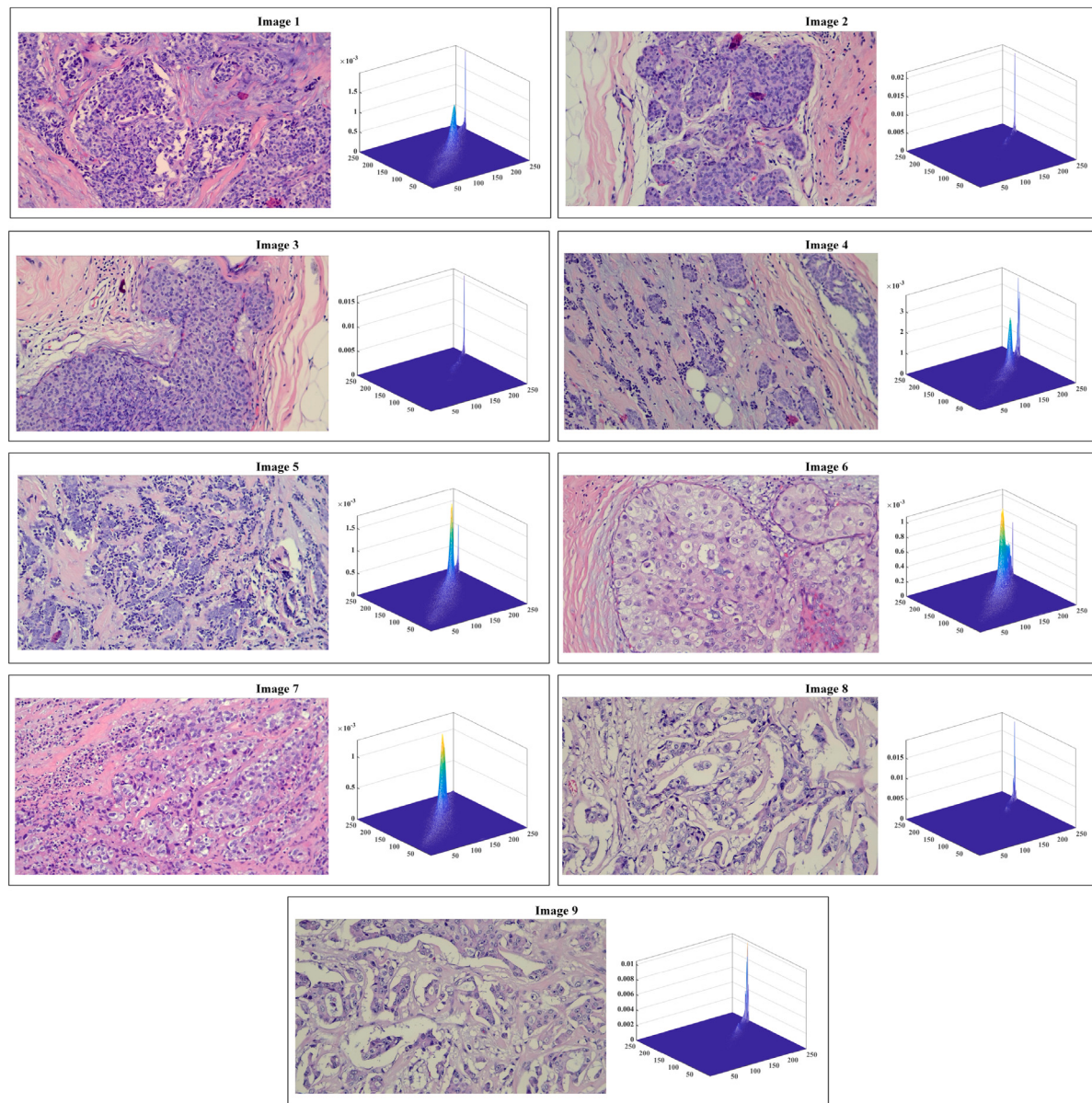


Fig. 13. The test images and corresponding histograms from hospital.

Table 4

The PSNR comparison results at different threshold level.

Thresholds	REBSA	BSA	DE	MGSMA	MDE	IGWO	GLSMA
15	+/-=	~	9/0/0	3/0/6	9/0/0	8/0/1	9/0/0
	Mean	1.2222	3.6667	1.7778	5.4444	3.3333	5.8889
	Rank	1	4	2	5	3	6
20	+/-=	~	9/0/0	2/0/7	9/0/0	8/0/1	9/0/0
	Mean	1.2222	3.5556	1.7778	5.2222	3.4444	6.0000
	Rank	1	4	2	5	3	6
25	+/-=	~	9/0/0	3/0/6	9/0/0	9/0/0	9/0/0
	Mean	1.0000	3.2222	2.0000	5.7778	3.7778	5.7778
	Rank	1	3	2	5	4	5
30	+/-=	~	9/0/0	4/0/5	9/0/0	9/0/0	9/0/0
	Mean	1.0000	3.1111	2.0000	5.8889	3.8889	6.2222
	Rank	1	3	2	5	4	7

Fig. 14 shows the convergence curves on 9 breast cancer pathology images with a threshold level of 15. Other threshold levels (20, 25, 30) are provided in the appendix as Figs. B.1–B.3. It can be observed that the REBSA method demonstrates greater convergence accuracy and faster convergence speed. During the evaluation process, REBSA exhibited excellent exploitation and the capacity to jump LO, effectively

identifying the optimal threshold sets and significantly enhancing IS results.

Fig. 15 shows the segmentation results of image E at a threshold level of 15, along with the corresponding thresholded images. It illustrates that REBSA, compared to other algorithms, produces more

Table 5
The SSIM comparison results at different threshold level.

Thresholds	REBSA	BSA	DE	MGSMA	MDE	IGWO	GLSMA
15	+/-/=	~	9/0/0	3/0/6	9/0/0	8/0/1	9/0/0
	Mean	1.2222	3.7778	1.7778	5.2222	3.2222	6.2222
	Rank	1	4	2	5	3	6
20	+/-/=	~	9/0/0	1/0/8	9/0/0	9/0/0	9/0/0
	Mean	1.0000	3.5556	2.0000	5.3333	3.4444	6.1111
	Rank	1	4	2	5	3	6
25	+/-/=	~	9/0/0	5/0/4	9/0/0	9/0/0	9/0/0
	Mean	1.0000	3.3333	2.0000	6.0000	3.6667	5.5556
	Rank	1	3	2	6	4	5
30	+/-/=	~	9/0/0	4/0/5	9/0/0	9/0/0	9/0/0
	Mean	1.0000	3.4444	2.0000	6.0000	3.5556	6.2222
	Rank	1	3	2	6	4	7

Table 6
The FSIM comparison results at different threshold level.

Thresholds	REBSA	BSA	DE	MGSMA	MDE	IGWO	GLSMA
15	+/-/=	~	9/0/0	3/0/6	9/0/0	9/0/0	9/0/0
	Mean	1.0000	3.6667	2.0000	5.3333	3.3333	6.2222
	Rank	1	4	2	5	3	6
20	+/-/=	~	9/0/0	4/0/5	9/0/0	9/0/0	9/0/0
	Mean	1.1111	4.0000	1.8889	5.6667	3.0000	6.1111
	Rank	1	4	2	5	3	6
25	+/-/=	~	9/0/0	5/0/4	9/0/0	9/0/0	9/0/0
	Mean	1.0000	3.7778	2.0000	6.1111	3.2222	5.5556
	Rank	1	4	2	6	3	5
30	+/-/=	~	9/0/0	6/0/3	9/0/0	9/0/0	9/0/0
	Mean	1.0000	3.6667	2.0000	6.0000	3.3333	5.5556
	Rank	1	4	2	6	3	5

Table 7
The PSNR comparison results at different threshold level.

Thresholds	REBSA	BSA	DE	MGSMA	MDE	IGWO	GLSMA
15	+/-/=	~	9/0/0	7/0/2	9/0/0	8/0/1	9/0/0
	Mean	1.00	3.56	2.56	5.22	2.89	6.33
	Rank	1	4	2	5	3	6
20	+/-/=	~	9/0/0	1/0/8	9/0/0	9/0/0	9/0/0
	Mean	1.22	3.11	1.78	5.78	3.89	5.89
	Rank	1	3	2	5	4	6
25	+/-/=	~	9/0/0	0/0/9	9/0/0	9/0/0	9/0/0
	Mean	1.11	3.44	1.89	5.78	3.56	6.78
	Rank	1	3	2	6	4	5
30	+/-/=	~	9/0/0	2/0/7	9/0/0	9/0/0	9/0/0
	Mean	1.11	3.22	1.89	5.89	3.78	6.00
	Rank	1	3	2	5	4	6

refined segmentation boundaries. This demonstrates REBSA's superior ability to segment images more effectively.

6.4. Experimental analysis of hospital breast cancer images

To confirm the efficacy of the REBSA in practical applications, this section selected 9 breast cancer medical images from the First Affiliated Hospital of Wenzhou Medical University, China. The image size was set to 1920×1080 , and segmentation experiments were conducted at threshold levels of 15, 20, 25, and 30.

Tables 7–9 present the PSNR, SSIM, and FSIM results using WSRT across all threshold levels. The MTIS method based on REBSA consistently achieved the highest ranking results, significantly outperforming BSA, GLSMA, IGWO, MDE, and MGSMA.

The convergence curves of many methods at the 15 threshold level are displayed in Fig. 16. It is evident that among all the algorithms, REBSA achieved the best convergence accuracy. Moreover, REBSA also demonstrated faster convergence speed, and when other algorithms gradually converged in the later iterations, REBSA, due to the introduction of the RR strategy and EQ mechanism, was able to escape local optima, finding better solutions and enabling a more comprehensive search within the solution space. The convergence curves at the other threshold levels (20, 25, 30) can be shown in the appendix in Figs. B.4–B.6.

Fig. 17 shows the segmented grayscale and jet-colored images of Image 3 at the 15 threshold level using all methods. It is evident that the segmentation method based on REBSA was able to retain more local features, display more distinct segmentation boundaries, and preserve the image information to the greatest extent.

7. Discussion

In this part, we will cover the strengths, weaknesses, and forthcoming advancements of REBSA based on all the experiments conducted in this study.

Firstly, through the diversity balance analysis, We have confirmed that the method successfully strikes a balance between local exploitation and global search. This capability indicates that REBSA has great potential in complex optimization problems, as it can avoid getting trapped in LO while precisely exploring the solution space.

Secondly, we conducted detailed experiments on the key parameter settings in the REBSA. The findings indicate that the method's performance does not significantly vary with different parameter values, demonstrating REBSA's insensitivity to parameter changes. This characteristic makes REBSA more adaptable and robust in various application scenarios, achieving good optimization results without the need for frequent parameter adjustments.

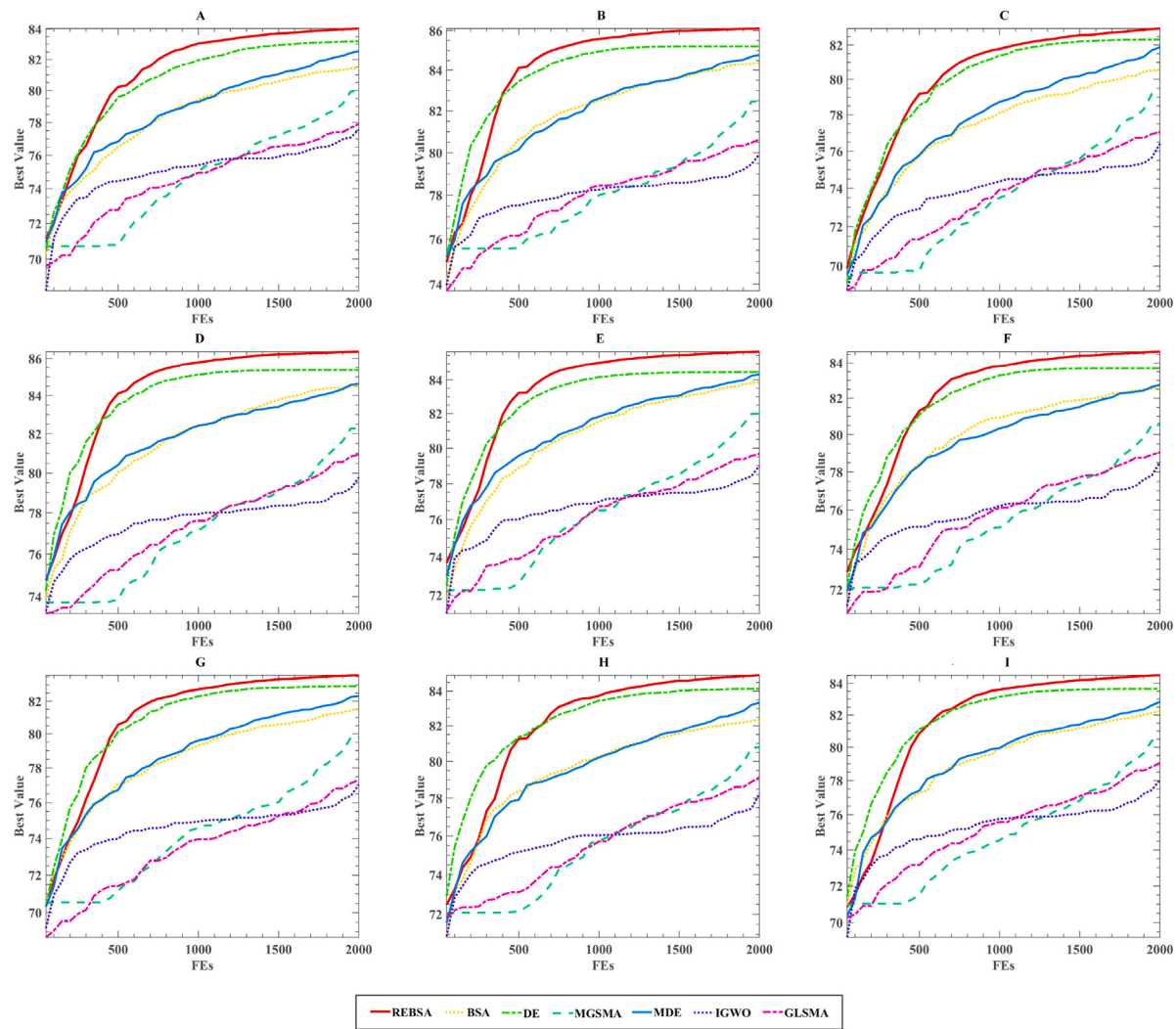


Fig. 14. Convergence curves of all competitive algorithms with threshold = 15.

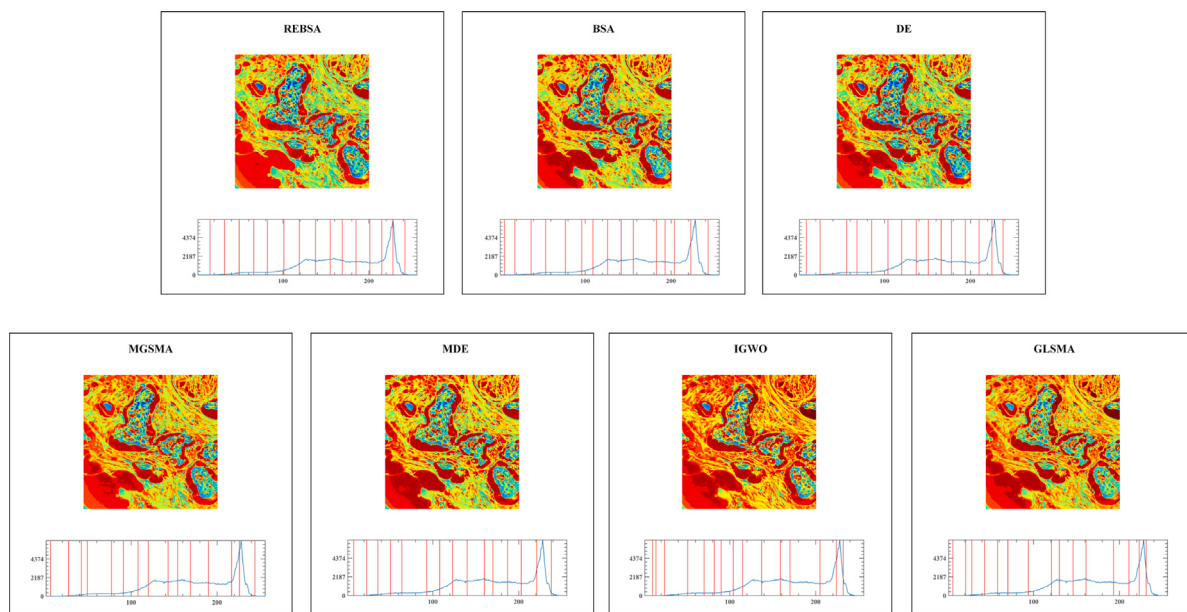


Fig. 15. Segmented results of all competitive algorithms with threshold = 15 on the image E.

Table 8
The SSIM comparison results at different threshold level.

Thresholds	REBSA	BSA	DE	MGSMA	MDE	IGWO	GLSMA
15	+/-/=	~	9/0/0	4/0/5	9/0/0	8/0/1	9/0/0
	Mean	1.00	3.56	2.44	5.11	3.11	6.67
	Rank	1	4	2	5	3	6
20	+/-/=	~	8/0/1	1/0/8	9/0/0	9/0/0	9/0/0
	Mean	1.22	3.22	1.78	5.78	3.78	5.89
	Rank	1	3	2	5	4	6
25	+/-/=	~	9/0/0	0/0/9	9/0/0	9/0/0	9/0/0
	Mean	1.11	3.56	1.89	5.56	3.44	6.78
	Rank	1	4	2	5	3	6
30	+/-/=	~	9/0/0	2/0/7	9/0/0	9/0/0	9/0/0
	Mean	1.11	3.33	1.89	6.00	3.67	5.89
	Rank	1	3	2	6	4	5

Table 9
The FSIM comparison results at different threshold level.

Thresholds	REBSA	BSA	DE	MGSMA	MDE	IGWO	GLSMA
15	+/-/=	~	8/0/1	7/0/2	9/0/0	9/0/0	9/0/0
	Mean	1.00	3.44	2.56	5.22	3.00	6.44
	Rank	1	4	2	5	3	6
20	+/-/=	~	8/0/1	2/1/6	9/0/0	9/0/0	9/0/0
	Mean	1.11	3.33	1.89	6.00	3.67	5.56
	Rank	1	3	2	6	4	5
25	+/-/=	~	9/0/0	4/0/5	9/0/0	9/0/0	9/0/0
	Mean	1.11	3.44	1.89	5.67	3.56	6.67
	Rank	1	3	2	5	4	5
30	+/-/=	~	9/0/0	3/0/6	9/0/0	9/0/0	9/0/0
	Mean	1.00	3.33	2.00	6.00	3.67	5.78
	Rank	1	3	2	6	4	5

In stability experiments, REBSA also demonstrated stable performance across optimization tasks of different dimensions. The experiments showed that REBSA provides high-quality solutions and surpasses the compared algorithms in terms of stability and optimization efficiency. This validates that in multi-dimensional optimization tasks, REBSA not only has strong optimization capabilities but also maintains stable performance in complex and variable optimization environments.

Then, to demonstrate the algorithm's superiority, we evaluated its performance on the 29 functions from CEC 2017, comparing it against several strong algorithms. These included other baseline algorithms, enhanced BSA algorithms, other improved MAs, and several champion algorithms. The experimental results consistently showed that REBSA significantly outperformed other algorithms across multiple tests, particularly excelling on composite F11–F20. The introduction of the RR strategy enhanced the algorithm's exploration capabilities, allowing REBSA to search the solution space more extensively. Meanwhile, the EQ strategy ensured that the algorithm could both exploit local regions effectively and have opportunities to escape LO. The combination of these strategies enables REBSA to perform exceptionally well on complex problems. It not only balances development and escape from LO but also further explores potential solution areas, ensuring the algorithm's stability and reliability.

Finally, To confirm the efficacy of the REBSA in practical applications, we employed Renyi entropy as the fitness function and REBSA as the search strategy for threshold search, and used the obtained optimal segmentation threshold for MIS. In the MIS experiment, it was verified that REBSA has excellent threshold search capabilities and shows a small standard deviation value at each threshold level. This is because REBSA introduces the EQ and RR methods. Among them, the EQ method can more effectively explore high-quality solutions in the solution space, making it easier for the algorithm to find the optimal segmentation threshold combination. This directly improves the accuracy of MIS and ensures that the diseased tissue area can be separated more clearly. At the same time, through more precise threshold optimization, the EQ strategy can better preserve the detailed features in pathological images, especially key areas such as tumor

boundaries, thereby providing doctors with a more reliable basis for diagnosis. In addition, medical images often have large noise and artifact interference. The RR strategy introduces new solutions, expands the coverage of the solution space, enhances the diversity, and enables the algorithm to more effectively avoid getting stuck in LO, thereby more comprehensively exploring possible threshold combinations and enhancing the applicability of segmentation results in different images. Compared to other algorithms, REBSA exhibited faster convergence rates, higher convergence accuracy, outstanding development capability, and the capacity to get away from LO. This capability enabled REBSA to identify optimal threshold sets, significantly improving the effectiveness of MIS.

However, REBSA also has its limitations. For instance, its segmentation performance at low threshold levels is not ideal, and at high threshold levels, its advantage over other algorithms diminishes as the threshold level increases. This is also an area that needs improvement going forward.

8. Conclusions and future works

This research enhanced the traditional BSA by introducing the RR method and EQ strategy, resulting in the REBSA algorithm. Traditional BSA frequently has problems such as LO trapping, premature convergence, and poor convergence accuracy in optimization problems. To address these issues, the RR strategy enhances population diversity, providing the algorithm with opportunities to escape LO. The EQ strategy improves the quality of candidate solutions while maintaining a degree of randomness, further enhancing the algorithm's performance. Experimental comparisons across 29 benchmark functions demonstrated the outstanding results of REBSA compared to other algorithms. Moreover, in the domain of medical IS, REBSA exhibited a strong capability for threshold searching. These findings indicate that REBSA excels in theoretical tests and practical applications, effectively solving problems across different scenarios.

Although REBSA has demonstrated significant advantages in experiments, there is still room for improvement. Future research can

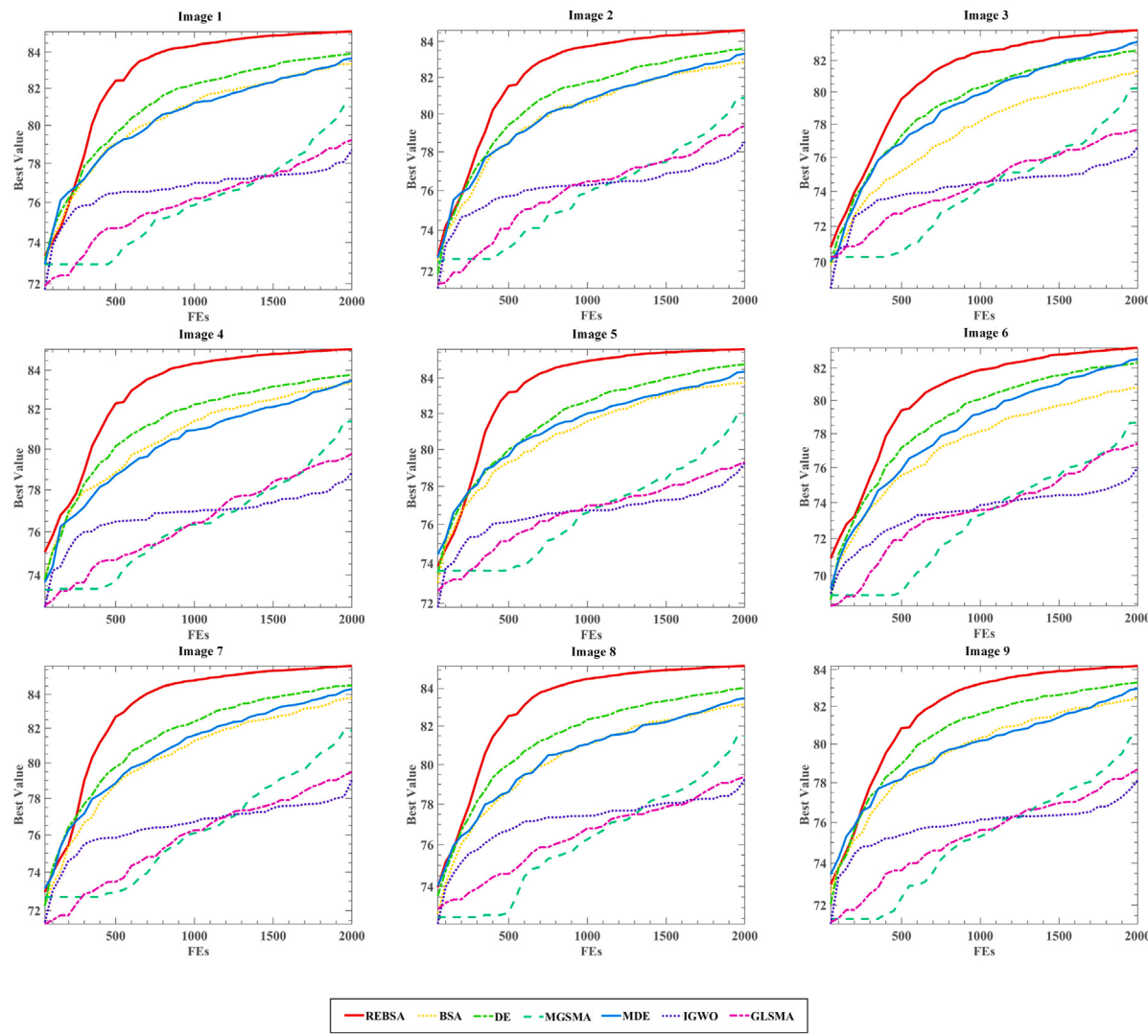


Fig. 16. Convergence curves of all competitive algorithms with threshold = 15.

focus on several areas for enhancement and expansion. Firstly, despite its superior optimization performance, REBSA's time efficiency needs improvement. Future studies could explore algorithmic structures and parallel computing techniques to reduce computational costs and enhance algorithm efficiency. Additionally, the segmentation performance of REBSA at low threshold levels could be further improved. Specialized improvements targeting this issue, such as introducing new strategies or mechanisms, could enhance REBSA's performance at low threshold levels. Furthermore, extending REBSA's application to other practical optimization problems is another avenue for improvement. Examples include feature selection, energy optimization, traffic flow optimization, financial investment optimization, and more. This would further validate REBSA's versatility and practical value. Finally, exploring hybrid strategies by combining REBSA with other excellent optimization algorithms could further enhance its performance and applicability. REBSA is poised to have a major part in a broader range of optimization problems through these improvements and expansions, becoming an efficient and stable optimization tool.

CRediT authorship contribution statement

Shiqi Xu: Writing – original draft. **Wei Jiang:** Investigation. **Yi Chen:** Methodology. **Ali Asghar Heidari:** Writing – review & editing. **Lei Liu:** Methodology. **Huiling Chen:** Funding acquisition. **Guoxi Liang:** Funding acquisition.

Declaration of Generative AI and AI-assisted technologies in the writing process

During the preparation of this work the author(s) used ChatGPT as a grammar checker in order to enhance the language and proofread the English grammar of the paper. After using this tool/service, the author(s) reviewed and edited the content as needed and take(s) full responsibility for the content of the publication.

Declaration of competing interest

The authors declare that they have no known competing financial interests or personal relationships that could have appeared to influence the work reported in this paper.

Acknowledgment

This work was supported by Zhejiang Provincial Natural Science Foundation of China (LTGY24C060004).

Appendix A

See Tables A.1–A.7.

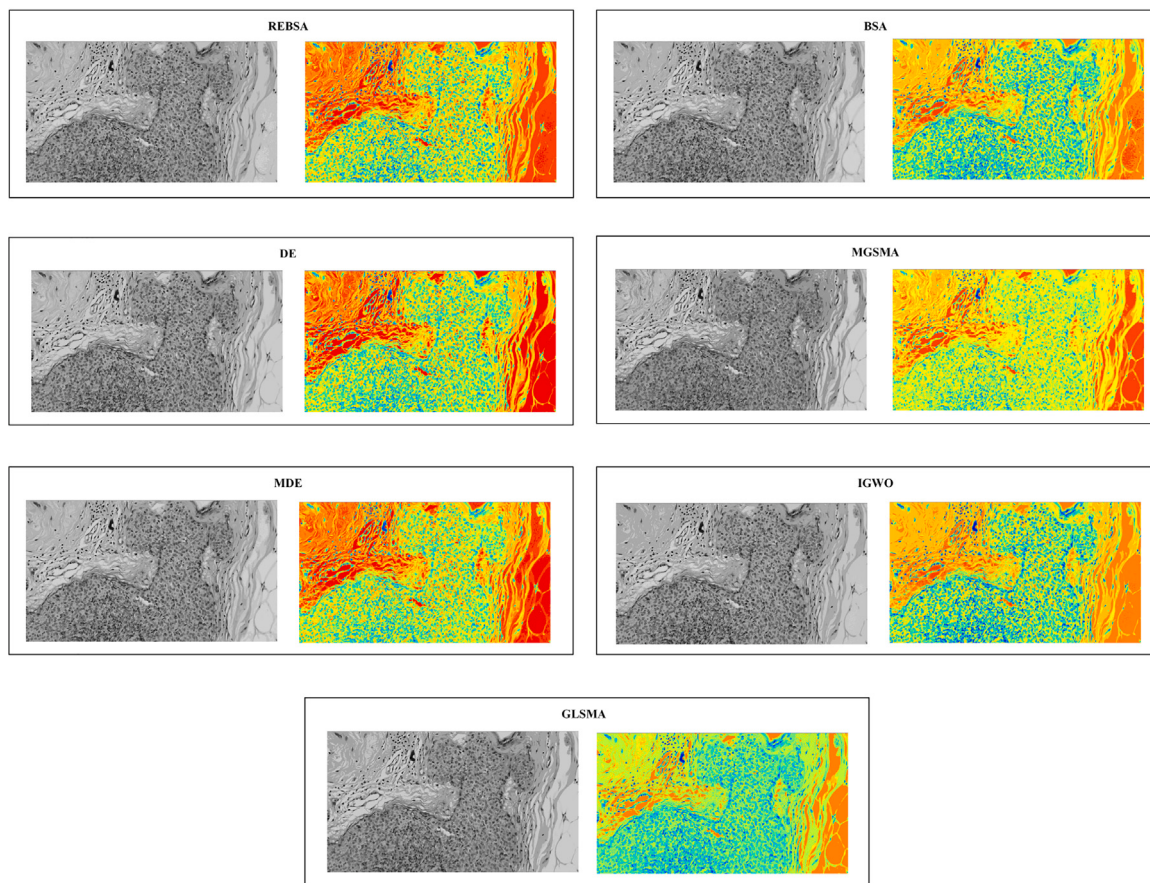


Fig. 17. Segmentation results for each method at threshold level 15 of Image 3.

Table A.1
Details of the CEC 2017.

ID	Function equation	Class	Optimum
F1	Shifted and Rotated Bent Cigar Function	Unimodal Functions	100
F3	Shifted and Rotated Zakharov Function		300
F4	Shifted and Rotated Rosenbrock's Function		400
F5	Shifted and Rotated Rastrigin's Function		500
F6	Shifted and Rotated Expanded Saffer's F6 Function		600
F7	Shifted and Rotated Lunacek Bi-Rastrigin Function	Multimodal Functions	700
F8	Shifted and Rotated Non-Continuous Rastrigin's Function		800
F9	Shifted and Rotated Lévy Function		900
F10	Shifted and Rotated Schwefel's Function		1000
F11	Hybrid Function 1 ($N = 3$)		1100
F12	Hybrid Function 2 ($N = 3$)		1200
F13	Hybrid Function 3 ($N = 3$)		1300
F14	Hybrid Function 4 ($N = 4$)		1400
F15	Hybrid Function 5 ($N = 4$)	Hybrid Functions	1500
F16	Hybrid Function 6 ($N = 4$)		1600
F17	Hybrid Function 7 ($N = 5$)		1700
F18	Hybrid Function 8 ($N = 5$)		1800
F19	Hybrid Function 9 ($N = 5$)		1900
F20	Hybrid Function 10 ($N = 6$)		2000
F21	Composition Function 1 ($N = 3$)		2100
F22	Composition Function 2 ($N = 3$)		2200
F23	Composition Function 3 ($N = 4$)		2300
F24	Composition Function 4 ($N = 4$)		2400
F25	Composition Function 5 ($N = 5$)	Composition Functions	2500
F26	Composition Function 6 ($N = 5$)		2600
F27	Composition Function 7 ($N = 6$)		2700
F28	Composition Function 8 ($N = 6$)		2800
F29	Composition Function 9 ($N = 3$)		2900
F30	Composition Function 10 ($N = 3$)		3000

Table A.2
Mean and standard deviation of REBSA and BSA on different dimensions.

Functions	Algorithm	dim = 10		dim = 30	
		Avg	Std	Avg	Std
F1	REBSA	1.0000E+02	0.0000E+00	1.0000E+02	2.1833E-13
	BSA	1.0000E+02	2.2649E-04	1.0093E+02	1.2547E+00
F3	REBSA	3.0000E+02	0.0000E+00	3.0000E+02	2.0038E-07
	BSA	3.0188E+02	3.2749E+00	5.6361E+04	1.2957E+04
F4	REBSA	4.0000E+02	0.0000E+00	4.2136E+02	2.7794E+01
	BSA	4.0058E+02	7.4823E-01	4.6962E+02	1.7995E+01
F5	REBSA	5.0484E+02	2.1345E+00	5.7689E+02	1.4898E+01
	BSA	5.0528E+02	1.5060E+00	5.6417E+02	6.8259E+00
F6	REBSA	6.0000E+02	0.0000E+00	6.0001E+02	5.3733E-03
	BSA	6.0000E+02	2.9856E-14	6.0000E+02	9.6743E-14
F7	REBSA	7.1489E+02	2.2060E+00	7.9539E+02	1.3178E+01
	BSA	7.1517E+02	2.2779E+00	7.9379E+02	1.1035E+01
F8	REBSA	8.0541E+02	2.7613E+00	8.7242E+02	1.2120E+01
	BSA	8.0601E+02	2.2612E+00	8.6686E+02	1.0644E+01
F9	REBSA	9.0000E+02	0.0000E+00	9.8247E+02	1.1343E+02
	BSA	9.0000E+02	0.0000E+00	1.1244E+03	1.7181E+02
F10	REBSA	1.1671E+03	8.3942E+01	3.4595E+03	3.7309E+02
	BSA	1.1808E+03	8.8423E+01	3.3288E+03	2.9829E+02
F11	REBSA	1.1006E+03	8.5711E-01	1.1293E+03	1.5434E+01
	BSA	1.1016E+03	7.1410E-01	1.1274E+03	6.8511E+00
F12	REBSA	1.2006E+03	2.0541E+00	1.4003E+04	7.9599E+03
	BSA	2.3982E+03	1.0610E+03	5.6409E+05	3.1141E+05
F13	REBSA	1.3029E+03	1.8684E+00	1.3786E+03	7.3944E+01
	BSA	1.3055E+03	1.4009E+00	7.5055E+03	4.8118E+03
F14	REBSA	1.4006E+03	6.7126E-01	1.4293E+03	1.2276E+01
	BSA	1.4008E+03	5.6392E-01	1.8920E+04	1.1752E+04
F15	REBSA	1.5001E+03	2.5153E-01	1.5192E+03	1.2459E+01
	BSA	1.5004E+03	4.0583E-01	3.8170E+03	1.7758E+03
F16	REBSA	1.6054E+03	2.2472E+01	2.0989E+03	1.2636E+02
	BSA	1.6010E+03	2.1187E+00	2.2345E+03	1.4579E+02
F17	REBSA	1.7027E+03	5.7222E+00	1.7732E+03	5.0660E+01
	BSA	1.7004E+03	3.5069E-01	1.8580E+03	7.1961E+01
F18	REBSA	1.8000E+03	7.1991E-02	2.2931E+03	5.7550E+02
	BSA	1.8000E+03	3.3209E-02	3.0813E+05	1.5448E+05
F19	REBSA	1.9000E+03	9.0879E-03	1.9114E+03	3.2763E+00
	BSA	1.9000E+03	1.0225E-02	3.6175E+03	1.3799E+03
F20	REBSA	2.0002E+03	2.6725E-01	2.1295E+03	6.1852E+01
	BSA	2.0000E+03	2.6363E-04	2.1840E+03	9.5557E+01
F21	REBSA	2.2144E+03	3.7362E+01	2.3505E+03	3.1566E+01
	BSA	2.2134E+03	2.7372E+01	2.3694E+03	1.1138E+01
F22	REBSA	2.2980E+03	1.1856E+01	2.4626E+03	6.4492E+02
	BSA	2.2574E+03	3.2141E+01	2.8231E+03	1.0282E+03
F23	REBSA	2.6067E+03	2.5787E+00	2.6968E+03	1.2526E+01
	BSA	2.6094E+03	1.9123E+00	2.7170E+03	1.1779E+01
F24	REBSA	2.6654E+03	1.1014E+02	2.8733E+03	1.4238E+01
	BSA	2.5464E+03	7.8719E+01	2.9225E+03	1.6605E+01
F25	REBSA	2.9009E+03	1.1547E+01	2.8843E+03	1.8697E+00
	BSA	2.8295E+03	1.1397E+02	2.8860E+03	1.4171E+00
F26	REBSA	2.8700E+03	7.9438E+01	3.5352E+03	7.0195E+02
	BSA	2.7889E+03	9.9946E+01	3.7747E+03	7.0785E+02
F27	REBSA	3.0892E+03	5.5983E-01	3.2035E+03	8.3947E+00
	BSA	3.0889E+03	7.1305E-01	3.2114E+03	6.2065E+00
F28	REBSA	3.1127E+03	5.4142E+01	3.1035E+03	1.9365E+01
	BSA	3.0891E+03	1.0120E+02	3.2070E+03	5.1017E+00
F29	REBSA	3.1374E+03	5.6260E+00	3.4100E+03	5.2268E+01
	BSA	3.1459E+03	6.4163E+00	3.5127E+03	9.0077E+01
F30	REBSA	3.4135E+03	3.1433E+01	5.4791E+03	3.8631E+02
	BSA	1.0564E+04	1.1159E+04	1.0266E+04	2.4691E+03
Functions	Algorithm	dim = 50		dim = 100	
		Avg	Std	Avg	Std
F1	REBSA	1.0000E+02	9.7162E-13	1.0000E+02	9.7162E-13
	BSA	1.0498E+02	1.2965E+01	1.0498E+02	1.2965E+01
F3	REBSA	3.0000E+02	2.0477E-09	3.0000E+02	2.0477E-09
	BSA	5.7160E+04	1.1986E+04	5.7160E+04	1.1986E+04
F4	REBSA	4.1626E+02	2.4212E+01	4.1626E+02	2.4212E+01
	BSA	4.6414E+02	2.1358E+01	4.6414E+02	2.1358E+01
F5	REBSA	5.8068E+02	1.3197E+01	5.8068E+02	1.3197E+01
	BSA	5.6214E+02	1.1801E+01	5.6214E+02	1.1801E+01
F6	REBSA	6.0001E+02	5.2560E-03	6.0001E+02	5.2560E-03
	BSA	6.0000E+02	1.0125E-13	6.0000E+02	1.0125E-13
F7	REBSA	7.9572E+02	1.6187E+01	7.9572E+02	1.6187E+01
	BSA	7.9145E+02	9.5611E+00	7.9145E+02	9.5611E+00

(continued on next page)

Table A.2 (continued).

F8	REBSA	8.7184E+02	1.0736E+01	8.7184E+02	1.0736E+01
	BSA	8.7044E+02	9.5041E+00	8.7044E+02	9.5041E+00
F9	REBSA	9.7831E+02	7.3057E+01	9.7831E+02	7.3057E+01
	BSA	1.0783E+03	1.0613E+02	1.0783E+03	1.0613E+02
F10	REBSA	3.4523E+03	3.2753E+02	3.4523E+03	3.2753E+02
	BSA	3.2889E+03	2.9814E+02	3.2889E+03	2.9814E+02
F11	REBSA	1.1297E+03	1.6323E+01	1.1297E+03	1.6323E+01
	BSA	1.1261E+03	7.2508E+00	1.1261E+03	7.2508E+00
F12	REBSA	9.5996E+03	6.4764E+03	9.5996E+03	6.4764E+03
	BSA	7.4180E+05	3.8359E+05	7.4180E+05	3.8359E+05
F13	REBSA	1.3668E+03	3.8608E+01	1.3668E+03	3.8608E+01
	BSA	9.5096E+03	7.4881E+03	9.5096E+03	7.4881E+03
F14	REBSA	1.4310E+03	9.4509E+00	1.4310E+03	9.4509E+00
	BSA	2.2302E+04	1.1201E+04	2.2302E+04	1.1201E+04
F15	REBSA	1.5167E+03	6.8576E+00	1.5167E+03	6.8576E+00
	BSA	3.4802E+03	2.1961E+03	3.4802E+03	2.1961E+03
F16	REBSA	2.0885E+03	1.7601E+02	2.0885E+03	1.7601E+02
	BSA	2.1985E+03	1.5792E+02	2.1985E+03	1.5792E+02
F17	REBSA	1.7807E+03	6.2536E+01	1.7807E+03	6.2536E+01
	BSA	1.8573E+03	5.5008E+01	1.8573E+03	5.5008E+01
F18	REBSA	1.8992E+03	6.6178E+01	1.8992E+03	6.6178E+01
	BSA	2.8757E+05	1.4990E+05	2.8757E+05	1.4990E+05
F19	REBSA	1.9116E+03	4.0907E+00	1.9116E+03	4.0907E+00
	BSA	3.2881E+03	1.3922E+03	3.2881E+03	1.3922E+03
F20	REBSA	2.1417E+03	7.5075E+01	2.1417E+03	7.5075E+01
	BSA	2.1882E+03	6.7846E+01	2.1882E+03	6.7846E+01
F21	REBSA	2.3562E+03	1.1414E+01	2.3562E+03	1.1414E+01
	BSA	2.3658E+03	2.6033E+01	2.3658E+03	2.6033E+01
F22	REBSA	2.5929E+03	8.9899E+02	2.5929E+03	8.9899E+02
	BSA	3.0041E+03	1.1675E+03	3.0041E+03	1.1675E+03
F23	REBSA	2.6995E+03	1.1916E+01	2.6995E+03	1.1916E+01
	BSA	2.7197E+03	1.1973E+01	2.7197E+03	1.1973E+01
F24	REBSA	2.8842E+03	1.8339E+01	2.8842E+03	1.8339E+01
	BSA	2.9198E+03	2.3477E+01	2.9198E+03	2.3477E+01
F25	REBSA	2.8842E+03	1.6955E+00	2.8842E+03	1.6955E+00
	BSA	2.8855E+03	1.3242E+00	2.8855E+03	1.3242E+00
F26	REBSA	3.6038E+03	6.8642E+02	3.6038E+03	6.8642E+02
	BSA	3.6003E+03	7.2050E+02	3.6003E+03	7.2050E+02
F27	REBSA	3.2047E+03	7.0200E+00	3.2047E+03	7.0200E+00
	BSA	3.2085E+03	7.7618E+00	3.2085E+03	7.7618E+00
F28	REBSA	3.1142E+03	3.6810E+01	3.1142E+03	3.6810E+01
	BSA	3.2073E+03	4.9333E+00	3.2073E+03	4.9333E+00
F29	REBSA	3.3794E+03	4.7622E+01	3.3794E+03	4.7622E+01
	BSA	3.5118E+03	8.0212E+01	3.5118E+03	8.0212E+01
F30	Avg	5.1575E+03	1.4109E+02	5.1575E+03	1.4109E+02
	Std	1.0795E+04	2.1267E+03	1.0795E+04	2.1267E+03

Table A.3

The Avg and Std results of PSNR, SSIM, and FSIM with threshold = 15.

Image	Paradigm	REBSA	BSA	DE	MGSMA	MDE	IGWO	GLSMA
A	PSNR	Avg	2.8021E+01	2.7148E+01	2.7748E+01	2.5678E+01	2.7289E+01	2.5623E+01
		Std	1.2480E+00	1.3750E+00	1.3293E+00	2.2778E+00	1.5282E+00	2.8188E+00
		Rank	1	4	2	6	3	5
B	PSNR	Avg	2.8932E+01	2.7718E+01	2.8523E+01	2.6103E+01	2.7829E+01	2.5432E+01
		Std	4.0164E-01	7.0427E-01	5.3073E-01	1.4795E+00	6.3852E-01	1.1290E+00
		Rank	1	4	2	5	3	7
C	PSNR	Avg	2.7557E+01	2.6866E+01	2.7668E+01	2.5177E+01	2.6840E+01	2.4679E+01
		Std	7.9764E-01	1.2721E+00	1.1613E+00	1.9685E+00	1.1458E+00	2.1577E+00
		Rank	2	3	1	5	4	6
D	PSNR	Avg	2.8804E+01	2.7488E+01	2.8474E+01	2.6023E+01	2.7377E+01	2.5629E+01
		Std	5.1972E-01	1.0055E+00	8.6724E-01	1.4204E+00	8.8310E-01	1.7604E+00
		Rank	1	3	2	5	4	6
E	PSNR	Avg	2.8738E+01	2.7608E+01	2.8430E+01	2.6396E+01	2.7842E+01	2.5572E+01
		Std	4.8234E-01	1.0917E+00	7.7690E-01	1.3252E+00	9.3420E-01	1.4854E+00
		Rank	1	4	2	5	3	7
F	PSNR	Avg	2.8629E+01	2.7418E+01	2.8305E+01	2.5510E+01	2.7633E+01	2.5961E+01
		Std	5.2867E-01	1.0446E+00	6.4756E-01	1.6624E+00	8.8030E-01	1.6942E+00
		Rank	1	4	2	6	3	5
G	PSNR	Avg	2.8831E+01	2.7724E+01	2.8796E+01	2.6087E+01	2.8085E+01	2.5784E+01
		Std	9.1429E-01	1.1064E+00	9.5715E-01	2.2117E+00	8.9050E-01	1.9155E+00
		Rank	1	4	2	5	3	7
H	PSNR	Avg	2.8651E+01	2.7922E+01	2.8920E+01	2.6012E+01	2.7868E+01	2.6184E+01
		Std	8.6209E-01	1.3665E+00	1.1564E+00	2.1804E+00	1.0435E+00	2.4489E+00
		Rank	2	3	1	7	4	6
I	PSNR	Avg	2.8624E+01	2.7301E+01	2.7880E+01	2.6107E+01	2.7330E+01	2.5998E+01
		Std	6.6499E-01	1.3646E+00	1.1219E+00	1.5735E+00	1.0758E+00	1.5134E+00
		Rank	1	4	2	5	3	7

(continued on next page)

Table A.3 (continued).

Image	Paradigm	REBSA	BSA	DE	MGSMA	MDE	IGWO	GLSMA
A	Avg	8.9114E-01	8.6811E-01	8.8575E-01	8.3509E-01	8.7375E-01	8.3160E-01	8.3465E-01
	Std	2.3741E-02	3.3079E-02	2.9363E-02	5.6930E-02	3.4051E-02	7.8222E-02	5.2733E-02
	Rank	1 4	2	5	3	7	6	
B	Avg	9.8168E-01	9.7491E-01	9.7935E-01	9.6465E-01	9.7600E-01	9.5879E-01	9.6237E-01
	Std	1.8922E-03	5.2139E-03	3.3914E-03	1.4670E-02	5.1359E-03	9.3885E-03	2.4366E-02
	Rank	1 4	2	5	3	7	6	
C	Avg	9.1073E-01	8.9786E-01	9.1086E-01	8.6617E-01	8.9545E-01	8.5264E-01	8.4828E-01
	Std	1.2597E-02	2.1111E-02	1.9441E-02	4.4106E-02	2.3771E-02	4.9839E-02	6.2201E-02
	Rank	2 3	1	5	4	6	7	
D	Avg	9.5630E-01	9.4414E-01	9.5250E-01	9.2869E-01	9.4147E-01	9.2471E-01	9.2343E-01
	Std	8.9569E-03	1.0449E-02	1.2346E-02	1.9391E-02	1.1777E-02	2.7866E-02	2.4948E-02
	Rank	1 3	2	5	4	6	7	
E	Avg	9.4687E-01	9.3185E-01	9.4320E-01	9.1691E-01	9.3483E-01	9.0298E-01	9.0099E-01
	Std	5.4941E-03	1.6370E-02	9.8183E-03	2.3252E-02	1.2385E-02	2.7908E-02	2.9853E-02
	Rank	1 4	2	5	3	6	7	
F	Avg	9.7997E-01	9.7027E-01	9.7745E-01	9.4985E-01	9.7156E-01	9.5281E-01	9.4694E-01
	Std	2.6043E-03	8.9684E-03	3.8491E-03	1.9348E-02	7.5483E-03	2.9329E-02	1.9997E-02
	Rank	1 4	2	6	3	5	7	
G	Avg	9.5487E-01	9.3817E-01	9.5315E-01	9.0927E-01	9.4463E-01	9.0660E-01	9.0194E-01
	Std	1.0453E-02	1.6528E-02	1.0033E-02	4.4959E-02	1.2425E-02	3.9147E-02	4.0465E-02
	Rank	1 4	2	5	3	6	7	
H	Avg	9.7721E-01	9.6825E-01	9.7726E-01	9.4588E-01	9.6971E-01	9.4481E-01	9.5298E-01
	Std	5.0712E-03	1.1055E-02	7.4522E-03	3.6364E-02	8.8057E-03	4.9020E-02	2.4383E-02
	Rank	2 4	1	6	3	7	5	
I	Avg	9.6504E-01	9.4758E-01	9.5631E-01	9.3278E-01	9.5040E-01	9.2963E-01	9.1572E-01
	Std	5.4631E-03	2.2745E-02	1.1933E-02	2.7885E-02	1.3276E-02	2.0977E-02	4.2721E-02
	Rank	1 4	2	5	3	6	7	
A	Avg	9.7701E-01	9.6368E-01	9.7348E-01	9.4010E-01	9.6740E-01	9.3424E-01	9.3844E-01
	Std	7.5475E-03	1.6331E-02	1.0065E-02	3.2599E-02	1.3739E-02	4.5313E-02	2.6639E-02
	Rank	1 4	2	5	3	7	6	
B	Avg	9.9439E-01	9.9191E-01	9.9277E-01	9.8841E-01	9.9147E-01	9.8235E-01	9.8590E-01
	Std	9.6020E-04	3.0666E-03	2.3895E-03	5.5783E-03	4.5232E-03	1.0097E-02	1.4487E-02
	Rank	1 3	2	5	4	7	6	
C	Avg	9.8118E-01	9.7188E-01	9.7900E-01	9.5072E-01	9.7185E-01	9.4076E-01	9.4292E-01
	Std	5.8634E-03	1.3477E-02	1.1657E-02	3.1910E-02	1.5321E-02	3.9991E-02	4.5830E-02
	Rank	1 3	2	5	4	7	6	
D	Avg	9.8733E-01	9.8233E-01	9.8459E-01	9.7356E-01	9.8143E-01	9.7197E-01	9.7264E-01
	Std	8.1471E-03	7.6116E-03	1.0739E-02	1.5606E-02	8.2633E-03	1.4882E-02	1.7890E-02
	Rank	1 3	2	5	4	7	6	
E	Avg	9.8479E-01	9.7883E-01	9.8268E-01	9.6856E-01	9.7883E-01	9.5732E-01	9.5558E-01
	Std	2.8755E-03	6.9341E-03	4.3883E-03	1.1960E-02	8.3359E-03	2.4712E-02	2.2404E-02
	Rank	1 4	2	5	3	6	7	
F	Avg	9.9595E-01	9.9201E-01	9.9549E-01	9.8464E-01	9.9442E-01	9.8685E-01	9.8357E-01
	Std	1.4135E-03	6.3716E-03	1.0955E-03	1.1404E-02	1.9833E-03	1.3317E-02	1.2830E-02
	Rank	1 4	2	6	3	5	7	
G	Avg	9.9307E-01	9.8704E-01	9.9147E-01	9.7066E-01	9.8966E-01	9.7140E-01	9.6958E-01
	Std	3.0295E-03	8.3819E-03	3.7635E-03	2.3830E-02	4.2017E-03	2.6900E-02	2.3060E-02
	Rank	1 4	2	6	3	5	7	
H	Avg	9.9521E-01	9.9244E-01	9.9495E-01	9.8424E-01	9.9337E-01	9.8326E-01	9.8412E-01
	Std	1.3968E-03	4.1609E-03	1.8555E-03	1.6158E-02	2.6062E-03	1.6780E-02	1.4438E-02
	Rank	1 4	2	5	3	7	6	
I	Avg	9.9378E-01	9.8583E-01	9.9178E-01	9.7999E-01	9.8752E-01	9.8154E-01	9.7131E-01
	Std	1.5244E-03	8.7446E-03	3.2659E-03	1.0564E-02	5.3165E-03	1.3934E-02	2.3755E-02
	Rank	1 4	2	6	3	5	7	

Table A.4

The Avg and Std results of PSNR, SSIM, and FSIM with threshold = 20.

Image	Paradigm	REBSA	BSA	DE	MGSMA	MDE	IGWO	GLSMA
A	Avg	3.0050E+01	2.8661E+01	2.9720E+01	2.7427E+01	2.9162E+01	2.7182E+01	2.6877E+01
	Std	1.3354E+00	1.3305E+00	1.7440E+00	2.1359E+00	1.4998E+00	2.0803E+00	2.3683E+00
	Rank	1 4	2	5	3	6	7	
B	Avg	3.1246E+01	2.9366E+01	3.0829E+01	2.7782E+01	2.9573E+01	2.7500E+01	2.7490E+01
	Std	3.2965E-01	1.1096E+00	5.2618E-01	1.3427E+00	6.1009E-01	1.2356E+00	1.3015E+00
	Rank	1 4	2	5	3	6	7	
C	Avg	3.0008E+01	2.8847E+01	2.9772E+01	2.7746E+01	2.8783E+01	2.5895E+01	2.6248E+01
	Std	9.0310E-01	1.3066E+00	1.3519E+00	1.8580E+00	1.0062E+00	1.8558E+00	1.9496E+00
	Rank	1 3	2	5	4	7	6	
D	Avg	3.1022E+01	2.9709E+01	3.0543E+01	2.7812E+01	2.9425E+01	2.7739E+01	2.7354E+01
	Std	6.8643E-01	1.0544E+00	7.5339E-01	1.6507E+00	9.2228E-01	1.3055E+00	1.8337E+00
	Rank	1 3	2	5	4	6	7	
E	Avg	3.0715E+01	2.9470E+01	3.0820E+01	2.8009E+01	2.9305E+01	2.7267E+01	2.7977E+01
	Std	7.3964E-01	1.1966E+00	7.0550E-01	1.5944E+00	9.7386E-01	1.8624E+00	1.4244E+00
	Rank	2 3	1	5	4	7	6	
F	Avg	3.0725E+01	2.9735E+01	3.0806E+01	2.7149E+01	2.9696E+01	2.8236E+01	2.6816E+01
	Std	5.0682E-01	7.9063E-01	9.0707E-01	2.1922E+00	8.6545E-01	1.5260E+00	1.9763E+00
	Rank	2 3	1	6	4	5	7	
G	Avg	3.0815E+01	2.9544E+01	3.0752E+01	2.7357E+01	2.9884E+01	2.7430E+01	2.6975E+01
	Std	6.7647E-01	1.0294E+00	1.1910E+00	2.5086E+00	7.5037E-01	1.8999E+00	2.1979E+00
	Rank	1 4	2	6	3	5	7	
H	Avg	3.1027E+01	2.9494E+01	3.0675E+01	2.7415E+01	2.9901E+01	2.7356E+01	2.7290E+01
	Std	9.2271E-01	9.7622E-01	1.4414E+00	1.9547E+00	8.8224E-01	2.3239E+00	1.9123E+00
	Rank	1 4	2	5	3	6	7	

(continued on next page)

Table A.4 (continued).

Image	Paradigm	REBSA	BSA	DE	MGSMA	MDE	IGWO	GLSMA
I	Avg	3.0503E+01	2.9230E+01	3.0096E+01	2.7410E+01	2.9430E+01	2.7337E+01	2.6702E+01
	Std	9.5284E-01	1.0692E+00	9.8279E-01	2.1806E+00	1.1127E+00	2.0588E+00	2.4528E+00
	Rank	1	4	2	5	3	6	7
A	Avg	9.2258E-01	8.9626E-01	9.1423E-01	8.6690E-01	9.0393E-01	8.6318E-01	8.5752E-01
	Std	1.9010E-02	2.4794E-02	2.8208E-02	4.7617E-02	2.7079E-02	4.9951E-02	5.2102E-02
	Rank	1	4	2	5	3	6	7
B	Avg	9.8824E-01	9.8122E-01	9.8651E-01	9.7266E-01	9.8214E-01	9.7113E-01	9.7096E-01
	Std	1.1908E-03	4.9350E-03	2.3161E-03	8.9315E-03	3.2530E-03	8.9208E-03	9.7003E-03
	Rank	1	4	2	5	3	6	7
C	Avg	9.3995E-01	9.2231E-01	9.3546E-01	9.0649E-01	9.2149E-01	8.7646E-01	8.8313E-01
	Std	9.8672E-03	1.8330E-02	1.8087E-02	3.0095E-02	1.5058E-02	3.6885E-02	3.8284E-02
	Rank	1	3	2	5	4	7	6
D	Avg	9.6908E-01	9.5881E-01	9.6642E-01	9.4676E-01	9.5868E-01	9.4409E-01	9.4126E-01
	Std	6.2821E-03	1.2026E-02	5.5005E-03	1.4071E-02	8.5393E-03	1.3792E-02	2.0683E-02
	Rank	1	3	2	5	4	6	7
E	Avg	9.6084E-01	9.5037E-01	9.5998E-01	9.3486E-01	9.4930E-01	9.2817E-01	9.3266E-01
	Std	6.4044E-03	9.9152E-03	7.1281E-03	1.7069E-02	1.1661E-02	2.3407E-02	1.9726E-02
	Rank	1	3	2	5	4	7	6
F	Avg	9.8661E-01	9.8110E-01	9.8615E-01	9.6039E-01	9.8075E-01	9.7137E-01	9.5898E-01
	Std	1.9752E-03	3.6602E-03	3.7477E-03	2.4296E-02	5.2311E-03	1.2816E-02	2.1668E-02
	Rank	1	3	2	6	4	5	7
G	Avg	9.6852E-01	9.5533E-01	9.6582E-01	9.2170E-01	9.5941E-01	9.2916E-01	9.1769E-01
	Std	5.1496E-03	1.1448E-02	1.3441E-02	4.9835E-02	8.7493E-03	2.7252E-02	3.8091E-02
	Rank	1	4	2	6	3	5	7
H	Avg	9.8601E-01	9.7666E-01	9.8311E-01	9.5862E-01	9.7945E-01	9.5390E-01	9.5866E-01
	Std	3.3328E-03	6.5388E-03	7.1156E-03	1.9999E-02	5.7736E-03	2.9266E-02	1.8320E-02
	Rank	1	4	2	6	3	7	5
I	Avg	9.7523E-01	9.6439E-01	9.7175E-01	9.4053E-01	9.6562E-01	9.4003E-01	9.2998E-01
	Std	6.5929E-03	9.2666E-03	7.9178E-03	3.5656E-02	1.0422E-02	3.1499E-02	5.3716E-02
	Rank	1	4	2	5	3	6	7
A	Avg	9.8407E-01	9.7307E-01	9.7929E-01	9.5266E-01	9.7563E-01	9.5180E-01	9.5110E-01
	Std	6.3105E-03	1.2636E-02	1.1788E-02	2.8566E-02	1.2942E-02	2.6626E-02	3.1977E-02
	Rank	1	4	2	5	3	6	7
B	Avg	9.9633E-01	9.9355E-01	9.9549E-01	9.8897E-01	9.9439E-01	9.8822E-01	9.8940E-01
	Std	9.8776E-04	4.7684E-03	2.0650E-03	7.3094E-03	2.1349E-03	7.0677E-03	6.5421E-03
	Rank	1	4	2	6	3	7	5
C	Avg	9.8899E-01	9.8050E-01	9.8575E-01	9.7199E-01	9.8192E-01	9.5531E-01	9.5863E-01
	Std	3.6365E-03	8.9370E-03	8.6369E-03	1.4881E-02	6.9125E-03	2.3928E-02	2.1481E-02
	Rank	1	4	2	5	3	7	6
D	Avg	9.9048E-01	9.8667E-01	9.8921E-01	9.7988E-01	9.8735E-01	9.8094E-01	9.7894E-01
	Std	5.2792E-03	8.0278E-03	4.0310E-03	1.0345E-02	4.8895E-03	8.9601E-03	1.5531E-02
	Rank	1	4	2	6	3	5	7
E	Avg	9.8820E-01	9.8215E-01	9.8857E-01	9.7658E-01	9.8315E-01	9.7105E-01	9.7750E-01
	Std	5.0659E-03	8.6001E-03	3.4270E-03	1.3316E-02	6.0423E-03	1.5737E-02	8.4919E-03
	Rank	2	4	1	6	3	7	5
F	Avg	9.9768E-01	9.9623E-01	9.9731E-01	9.8906E-01	9.9627E-01	9.9219E-01	9.8955E-01
	Std	8.9179E-04	1.5968E-03	9.1083E-04	9.3035E-03	1.2238E-03	5.0419E-03	8.5389E-03
	Rank	1	4	2	7	3	5	6
G	Avg	9.9472E-01	9.9175E-01	9.9349E-01	9.7808E-01	9.9217E-01	9.7920E-01	9.7723E-01
	Std	3.1273E-03	4.3352E-03	4.2192E-03	2.0264E-02	4.8195E-03	1.5274E-02	1.4121E-02
	Rank	1	4	2	6	3	5	7
H	Avg	9.9717E-01	9.9457E-01	9.9666E-01	9.8857E-01	9.9558E-01	9.8535E-01	9.8811E-01
	Std	8.1425E-04	2.2854E-03	1.5216E-03	7.0839E-03	1.5735E-03	1.7693E-02	7.4404E-03
	Rank	1	4	2	5	3	7	6
I	Avg	9.9560E-01	9.9076E-01	9.9347E-01	9.8405E-01	9.9297E-01	9.8374E-01	9.7978E-01
	Std	1.4230E-03	5.4275E-03	3.4903E-03	1.2180E-02	2.7666E-03	1.2496E-02	2.2488E-02

Table A.5

The Avg and Std results of PSNR, SSIM, and FSIM with threshold = 25.

Image	Paradigm	REBSA	BSA	DE	MGSMA	MDE	IGWO	GLSMA
A	Avg	3.2383E+01	3.0557E+01	3.1614E+01	2.8451E+01	3.0690E+01	2.9086E+01	2.8113E+01
	Std	1.2862E+00	1.6802E+00	1.1911E+00	2.3682E+00	1.6022E+00	1.8325E+00	2.1493E+00
	Rank	1	4	2	6	3	5	7
B	Avg	3.2885E+01	3.1137E+01	3.2120E+01	2.8803E+01	3.1006E+01	2.8778E+01	2.8714E+01
	Std	3.9662E-01	9.7914E-01	9.1217E-01	1.6193E+00	1.0967E+00	1.2854E+00	1.4992E+00
	Rank	1	3	2	5	4	6	7
C	Avg	3.2100E+01	3.0503E+01	3.1649E+01	2.8390E+01	3.0476E+01	2.8023E+01	2.8337E+01
	Std	5.7830E-01	9.1085E-01	1.1489E+00	1.8086E+00	1.0893E+00	1.9055E+00	2.3867E+00
	Rank	1	3	2	5	4	7	6
D	Avg	3.2818E+01	3.1273E+01	3.2434E+01	2.8959E+01	3.1271E+01	2.8816E+01	2.8183E+01
	Std	7.2582E-01	1.1165E+00	9.4310E-01	1.6207E+00	7.4712E-01	1.4701E+00	2.0145E+00
	Rank	1	3	2	5	4	6	7
E	Avg	3.2581E+01	3.0892E+01	3.2391E+01	2.8654E+01	3.1079E+01	2.9017E+01	2.8688E+01
	Std	6.3726E-01	1.4364E+00	6.3016E-01	2.0975E+00	8.6251E-01	1.4790E+00	1.5376E+00
	Rank	1	4	2	7	3	5	6
F	Avg	3.2628E+01	3.1240E+01	3.2323E+01	2.9041E+01	3.1149E+01	2.8755E+01	2.8907E+01
	Std	5.6969E-01	1.0108E+00	6.2555E-01	1.4792E+00	7.1278E-01	2.0140E+00	1.8818E+00
	Rank	1	3	2	5	4	7	6

(continued on next page)

Table A.5 (continued).

Image	Paradigm	REBSA	BSA	DE	MGSMA	MDE	IGWO	GLSMA
G	Avg	3.2505E+01	3.1187E+01	3.2322E+01	2.8594E+01	3.1156E+01	2.9377E+01	2.8117E+01
	Std	9.1146E-01	1.0915E+00	9.5247E-01	1.7243E+00	1.1435E+00	1.9300E+00	2.5812E+00
	Rank	1 3 2	3 2 2	6 4 6	4 5 4	5 7 5	5 7 7	5 7 7
H	Avg	3.2527E+01	3.1155E+01	3.2462E+01	2.8698E+01	3.1097E+01	2.9394E+01	2.8290E+01
	Std	6.2632E-01	1.5370E+00	1.0020E+00	1.8645E+00	1.3220E+00	1.8222E+00	2.7893E+00
	Rank	1 3 2	3 2 2	6 4 6	4 5 4	5 7 5	5 7 7	5 7 7
I	Avg	3.2414E+01	3.1387E+01	3.2141E+01	2.7222E+01	3.0700E+01	2.8433E+01	2.9003E+01
	Std	8.9466E-01	1.3301E+00	1.3520E+00	2.9011E+00	1.0296E+00	2.5325E+00	1.9298E+00
	Rank	1 3	3 2	7	4	6	6	5
A	Avg	9.4897E-01	9.2305E-01	9.3872E-01	8.8286E-01	9.2419E-01	8.9773E-01	8.8165E-01
	Std	1.3733E-02	2.6282E-02	1.4963E-02	4.8974E-02	2.5297E-02	3.4378E-02	4.2288E-02
	Rank	1 4	4 2	6 3	3 5	5 7	5 7	5 7
B	Avg	9.9116E-01	9.8632E-01	9.8892E-01	9.7509E-01	9.8585E-01	9.7672E-01	9.7649E-01
	Std	1.2592E-03	3.4855E-03	3.3187E-03	9.7640E-03	4.0358E-03	6.3100E-03	9.3151E-03
	Rank	1 3	3 2	7 4	4 5	5 6	5 6	5 6
C	Avg	9.5853E-01	9.4078E-01	9.5323E-01	9.1570E-01	9.4074E-01	9.0823E-01	9.1493E-01
	Std	4.9572E-03	1.0340E-02	1.0714E-02	2.8994E-02	1.2213E-02	3.0591E-02	3.0585E-02
	Rank	1 3	3 2	5 4	4 7	6 7	6 7	6 7
D	Avg	9.7835E-01	9.6970E-01	9.7625E-01	9.5200E-01	9.6883E-01	9.5435E-01	9.4688E-01
	Std	3.7876E-03	8.0417E-03	4.2919E-03	1.5266E-02	7.2711E-03	9.1923E-03	2.0002E-02
	Rank	1 3	3 2	6 4	4 5	5 7	5 7	5 7
E	Avg	9.7200E-01	9.5963E-01	9.7072E-01	9.3887E-01	9.6052E-01	9.4186E-01	9.3859E-01
	SSIM	Std 3.8123E-03	1.3720E-02	4.0031E-03	2.4356E-02	7.0428E-03	1.6214E-02	1.7911E-02
	Rank	1 4	4 2	6 3	3 5	5 7	5 7	5 7
F	Avg	9.9076E-01	9.8547E-01	9.8956E-01	9.7417E-01	9.8539E-01	9.7116E-01	9.7265E-01
	Std	1.4957E-03	4.2823E-03	1.9889E-03	1.0226E-02	3.4040E-03	1.8181E-02	1.2439E-02
	Rank	1 3	3 2	5 4	4 7	5 6	5 6	5 6
G	Avg	9.7692E-01	9.6728E-01	9.7496E-01	9.3985E-01	9.6585E-01	9.4701E-01	9.3002E-01
	Std	5.9461E-03	8.7346E-03	6.7160E-03	2.5713E-02	1.0207E-02	2.5537E-02	4.7191E-02
	Rank	1 3	3 2	6 4	4 5	5 7	5 7	5 7
H	Avg	9.8970E-01	9.8249E-01	9.8882E-01	9.6704E-01	9.8290E-01	9.7188E-01	9.5990E-01
	Std	1.6861E-03	8.5478E-03	3.2147E-03	1.7976E-02	6.4147E-03	1.5796E-02	3.4474E-02
	Rank	1 4	4 2	6 3	3 5	5 7	5 7	5 7
I	Avg	9.8304E-01	9.7589E-01	9.8019E-01	9.2685E-01	9.7304E-01	9.4622E-01	9.5773E-01
	Std	4.0385E-03	9.1365E-03	9.1471E-03	6.6130E-02	7.4562E-03	3.6644E-02	1.9600E-02
	Rank	1 3	3 2	7 4	4 6	6 5	6 5	6 5
A	Avg	9.8945E-01	9.7741E-01	9.8748E-01	9.5955E-01	9.8261E-01	9.6848E-01	9.5952E-01
	Std	3.7626E-03	1.4049E-02	4.3194E-03	2.6691E-02	7.0840E-03	1.5047E-02	2.4133E-02
	Rank	1 4	4 2	6 3	3 5	5 7	5 7	5 7
B	Avg	9.9698E-01	9.9519E-01	9.9622E-01	9.9014E-01	9.9491E-01	9.9230E-01	9.9056E-01
	Std	1.2360E-03	2.7986E-03	2.0486E-03	5.3468E-03	3.9737E-03	3.9697E-03	6.8887E-03
	Rank	1 3	3 2	7 4	4 5	5 6	5 6	5 6
C	Avg	9.9323E-01	9.8669E-01	9.9113E-01	9.7312E-01	9.8728E-01	9.6919E-01	9.7300E-01
	Std	1.6304E-03	3.8817E-03	3.1846E-03	1.7951E-02	5.1992E-03	2.1855E-02	1.9741E-02
	Rank	1 4	4 2	5 3	3 5	5 7	5 6	5 6
D	Avg	9.9368E-01	9.8952E-01	9.9333E-01	9.8161E-01	9.9060E-01	9.8287E-01	9.7877E-01
	Std	2.4707E-03	6.2236E-03	3.0118E-03	9.8158E-03	5.0591E-03	8.1200E-03	1.2877E-02
	Rank	1 4	4 2	6 3	3 5	5 7	5 7	5 7
E	Avg	9.9188E-01	9.8548E-01	9.9186E-01	9.7445E-01	9.8853E-01	9.7884E-01	9.7563E-01
	FSIM	Std 1.9790E-03	1.0704E-02	3.1925E-03	1.5663E-02	4.1331E-03	1.0973E-02	1.1213E-02
	Rank	1 4	4 2	7 3	3 5	5 6	5 6	5 6
F	Avg	9.9851E-01	9.9707E-01	9.9811E-01	9.9389E-01	9.9722E-01	9.9141E-01	9.9343E-01
	Std	3.8637E-04	1.1046E-03	5.5931E-04	4.3680E-03	8.9166E-04	9.4241E-03	4.2545E-03
	Rank	1 4	4 2	5 3	3 5	5 7	5 6	5 6
G	Avg	9.9714E-01	9.9260E-01	9.9616E-01	9.8488E-01	9.9437E-01	9.8585E-01	9.8063E-01
	Std	8.7778E-04	6.7531E-03	1.4032E-03	1.2486E-02	2.2960E-03	8.1818E-03	2.0706E-02
	Rank	1 4	4 2	6 3	3 5	5 7	5 6	5 7
H	Avg	9.9792E-01	9.9598E-01	9.9773E-01	9.9141E-01	9.9623E-01	9.9291E-01	9.8724E-01
	Std	5.6681E-04	2.8510E-03	8.1967E-04	4.6467E-03	1.4789E-03	3.9803E-03	2.1089E-02
	Rank	1 4	4 2	6 3	3 5	5 7	5 6	5 7
I	Avg	9.9735E-01	9.9562E-01	9.9661E-01	9.7943E-01	9.9456E-01	9.8557E-01	9.8626E-01
	Std	6.7531E-04	1.6733E-03	1.9436E-03	2.5901E-02	2.7644E-03	1.3684E-02	1.3702E-02
	Rank	1 3	3 2	7 4	4 6	6 5	6 5	5 5

Table A.6

The Avg and Std results of PSNR, SSIM, and FSIM with threshold = 30.

Image	Paradigm	REBSA	BSA	DE	MGSMA	MDE	IGWO	GLSMA
A	Avg	3.3858E+01	3.1935E+01	3.3204E+01	2.9525E+01	3.2022E+01	2.9082E+01	2.9230E+01
	Std	1.2585E+00	1.9069E+00	1.3508E+00	2.3126E+00	1.4976E+00	2.9735E+00	2.3838E+00
	Rank	1 4	4 2	5 3	3 7	7 6	7 6	7 6
B	Avg	3.4384E+01	3.2647E+01	3.3816E+01	2.9376E+01	3.2297E+01	2.9733E+01	3.0365E+01
	Std	5.5368E-01	1.0043E+00	7.3653E-01	1.9396E+00	7.4501E-01	1.4431E+00	1.1832E+00
	Rank	1 3	3 2	7 4	4 6	6 5	6 5	6 5
C	Avg	3.3435E+01	3.1431E+01	3.3105E+01	2.9441E+01	3.1370E+01	2.9111E+01	2.9334E+01
	Std	8.1074E-01	1.2458E+00	9.9701E-01	2.2204E+00	1.3199E+00	1.8724E+00	2.2263E+00
	Rank	1 3	3 2	5 4	4 5	4 7	4 6	4 6
D	Avg	3.4191E+01	3.2377E+01	3.3955E+01	2.9722E+01	3.2223E+01	2.9625E+01	3.0041E+01
	Std	4.7840E-01	1.3368E+00	7.7254E-01	1.8620E+00	9.6706E-01	1.3107E+00	2.2661E+00
	Rank	1 3	3 2	6 4	4 7	7 5	7 5	7 5
E	Avg	3.4211E+01	3.3010E+01	3.3890E+01	2.9779E+01	3.2379E+01	2.9559E+01	2.9820E+01
	PSNR	Std 6.7309E-01	1.1238E+00	7.2129E-01	2.3385E+00	1.0065E+00	1.7991E+00	2.1576E+00
	Rank	1 3	3 2	6 4	4 7	7 5	7 5	5 5

(continued on next page)

Table A.6 (continued).

Image	Paradigm	REBSA	BSA	DE	MGSMA	MDE	IGWO	GLSMA
F	Avg	3.4060E+01	3.2531E+01	3.3825E+01	2.9129E+01	3.2327E+01	2.9778E+01	2.9296E+01
	Std	6.9918E-01	1.0740E+00	6.8564E-01	2.1001E+00	1.2173E+00	2.0435E+00	1.7050E+00
	Rank	1 3	2	7	4	5	6	
G	Avg	3.4254E+01	3.2733E+01	3.3373E+01	2.9138E+01	3.2522E+01	2.9241E+01	2.9013E+01
	Std	1.1063E+00	1.3074E+00	8.1245E-01	1.5273E+00	6.5102E-01	1.8185E+00	2.5002E+00
	Rank	1 3	2	6	4	5	7	
H	Avg	3.4062E+01	3.2797E+01	3.3762E+01	2.9675E+01	3.2136E+01	2.9928E+01	2.8834E+01
	Std	8.4300E-01	1.2262E+00	9.7433E-01	2.1845E+00	1.5566E+00	1.6149E+00	2.4761E+00
	Rank	1 3	2	6	4	5	7	
I	Avg	3.3749E+01	3.2225E+01	3.2873E+01	3.0057E+01	3.2145E+01	2.9250E+01	2.9448E+01
	Std	9.0797E-01	1.6080E+00	1.3651E+00	1.8953E+00	9.6989E-01	2.1925E+00	2.2896E+00
	Rank	1 3	2	5	4	7	6	
A	Avg	9.6080E-01	9.3787E-01	9.5390E-01	9.0266E-01	9.3825E-01	8.9034E-01	8.9904E-01
	Std	1.1237E-02	2.7702E-02	1.3236E-02	4.6054E-02	2.0551E-02	5.4718E-02	4.3151E-02
	Rank	1 4	2	5	3	7	6	
B	Avg	9.9321E-01	9.8979E-01	9.9220E-01	9.7824E-01	9.8872E-01	9.8027E-01	9.8327E-01
	Std	1.4324E-03	3.0439E-03	1.7854E-03	9.7580E-03	2.1106E-03	6.7243E-03	3.9122E-03
	Rank	1 3	2	7	4	6	5	
C	Avg	9.6656E-01	9.4757E-01	9.6348E-01	9.2488E-01	9.4752E-01	9.2200E-01	9.2746E-01
	Std	5.3349E-03	1.4920E-02	8.5652E-03	2.8862E-02	1.4956E-02	2.5642E-02	2.6663E-02
	Rank	1 3	2	6	4	7	5	
D	Avg	9.8212E-01	9.7345E-01	9.8055E-01	9.5921E-01	9.7380E-01	9.5788E-01	9.6040E-01
	Std	3.0049E-03	8.0732E-03	4.7383E-03	1.2340E-02	6.7932E-03	1.0586E-02	1.6455E-02
	Rank	1 4	2	6	3	7	5	
E	Avg	9.7779E-01	9.7277E-01	9.7682E-01	9.4529E-01	9.6745E-01	9.4627E-01	9.5093E-01
	Std	3.4133E-03	5.2121E-03	3.8884E-03	2.3666E-02	7.1657E-03	1.7393E-02	1.5907E-02
	Rank	1 3	2	7	4	6	5	
F	Avg	9.9302E-01	9.8869E-01	9.9221E-01	9.7205E-01	9.8772E-01	9.7558E-01	9.7395E-01
	Std	1.2824E-03	3.0269E-03	1.6210E-03	1.7809E-02	4.7070E-03	1.8073E-02	1.1763E-02
	Rank	1 3	2	7	4	5	6	
G	Avg	9.8368E-01	9.7420E-01	9.7882E-01	9.4638E-01	9.7463E-01	9.4421E-01	9.3870E-01
	Std	4.9785E-03	1.0196E-02	4.9415E-03	1.6884E-02	4.8570E-03	2.5234E-02	4.4654E-02
	Rank	1 4	2	5	3	6	7	
H	Avg	9.9230E-01	9.8823E-01	9.9136E-01	9.7130E-01	9.8553E-01	9.7482E-01	9.6591E-01
	Std	1.9241E-03	3.9305E-03	2.4362E-03	1.8005E-02	6.2608E-03	1.0157E-02	2.1560E-02
	Rank	1 3	2	6	4	5	7	
I	Avg	9.8681E-01	9.7819E-01	9.8221E-01	9.6427E-01	9.7924E-01	9.5402E-01	9.5702E-01
	Std	3.3923E-03	1.4362E-02	6.7205E-03	1.6760E-02	5.8537E-03	2.9702E-02	2.6600E-02
	Rank	1 4	2	5	3	7	6	
A	Avg	9.9242E-01	9.8457E-01	9.8958E-01	9.6771E-01	9.8573E-01	9.5913E-01	9.6153E-01
	Std	3.0399E-03	1.0893E-02	5.1957E-03	2.5917E-02	7.2931E-03	3.2026E-02	2.6214E-02
	Rank	1 4	2	5	3	7	6	
B	Avg	9.9780E-01	9.9606E-01	9.9746E-01	9.9115E-01	9.9647E-01	9.9334E-01	9.9246E-01
	Std	1.2144E-03	3.2561E-03	1.1944E-03	4.5030E-03	1.7277E-03	3.0878E-03	4.3624E-03
	Rank	1 4	2	7	3	5	6	
C	Avg	9.9472E-01	9.8861E-01	9.9331E-01	9.7645E-01	9.8815E-01	9.7617E-01	9.7590E-01
	Std	1.2852E-03	4.9708E-03	2.7551E-03	1.3974E-02	5.8279E-03	1.5522E-02	1.4671E-02
	Rank	1 3	2	5	4	6	7	
D	Avg	9.9439E-01	9.9097E-01	9.9343E-01	9.8402E-01	9.9151E-01	9.8684E-01	9.8575E-01
	Std	2.3415E-03	5.2518E-03	3.5578E-03	1.0414E-02	4.6615E-03	6.2440E-03	1.1323E-02
	Rank	1 4	2	7	3	5	6	
E	Avg	9.9411E-01	9.9160E-01	9.9310E-01	9.8022E-01	9.9040E-01	9.7987E-01	9.7958E-01
	Std	1.7609E-03	4.7706E-03	2.1375E-03	1.5876E-02	4.2468E-03	1.2143E-02	1.4250E-02
	Rank	1 3	2	5	4	6	7	
F	Avg	9.9885E-01	9.9764E-01	9.9845E-01	9.9216E-01	9.9787E-01	9.9442E-01	9.9335E-01
	Std	3.7199E-04	1.4150E-03	5.4609E-04	5.9347E-03	8.1502E-04	5.9072E-03	5.0588E-03
	Rank	1 4	2	7	3	5	6	
G	Avg	9.9775E-01	9.9523E-01	9.9670E-01	9.8157E-01	9.9592E-01	9.8488E-01	9.8200E-01
	Std	1.1770E-03	3.8604E-03	1.1614E-03	1.0646E-02	1.8337E-03	1.2004E-02	2.0167E-02
	Rank	1 4	2	7	3	5	6	
H	Avg	9.9846E-01	9.9697E-01	9.9831E-01	9.9140E-01	9.9679E-01	9.9370E-01	9.8980E-01
	Std	4.5715E-04	2.7479E-03	4.5492E-04	9.2036E-03	1.7629E-03	3.1295E-03	1.1955E-02
	Rank	1 3	2	6	4	5	7	
I	Avg	9.9791E-01	9.9552E-01	9.9687E-01	9.9112E-01	9.9623E-01	9.8847E-01	9.8692E-01
	Std	5.6766E-04	3.4208E-03	1.7517E-03	5.4133E-03	1.4521E-03	7.6771E-03	1.4390E-02
	Rank	1 4	2	5	3	6	7	

Table A.7

The fitness value results at different threshold level.

Image	Thresholds	REBSA	BSA	DE	MGSMA	MDE	IGWO	GLSMA
A	15	8.4727E+01	8.2793E+01	8.4476E+01	8.3014E+01	8.3385E+01	8.0272E+01	8.0620E+01
	20	1.0049E+02	9.8147E+01	9.9402E+01	9.6494E+01	9.8013E+01	9.3067E+01	9.5596E+01
	25	1.1324E+02	1.0936E+02	1.1205E+02	1.0706E+02	1.1041E+02	1.0504E+02	1.0577E+02
B	30	1.2320E+02	1.2036E+02	1.2222E+02	1.1101E+02	1.1920E+02	1.1010E+02	1.0993E+02
	15	8.6808E+01	8.5043E+01	8.6423E+01	8.4701E+01	8.5517E+01	8.2185E+01	8.3364E+01
	20	1.0271E+02	1.0117E+02	1.0206E+02	9.8120E+01	1.0034E+02	9.5488E+01	9.7474E+01
C	25	1.1615E+02	1.1340E+02	1.1512E+02	1.0911E+02	1.1479E+02	1.0519E+02	1.0899E+02
	30	1.2771E+02	1.2400E+02	1.2612E+02	1.1728E+02	1.2381E+02	1.1530E+02	1.1594E+02
	15	8.3989E+01	8.2557E+01	8.3601E+01	8.2425E+01	8.3374E+01	8.0406E+01	8.1086E+01
D	20	9.8992E+01	9.7056E+01	9.8532E+01	9.4297E+01	9.6999E+01	9.0848E+01	9.5159E+01
	25	1.1196E+02	1.0909E+02	1.1112E+02	1.0411E+02	1.0848E+02	9.9822E+01	1.0387E+02
	30	1.2300E+02	1.1678E+02	1.2157E+02	1.0861E+02	1.1745E+02	1.0793E+02	1.1441E+02
	15	8.6673E+01	8.5908E+01	8.6546E+01	8.4255E+01	8.5583E+01	8.1998E+01	8.3810E+01

(continued on next page)

Table A.7 (continued).

Image	Thresholds	REBSA	BSA	DE	MGSMA	MDE	IGWO	GLSMA
E	20	1.0283E+02	1.0162E+02	1.0236E+02	9.9143E+01	1.0075E+02	9.5000E+01	9.7476E+01
	25	1.1630E+02	1.1392E+02	1.1549E+02	1.0889E+02	1.1321E+02	1.0602E+02	1.0579E+02
	30	1.2750E+02	1.2565E+02	1.2696E+02	1.1981E+02	1.2225E+02	1.1222E+02	1.1821E+02
	15	8.6398E+01	8.5333E+01	8.5890E+01	8.4429E+01	8.5510E+01	8.1061E+01	8.2473E+01
	20	1.0258E+02	1.0003E+02	1.0122E+02	9.8167E+01	1.0020E+02	9.3837E+01	9.6198E+01
	25	1.1591E+02	1.1237E+02	1.1495E+02	1.0886E+02	1.1227E+02	1.0518E+02	1.0842E+02
F	30	1.2622E+02	1.2350E+02	1.2447E+02	1.1425E+02	1.2206E+02	1.1129E+02	1.1395E+02
	15	8.5294E+01	8.3742E+01	8.4949E+01	8.2891E+01	8.3904E+01	8.0881E+01	8.3173E+01
	20	1.0028E+02	9.9134E+01	9.9674E+01	9.5196E+01	9.8481E+01	9.5254E+01	9.4755E+01
G	25	1.1241E+02	1.0871E+02	1.1188E+02	1.0630E+02	1.1064E+02	1.0359E+02	1.0609E+02
	30	1.2382E+02	1.2231E+02	1.2338E+02	1.1331E+02	1.1910E+02	1.0870E+02	1.1254E+02
	15	8.5134E+01	8.3029E+01	8.4090E+01	8.1875E+01	8.4035E+01	8.0838E+01	8.1302E+01
	20	9.9515E+01	9.7222E+01	9.9297E+01	9.4411E+01	9.7504E+01	9.3831E+01	9.3445E+01
H	25	1.1194E+02	1.0884E+02	1.1180E+02	1.0391E+02	1.0838E+02	1.0303E+02	1.0671E+02
	30	1.2349E+02	1.1925E+02	1.2136E+02	1.1088E+02	1.1887E+02	1.0709E+02	1.0973E+02
	15	8.6198E+01	8.3600E+01	8.5025E+01	8.3552E+01	8.4817E+01	8.0389E+01	8.3547E+01
I	20	1.0133E+02	9.9271E+01	1.0052E+02	9.5494E+01	9.9580E+01	9.3020E+01	9.6632E+01
	25	1.1467E+02	1.1058E+02	1.1374E+02	1.0461E+02	1.1028E+02	1.0357E+02	1.0563E+02
	30	1.2560E+02	1.2137E+02	1.2371E+02	1.1339E+02	1.2016E+02	1.0941E+02	1.1594E+02
J	15	8.5334E+01	8.3393E+01	8.5052E+01	8.2565E+01	8.3849E+01	8.0409E+01	8.2282E+01
	20	1.0047E+02	9.7446E+01	9.9516E+01	9.6066E+01	9.8487E+01	9.3964E+01	9.4474E+01
	25	1.1309E+02	1.0933E+02	1.1212E+02	1.0396E+02	1.0928E+02	1.0027E+02	1.0671E+02
K	30	1.2361E+02	1.1882E+02	1.2221E+02	1.1580E+02	1.1885E+02	1.0642E+02	1.1296E+02

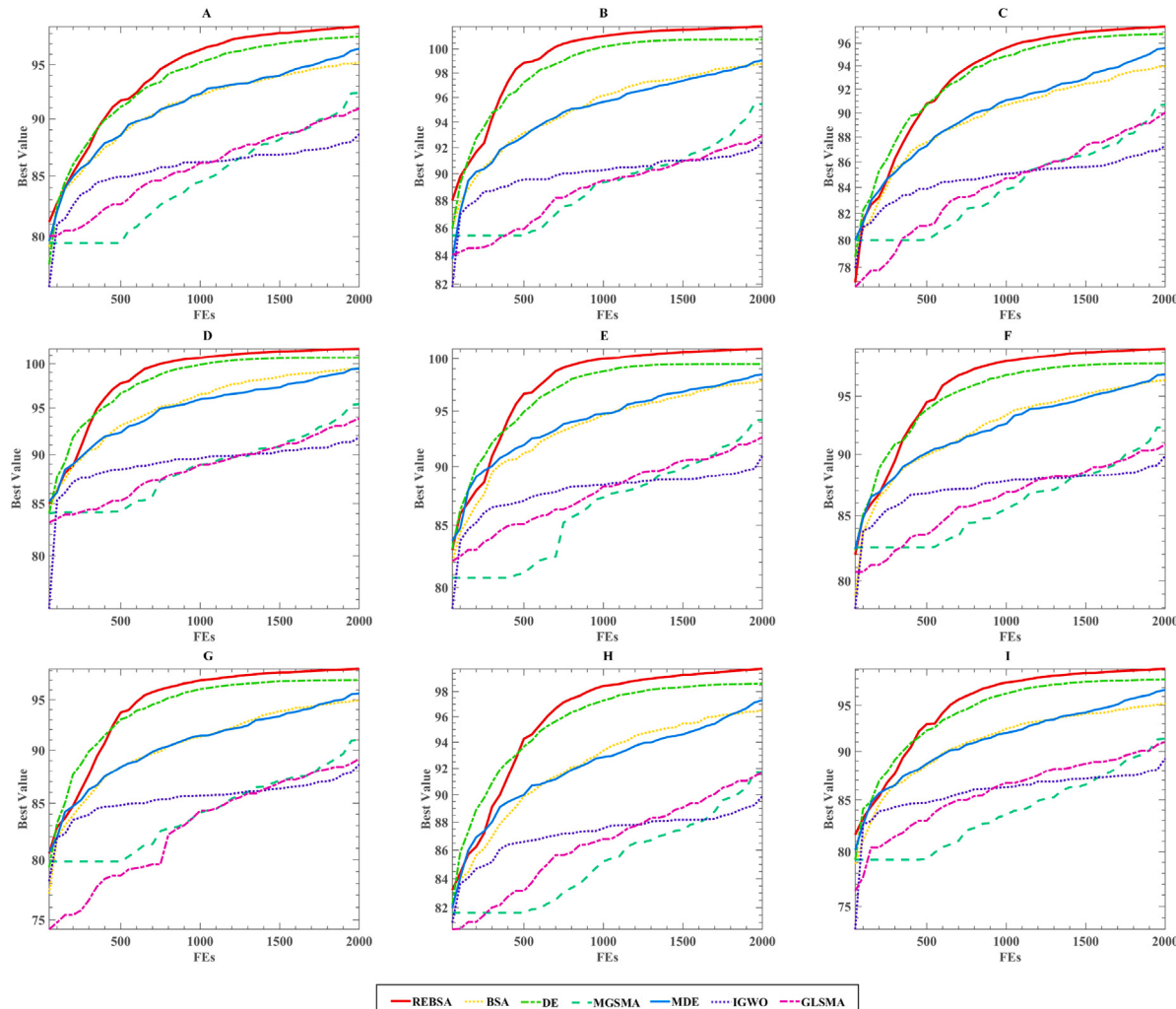
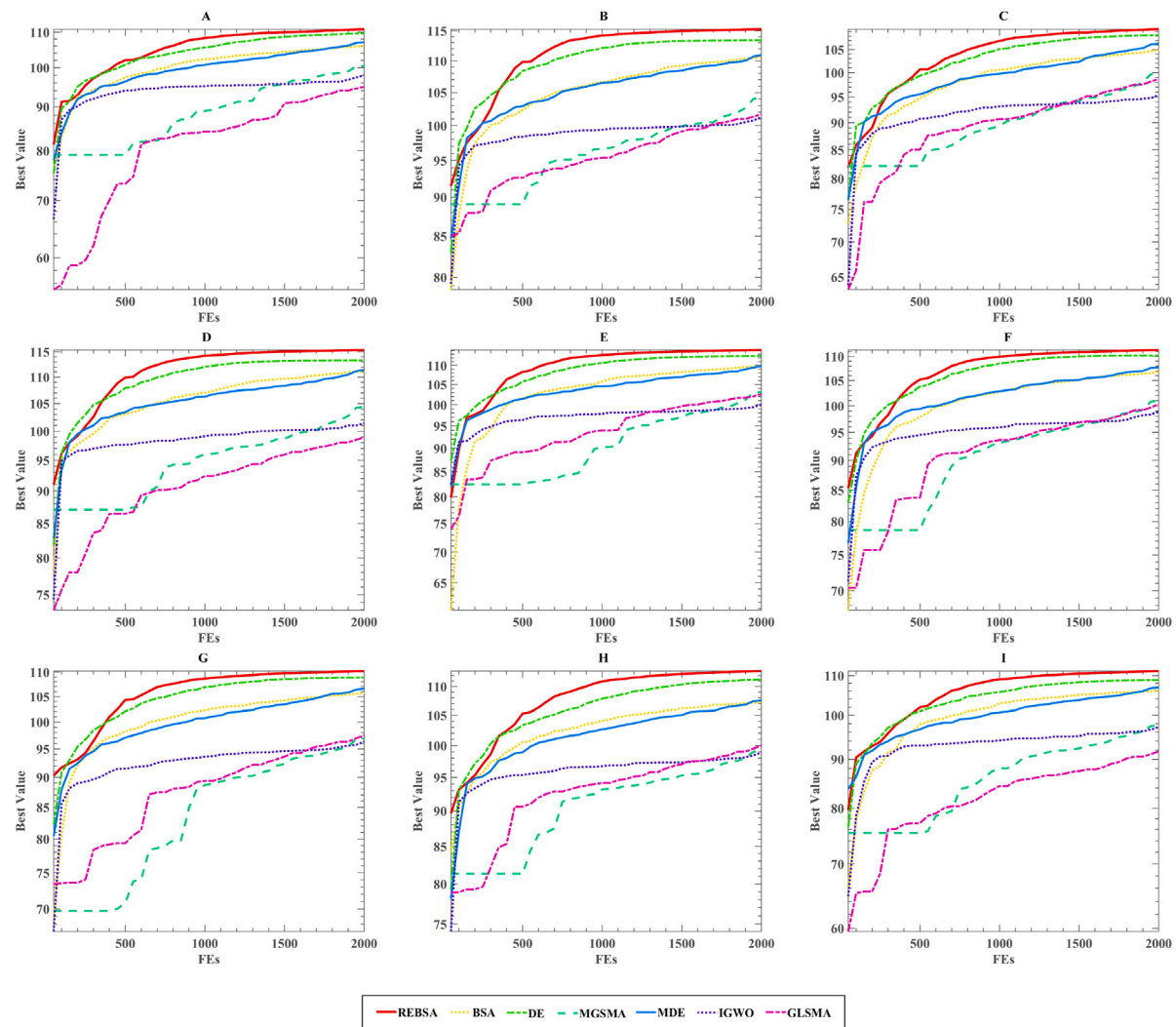


Fig. B.1. Convergence curves of all competitive algorithms with threshold = 20.

**Fig. B.2.** Convergence curves of all competitive algorithms with threshold = 25.**Appendix B****Data availability**

Data will be made available on request.

See Figs. B.1–B.6.

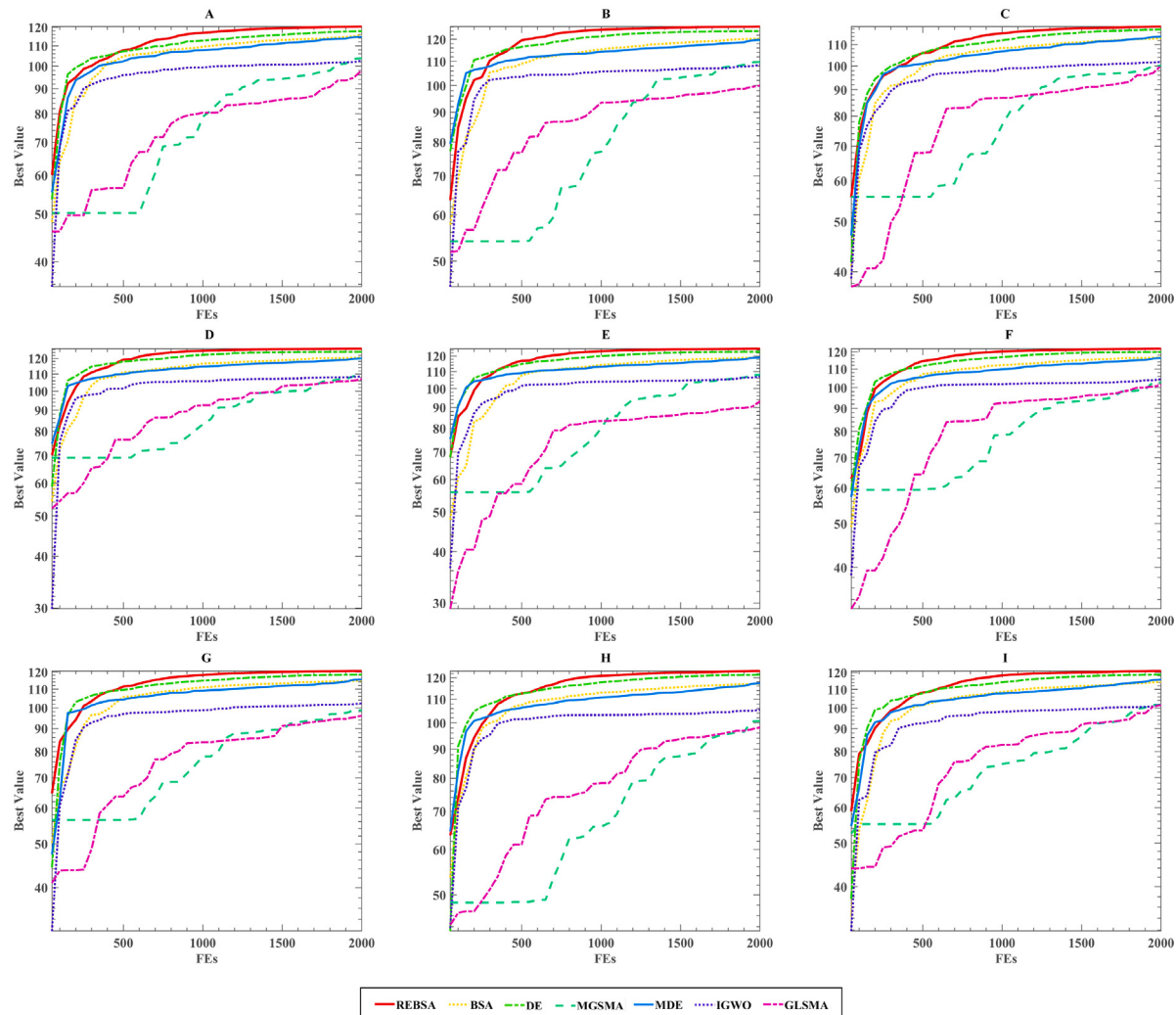


Fig. B.3. Convergence curves of all competitive algorithms with threshold = 30.

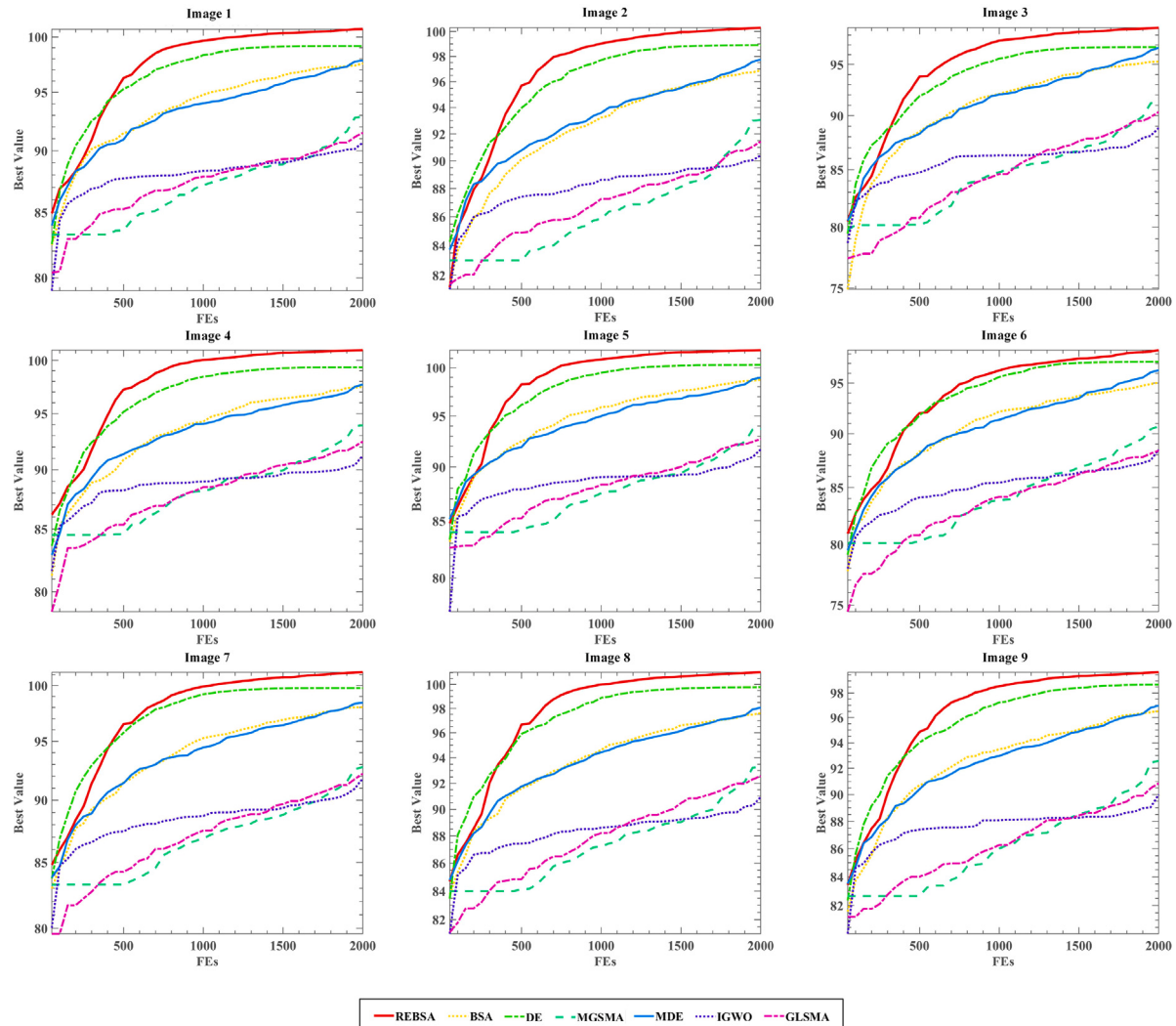


Fig. B.4. Convergence curves of all competitive algorithms with threshold = 20.

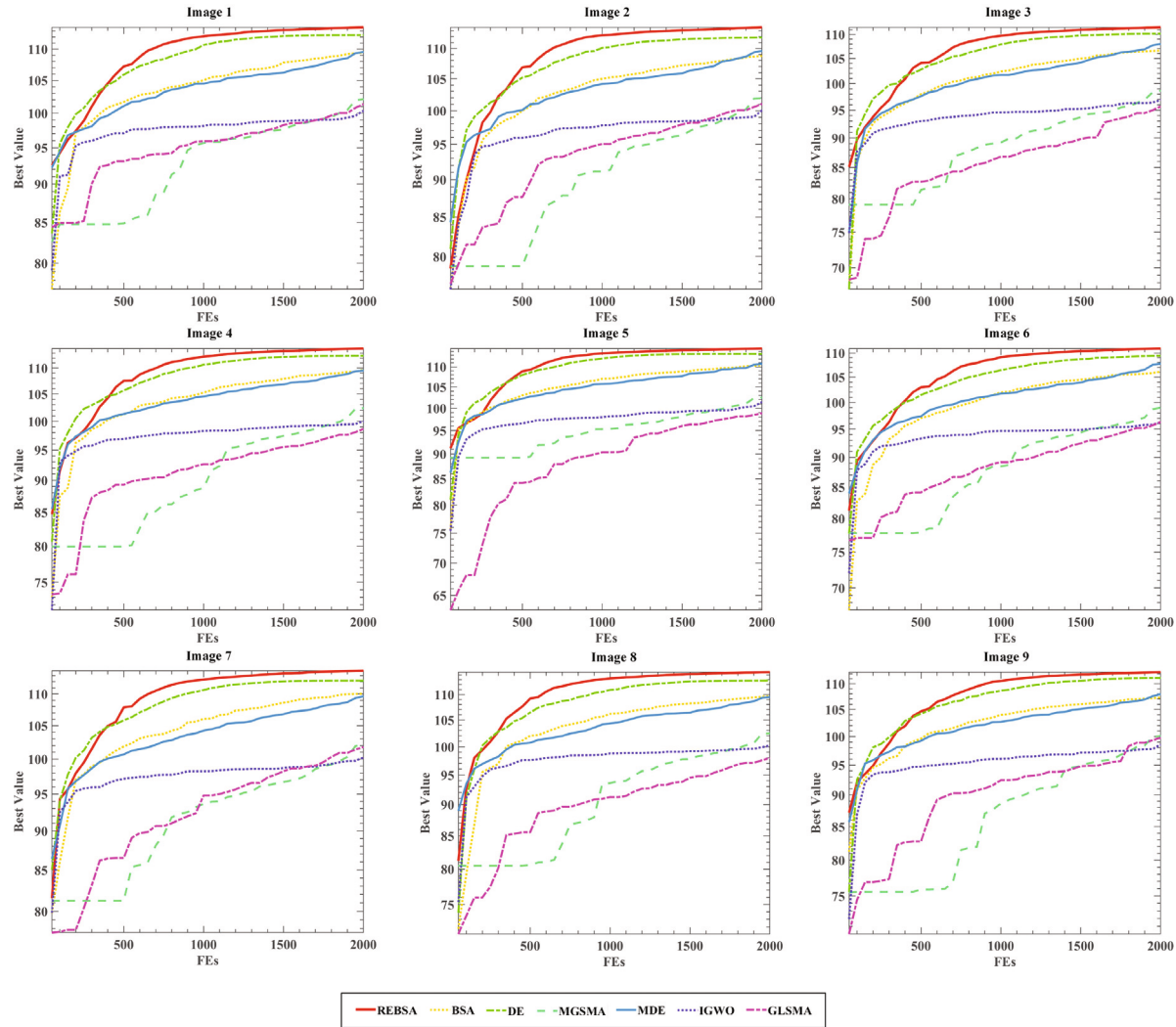


Fig. B.5. Convergence curves of all competitive algorithms with threshold = 25.

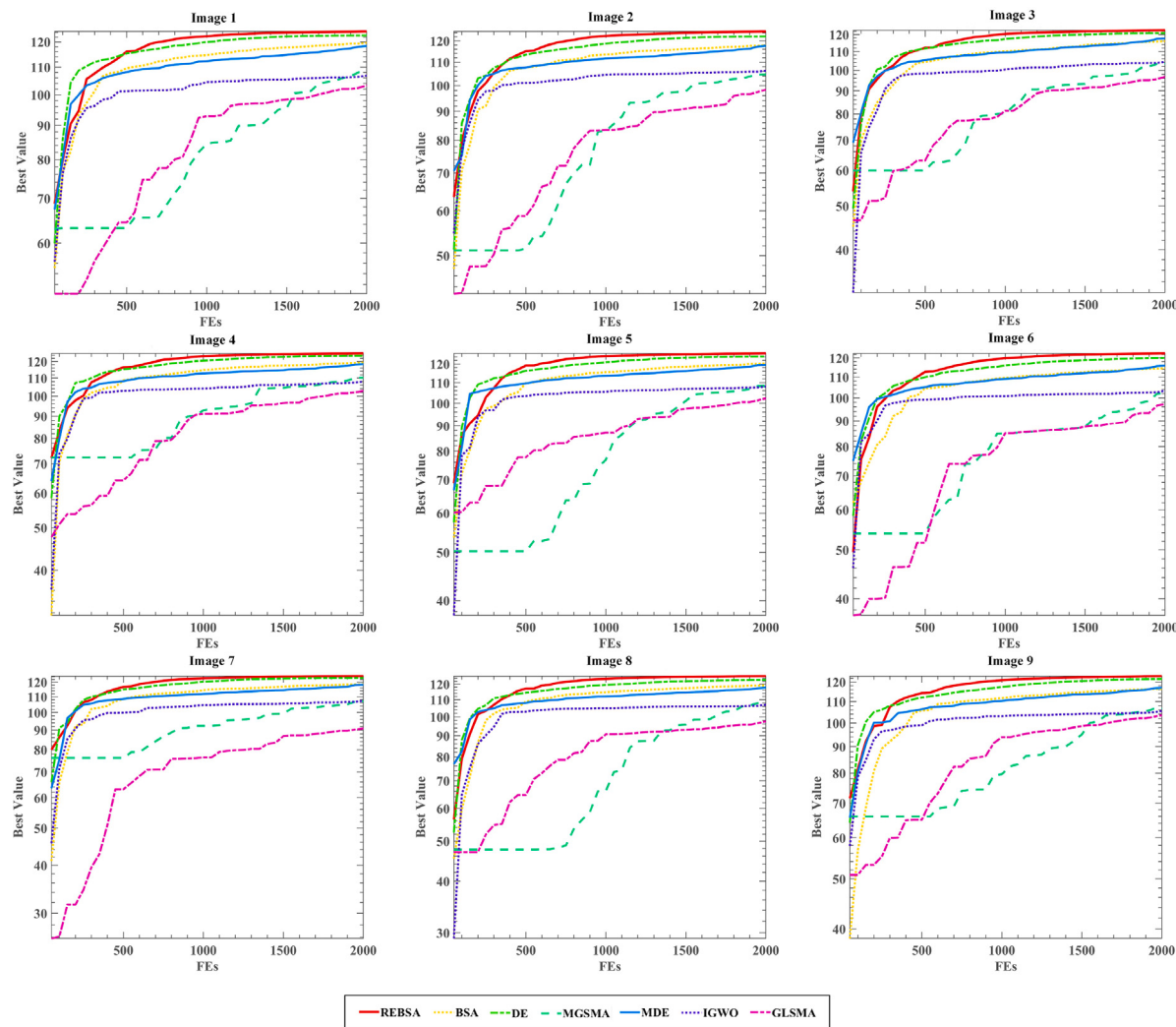


Fig. B.6. Convergence curves of all competitive algorithms with threshold = 30.

References

- [1] Dan-Dan Tang, Zhuo-Jun Ye, Wan-Wan Liu, Jing Wu, Jing-Yu Tan, Yan Zhang, Qun Xu, Yong-Bing Xiang, Survival feature and trend of female breast cancer: A comprehensive review of survival analysis from cancer registration data, *Breast* (2024) 103862.
- [2] Angela N. Giaquinto, Hyuna Sung, Kimberly D. Miller, Joan L. Kramer, Lisa A. Newman, Adair Minihan, Ahmedin Jemal, Rebecca L. Siegel, Breast cancer statistics, 2022, *CA: Cancer J. Clin.* 72 (6) (2022) 524–541.
- [3] Qinggang Zeng, Cheng Chen, Chen Chen, Haitao Song, Min Li, Junyi Yan, Xiaoyi Lv, Serum Raman spectroscopy combined with convolutional neural network for rapid diagnosis of HER2-positive and triple-negative breast cancer, *Spectrochim. Acta Part A: Mol. Biomol. Spectrosc.* 286 (2023) 122000.
- [4] Xiaorong Ma, Hong Cheng, Junwei Hou, Zhenhong Jia, Guohua Wu, Xiaoyi Lü, Hongyi Li, Xiangxiang Zheng, Chen Chen, Detection of breast cancer based on novel porous silicon Bragg reflector surface-enhanced Raman spectroscopy-active structure, *Chin. Opt. Lett.* 18 (5) (2020) 051701.
- [5] Xin Wen, Xing Guo, Shuihua Wang, Zhihai Lu, Yudong Zhang, Breast cancer diagnosis: A systematic review, *Biocybern. Biomed.* 44 (1) (2024) 119–148.
- [6] Ying Su, Xuecong Tian, Rui Gao, Wenjia Guo, Cheng Chen, Chen Chen, Dongfang Jia, Hongtao Li, Xiaoyi Lv, Colon cancer diagnosis and staging classification based on machine learning and bioinformatics analysis, *Comput. Biol. Med.* 145 (2022) 105409.
- [7] Zhiyuan Cheng, Hongyi Li, Chen Chen, Xiaoyi Lv, EnGuang Zuo, Xiaodong Xie, Zhongyuan Li, Pei Liu, Hongtao Li, Cheng Chen, Application of serum SERS technology based on thermally annealed silver nanoparticle composite substrate in breast cancer, *Photodiagnosis Photodyn. Ther.* 41 (2023) 103284.
- [8] Wenfeng Song, Xuan Wang, Yuting Guo, Shuai Li, Bin Xia, Aimin Hao, CenterFormer: a novel cluster center enhanced transformer for unconstrained dental plaque segmentation, *IEEE Trans. Multimed.* (2024).
- [9] Erik Cuevas, Carlos Guzmán-Rosales, Marco Perez, Ram Sarkar, A graph segmentation method based on compatibility subgraph aggregation, *IEEE Access* (2024).
- [10] Lin Yang, Dan Shao, Zhenxing Huang, Mengxiao Geng, Na Zhang, Long Chen, Xi Wang, Dong Liang, Zhi-Feng Pang, Zhanli Hu, Few-shot segmentation framework for lung nodules via an optimized active contour model, *Med. Phys.* 51 (4) (2024) 2788–2805.
- [11] Zhenxiang Chen, Tingfa Xu, Yongzhuo Pan, Ning Shen, Huan Chen, Jianan Li, Edge feature enhancement for fine-grained segmentation of remote sensing images, *IEEE Trans. Geosci. Remote Sens.* (2024).
- [12] Bo Li, Daoye Yang, ERT image reconstruction using marker region segmentation method, *Meas. Sci. Technol.* 35 (10) (2024) 105414.
- [13] Chetna Kaushal, Md Khairul Islam, Sara A. Althubiti, Fayadh Alenezi, Romany F. Mansour, A framework for interactive medical image segmentation using optimized swarm intelligence with convolutional neural networks, *Comput. Intell. Neurosci.* 2022 (1) (2022) 7935346.
- [14] Chetna Kaushal, Md Khairul Islam, Sara A. Althubiti, Fayadh Alenezi, Romany F. Mansour, A framework for interactive medical image segmentation using optimized swarm intelligence with convolutional neural networks, *Comput. Intell. Neurosci.* 2022 (1) (2022) 7935346.
- [15] Jianfu Xia, Zhenhao Cai, Ali A. Heidari, Yinghai Ye, Huiling Chen, Zhifang Pan, Enhanced moth-flame optimizer with quasi-reflection and refraction learning with application to image segmentation and medical diagnosis, *Curr. Bioinform.* 18 (2) (2023) 109–142.
- [16] Kumara Sastry, David Goldberg, Graham Kendall, Search methodologies, 2005,
- [17] Rainer Storn, Kenneth Price, Differential evolution—a simple and efficient heuristic for global optimization over continuous spaces, *J. Global Optim.* 11 (1997) 341–359.
- [18] Ingo Rechenberg, Evolutionsstrategien, in: *Simulationsmethoden in der Medizin und Biologie: Workshop*, Hannover, 29. Sept.–1. Okt. 1977, Springer, 1978, pp. 83–114.

- [19] Marco Dorigo, Mauro Birattari, Thomas Stutzle, Ant colony optimization, *IEEE Comput. Intell. Mag.* 1 (4) (2006) 28–39.
- [20] Mehdi Neshat, Ghodrat Sepidnam, Mehdi Sargolzaei, Adel Najarian Toosi, Artificial fish swarm algorithm: a survey of the state-of-the-art, hybridization, combinatorial and indicative applications, *Artif. Intell. Rev.* 42 (4) (2014) 965–997.
- [21] James Kennedy, Russell Eberhart, Particle swarm optimization, in: Proceedings of ICNN'95-International Conference on Neural Networks, Vol. 4, ieee, 1995, pp. 1942–1948.
- [22] Xin-She Yang, Firefly algorithm, stochastic test functions and design optimisation, *Int. J. Bio-Inspired Comput.* 2 (2) (2010) 78–84.
- [23] Kevin M. Passino, Bacterial foraging optimization, *Int. J. Swarm Intell. Res. (IJSIR)* 1 (1) (2010) 1–16.
- [24] Xin-She Yang, Amir Hossein Gandomi, Bat algorithm: a novel approach for global engineering optimization, *Eng. Comput.* 29 (5) (2012) 464–483.
- [25] Seyedali Mirjalili, Andrew Lewis, The whale optimization algorithm, *Adv. Eng. Softw.* 95 (2016) 51–67.
- [26] Seyedali Mirjalili, Amir H. Gandomi, Seyedeh Zahra Mirjalili, Shahrad Saremi, Hossam Faris, Seyed Mohammad Mirjalili, Salp swarm algorithm: A bio-inspired optimizer for engineering design problems, *Adv. Eng. Softw.* 114 (2017) 163–191.
- [27] Seyedali Mirjalili, Moth-flame optimization algorithm: A novel nature-inspired heuristic paradigm, *Knowl.-Based Syst.* 89 (2015) 228–249.
- [28] Jieming Ma, T.O. Ting, Ka Lok Man, Nan Zhang, Sheng-Uei Guan, Prudence W.H. Wong, et al., Parameter estimation of photovoltaic models via cuckoo search, *J. Appl. Math.* 2013 (2013).
- [29] Dervis Karaboga, Beyza Gorkemli, Celal Ozturk, Nurhan Karaboga, A comprehensive survey: artificial bee colony (ABC) algorithm and applications, *Artif. Intell. Rev.* 42 (2014) 21–57.
- [30] Ali Asghar Heidari, Seyedali Mirjalili, Hossam Faris, Ibrahim Aljarah, Majdi Mafarja, Huiling Chen, Harris hawks optimization: Algorithm and applications, *Future Gener. Comput. Syst.* 97 (2019) 849–872.
- [31] Seyedali Mirjalili, Seyed Mohammad Mirjalili, Andrew Lewis, Grey wolf optimizer, *Adv. Eng. Softw.* 69 (2014) 46–61.
- [32] Shimin Li, Huiling Chen, Mingjing Wang, Ali Asghar Heidari, Seyedali Mirjalili, Slime mould algorithm: A new method for stochastic optimization, *Future Gener. Comput. Syst.* 111 (2020) 300–323.
- [33] Yutao Yang, Huiling Chen, Ali Asghar Heidari, Amir H. Gandomi, Hunger games search: Visions, conception, implementation, deep analysis, perspectives, and towards performance shifts, *Expert Syst. Appl.* 177 (2021) 114864.
- [34] Iman Ahmadianfar, Ali Asghar Heidari, Amir H. Gandomi, Xuefeng Chu, Huiling Chen, RUN beyond the metaphor: An efficient optimization algorithm based on runge kutta method, *Expert Syst. Appl.* 181 (2021) 115079.
- [35] Seyedali Mirjalili, SCA: a sine cosine algorithm for solving optimization problems, *Knowl.-Based Syst.* 96 (2016) 120–133.
- [36] Hang Su, Dong Zhao, Ali Asghar Heidari, Lei Liu, Xiaoqin Zhang, Majdi Mafarja, Huiling Chen, RIME: A physics-based optimization, *Neurocomputing* 532 (2023) 183–214.
- [37] Ziyu Zhang, Yuelin Gao, Solving large-scale global optimization problems and engineering design problems using a novel biogeography-based optimization with Lévy and Brownian movements, *Int. J. Mach. Learn. Cybern.* 14 (1) (2023) 313–346.
- [38] Scott Kirkpatrick, C. Daniel Gelatt Jr., Mario P. Vecchi, Optimization by simulated annealing, *Science* 220 (4598) (1983) 671–680.
- [39] Esmat Rashedi, Hossein Nezamabadi-Pour, Saeid Saryazdi, GSA: a gravitational search algorithm, *Inform. Sci.* 179 (13) (2009) 2232–2248.
- [40] Pinar Civicioglu, Backtracking search optimization algorithm for numerical optimization problems, *Appl. Math. Comput.* 219 (15) (2013) 8121–8144.
- [41] Kai Han, Victor S. Sheng, Yuqing Song, Yi Liu, Chengjian Qiu, Siqi Ma, Zhe Liu, Deep semi-supervised learning for medical image segmentation: A review, *Expert Syst. Appl.* (2024) 123052.
- [42] C. Sahaya Pushpa Sarmila Star, T.M. Inbamalar, A. Milton, Automatic semantic segmentation of breast cancer in DCE-MRI using DeepLabV3+ with modified ResNet50, *Biomed. Signal Process. Control.* 99 (2025) 106691.
- [43] Yue Zhou, Houjin Chen, Yanfeng Li, Qin Liu, Xuanang Xu, Shu Wang, Pew-Thian Yap, Dinggang Shen, Multi-task learning for segmentation and classification of tumors in 3D automated breast ultrasound images, *Med. Image Anal.* 70 (2021) 101918.
- [44] Abeer Saber, Mohamed Sakr, Osama M. Abo-Seida, Arabi Keshk, Huiling Chen, A novel deep-learning model for automatic detection and classification of breast cancer using the transfer-learning technique, *IEE Access* 9 (2021) 71194–71209.
- [45] Yiqiu Shen, Nan Wu, Jason Phang, Jungkyu Park, Kangning Liu, Sudarshini Tyagi, Laura Heacock, S. Gene Kim, Linda Moy, Kyunghyun Cho, et al., An interpretable classifier for high-resolution breast cancer screening images utilizing weakly supervised localization, *Med. Image Anal.* 68 (2021) 101908.
- [46] Nikoleta Manakitsa, George S. Maraslis, Lazaros Moysis, George F. Frangulis, A review of machine learning and deep learning for object detection, semantic segmentation, and human action recognition in machine and robotic vision, *Technologies* 12 (2) (2024) 15.
- [47] Lihao Liu, Angelica I. Aviles-Rivero, Carola-Bibiane Schonlieb, Contrastive registration for unsupervised medical image segmentation, *IEEE Trans. Neural Networks Learn. Syst.* (2023).
- [48] Kang Li, Lequan Yu, Pheng-Ann Heng, Towards reliable cardiac image segmentation: Assessing image-level and pixel-level segmentation quality via self-reflective references, *Med. Image Anal.* 78 (2022).
- [49] Sheng He, Yanfang Feng, P. Ellen Grant, Yangming Ou, Segmentation ability map: Interpret deep features for medical image segmentation, *Med. Image Anal.* 84 (2023).
- [50] Melanie Gaillochet, Christian Desrosiers, Herve Lombaert, Active learning for medical image segmentation with stochastic batches, *Med. Image Anal.* 90 (2023).
- [51] Shunyao Luan, Xiangyang Yu, Shuang Lei, Chi Ma, Xiao Wang, Xudong Xue, Yi Ding, Teng Ma, Benpeng Zhu, Deep learning for fast super-resolution ultrasound microvessel imaging, *Phys. Med. Biol.* 68 (24) (2023) 245023.
- [52] Xiangyang Yu, Shunyao Luan, Shuang Lei, Jing Huang, Zeqing Liu, Xudong Xue, Teng Ma, Yi Ding, Benpeng Zhu, Deep learning for fast denoising filtering in ultrasound localization microscopy, *Phys. Med. Biol.* 68 (20) (2023) 205002.
- [53] Yanfei Jia, Guangda Chen, Haotian Chi, Retinal fundus image super-resolution based on generative adversarial network guided with vascular structure prior, *Sci. Rep.* 14 (1) (2024) 22786.
- [54] David H. Wolpert, William G. Macready, No free lunch theorems for optimization, *IEEE Trans. Evol. Comput.* 1 (1) (1997) 67–82.
- [55] Donglin Zhu, Jiaying Shen, Yangyang Zheng, Rui Li, Changjun Zhou, Shi Cheng, Yilin Yao, Multi-strategy learning-based particle swarm optimization algorithm for COVID-19 threshold segmentation, *Comput. Biol. Med.* (2024) 108498.
- [56] Yi Chen, Mingjing Wang, Ali Asghar Heidari, Beibei Shi, Zhongyi Hu, Qian Zhang, Huiling Chen, Majdi Mafarja, Hamza Turabieh, Multi-threshold image segmentation using a multi-strategy shuffled frog leaping algorithm, *Expert Syst. Appl.* 194 (2022) 116511.
- [57] Guohua Wu, Rammohan Mallipeddi, Ponnuthurai Nagaratnam Suganthan, Problem definitions and evaluation criteria for the CEC 2017 competition on constrained real-parameter optimization, in: National University of Defense Technology, Changsha, Hunan, PR China and Kyungpook National University, Daegu, South Korea and Nanyang Technological University, Singapore, Technical Report, Technical Report Zhengzhou, China, 2017.
- [58] Jie Xing, Ali Asghar Heidari, Huiling Chen, Hanli Zhao, WHRIME: A weight-based recursive hierarchical RIME optimizer for breast cancer histopathology image segmentation, *Displays* 82 (2024) 102648.
- [59] Jiaochen Chen, Zhennao Cai, Ali Asghar Heidari, Huiling Chen, Qiuxiang He, José Escorcia-Gutierrez, Romany F. Mansour, Multi-threshold image segmentation based on an improved differential evolution: case study of thyroid papillary carcinoma, *Biomed. Signal Process. Control.* 85 (2023) 104893.
- [60] Manrong Shi, Chi Chen, Lei Liu, Fangjun Kuang, Dong Zhao, Xiaowei Chen, A grade-based search adaptive random slime mould optimizer for lupus nephritis image segmentation, *Comput. Biol. Med.* 160 (2023) 106950.
- [61] Xiao Yang, Xiaojia Ye, Dong Zhao, Ali Asghar Heidari, Zhangze Xu, Huiling Chen, Yangyang Li, Multi-threshold image segmentation for melanoma based on Kapur's entropy using enhanced ant colony optimization, *Front. Neuroinformatics* 16 (2022) 1041799.
- [62] Ahmed S. Abutaleb, Automatic thresholding of gray-level pictures using two-dimensional entropy, *Comput. Vis. Graph. Image Process.* 47 (1) (1989) 22–32.
- [63] Antoni Buades, Bartomeu Coll, J.-M. Morel, A non-local algorithm for image denoising, in: 2005 IEEE Computer Society Conference on Computer Vision and Pattern Recognition, Vol. 2, CVPR'05, Ieee, 2005, pp. 60–65.
- [64] Leila Golshani, Einollah Pasha, Gholamhosseini Yari, Some properties of Rényi entropy and Rényi entropy rate, *Inform. Sci.* 179 (14) (2009) 2426–2433.
- [65] Jiaochen Chen, Zhennao Cai, Huiling Chen, Xiaowei Chen, José Escorcia-Gutierrez, Romany F. Mansour, Mahmoud Ragab, Renal pathology images segmentation based on improved cuckoo search with diffusion mechanism and adaptive beta-hill climbing, *J. Bionic Eng.* 20 (5) (2023) 2240–2275.
- [66] David J. Sheskin, *Handbook of Parametric and Nonparametric Statistical Procedures*, Chapman and hall/CRC, 2003.
- [67] J. Alcalá-Fdez, A. Fernandez, J. Luengo, J. Derrac, S. Garcia, L. Sanchez, F. Herrera, A software tool to assess evolutionary algorithms for data mining problems, *Multiple-Valued Log. Soft Comput.* 17 (2011) 2–3.
- [68] Jingqiao Zhang, Arthur C. Sanderson, JADE: adaptive differential evolution with optional external archive, *IEEE Trans. Evol. Comput.* 13 (5) (2009) 945–958.
- [69] Abhishek Kumar, Rakesh Kumar Misra, Devender Singh, Improving the local search capability of effective butterfly optimizer using covariance matrix adapted retreat phase, in: 2017 IEEE Congress on Evolutionary Computation, CEC, IEEE, 2017, pp. 1835–1842.
- [70] Noor H. Awad, Mostafa Z. Ali, Ponnuthurai N. Suganthan, Ensemble sinusoidal differential covariance matrix adaptation with euclidean neighborhood for solving CEC2017 benchmark problems, in: 2017 IEEE Congress on Evolutionary Computation, CEC, IEEE, 2017, pp. 372–379.
- [71] Yulian Cao, Han Zhang, Wenfeng Li, Mengchu Zhou, Yu Zhang, Wanpracha Art Chaovallitwongse, Comprehensive learning particle swarm optimization algorithm with local search for multimodal functions, *IEEE Trans. Evol. Comput.* 23 (4) (2018) 718–731.

- [72] DongLi Jia, GuoXin Zheng, BoYang Qu, Muhammad Khurram Khan, A hybrid particle swarm optimization algorithm for high-dimensional problems, *Comput. Ind. Eng.* 61 (4) (2011) 1117–1122.
- [73] Kunjie Yu, J.J. Liang, B.Y. Qu, Zhiping Cheng, Heshan Wang, Multiple learning backtracking search algorithm for estimating parameters of photovoltaic models, *Appl. Energy* 226 (2018) 408–422.
- [74] Mohamed Abd Elaziz, Diego Oliva, Shengwu Xiong, An improved opposition-based sine cosine algorithm for global optimization, *Expert Syst. Appl.* 90 (2017) 484–500.
- [75] Mohammed Azmi Al-Betar, Mohammed A. Awadallah, Hossam Faris, Ibrahim Al-Jarrah, Abdelaziz I. Hammouri, Natural selection methods for grey wolf optimizer, *Expert Syst. Appl.* 113 (2018) 481–498.
- [76] Lemin Peng, Caitou He, Ali Asghar Heidari, Qian Zhang, Huiling Chen, Guoxi Liang, Nojood O. Aljehane, Romany F. Mansour, Information sharing search boosted whale optimizer with nelder-mead simplex for parameter estimation of photovoltaic models, *Energy Convers. Manage.* 270 (2022) 116246.
- [77] Hamidreza Bolhasani, Elham Amjadi, Maryam Tabatabaeian, Somayyeh Jafarali Jassbi, A histopathological image dataset for grading breast invasive ductal carcinomas, *Informatics Med. Unlocked* 19 (2020) 100341.
- [78] Feng Qiu, Ran Guo, Huiling Chen, Guoxi Liang, Boosting slime mould algorithm for high-dimensional gene data mining: Diversity analysis and feature selection, *Comput. Math. Methods Med.* 2022 (1) (2022) 8011003.
- [79] Zhennao Cai, Jianhua Gu, Jie Luo, Qian Zhang, Huiling Chen, Zhifang Pan, Yuping Li, Chengye Li, Evolving an optimal kernel extreme learning machine by using an enhanced grey wolf optimization strategy, *Expert Syst. Appl.* 138 (2019) 112814.
- [80] Paul K. Bergey, Cliff Ragsdale, Modified differential evolution: a greedy random strategy for genetic recombination, *Omega* 33 (3) (2005) 255–265.
- [81] Lili Ren, Ali Asghar Heidari, Zhennao Cai, Qike Shao, Guoxi Liang, Hui-Ling Chen, Zhifang Pan, Gaussian kernel probability-driven slime mould algorithm with new movement mechanism for multi-level image segmentation, *Measurement* 192 (2022) 110884.
- [82] Quan Huynh-Thu, Mohammed Ghanbari, Scope of validity of PSNR in image/video quality assessment, *Electron. Lett.* 44 (13) (2008) 800–801.
- [83] Zhou Wang, Alan C. Bovik, Hamid R. Sheikh, Eero P. Simoncelli, Image quality assessment: from error visibility to structural similarity, *IEEE Trans. Image Process.* 13 (4) (2004) 600–612.
- [84] Lin Zhang, Lei Zhang, Xuanqin Mou, David Zhang, FSIM: A feature similarity index for image quality assessment, *IEEE Trans. Image Process.* 20 (8) (2011) 2378–2386.